

# **Mechatronics and Electrical Drives**

**Prof. Dr.-Ing. Joachim Böcker**

Lecture Notes

Last update 2017-07-17

University of Paderborn

Department of Power Electronics and  
Electrical Drives

## Contents

1	Mechatronic Systems .....	5
2	Magnetic Circuits.....	7
2.1	Magnetic Reluctance .....	7
2.2	Energy and Power.....	8
2.3	Magnetic Materials .....	15
2.4	Permanent Magnets .....	22
3	Magnetic Bearing.....	34
3.1	Magnetic Yoke.....	34
3.2	Construction with two Yokes .....	36
3.3	Control of a Magnetic Bearing with Bias Excitation by a Separate Winding .....	37
3.4	Magnetic Bearing with Permanent Magnets.....	46
3.5	Sensors.....	49
3.6	Current Converters.....	49
3.7	Pulse Width Modulation .....	50
3.8	Magnetic Bearing with Two Degrees of Freedom .....	55
4	Switched Reluctance Motor .....	57
4.1	Construction.....	57
4.2	Functional principle .....	58
4.3	Dynamic Behavior .....	64
4.4	Converter .....	70
5	Stepping Motors.....	73
6	Gleichstrommotor .....	75
6.1	Wirkprinzip.....	75
6.2	Aufbau .....	77
6.3	Kommutator und Ankerwicklungsschemata.....	78
6.4	Kommutierung und Wendepolwicklung.....	79
6.5	Ankerrückwirkung, Kompensations- und Kompoundwicklung.....	80
6.6	Mathematische Modellierung .....	81
6.7	Elektrische und mechanische Leistung, Wirkungsgrad.....	84
6.8	Schaltungsarten, Klemmenbezeichnungen und Schaltzeichen.....	84
6.9	Fremderregter und permanent erregter Motor .....	85
6.10	Nebenschlussmotor.....	89
6.11	Reihenschlussmotor.....	90
6.12	Controlled Operation .....	93
6.13	Operation at the Limits of Current and Voltages.....	99
7	Electronically Commutated Motors .....	102
7.1	Functional Principle.....	102
7.2	Induced Voltages .....	104
7.3	Equivalent Circuit Diagram and Torque.....	107
7.4	Converter .....	109
7.5	Commutation .....	110
7.6	Control.....	113
8	Design of Current and Speed Control.....	116
8.1	Controller Design with Pole-Zero-Cancellation (Magnitude Optimum).....	117
8.2	Symmetrical Optimum.....	125

## References

- R. Isermann  
Mechatronische Systeme  
Springer, 1999
- J. Pyrhönen, T. Jokinen and V. Hrabovcová  
Design of Rotating Electrical Machines  
Wiley & Sons, 2008
- D. Schröder  
Elektrische Antriebe – Grundlagen  
Springer Verlag, 2. Aufl., 2000
- Gerhard Müller, Bernd Ponick  
Grundlagen elektrischer Maschinen  
Wiley-VHC, 9. Auflage, 2006
- Gerhard Müller, Bernd Ponick  
Theorie elektrischer Maschinen  
Wiley-VHC, 4. Auflage
- H. Goldstein  
Klassische Mechanik  
Akademische Verlagsgesellschaft, 1981
- D. Hanselman  
Brushless Permanent Magnet Motor Design  
The Writer's Collective, 2003
- T. J. E. Miller  
Brushless Permanent-Magnet and Reluctance Motor Drives  
Oxford Science Publications, 1989
- D. Schröder  
Elektrische Antriebe – Grundlagen  
Springer Verlag, 2. Aufl., 2000
- Hans-Dieter Stölting, Eberhard Kallenbach  
Handbuch Elektrische Kleinantriebe  
Hanser Verlag, 3. Auflage, 2006
- R. Krishnan  
Electric Motor Drives  
Prentice Hall, 2001
- D. K. Miu  
Mechatronics – Electromechanics and Contromechanics  
Springer-Verlag, 1993
- G. Schweitzer, A. Traxler, H. Bleuler  
Magnetlager  
Springer-Verlag, 1993
- G. Schweitzer, E. H. Maslen (eds.)  
Magnetic Bearings  
Springer-Verlag 2009

H. Lutz, W. Wendt  
Taschenbuch der Regelungstechnik  
Verlag Harri Deutsch, 7. Auflage, 2007

W. Bolton  
Bausteine mechatronischer Systeme  
Pearson, 3. Auflage 2003  
Entwicklungsmethodik für mechatronische Systeme  
VDI-Richtlinie VDI 2206 (Entwurf), März 2003

## Greek Letters

Majuscule	Minuscule	Name
A <sup>1</sup>	α	Alpha
B <sup>1</sup>	β	Beta
Γ	γ	Gamma
Δ	δ	Delta
E <sup>1</sup>	ε	Epsilon
Z <sup>1</sup>	ζ	Zeta
H <sup>1</sup>	η	Eta
Θ	θ, ϑ <sup>2</sup>	Theta
I <sup>1</sup>	ι	Iota
K <sup>1</sup>	κ	Kappa
Λ	λ	Lambda
M <sup>1</sup>	μ	Mu
N <sup>1</sup>	ν	Nu
Ξ	ξ	Xi
O <sup>1</sup>	ο <sup>1</sup>	Omicron
Π	π	Pi
P <sup>1</sup>	ρ	Rho
Σ	σ, ς <sup>1</sup>	Sigma
T <sup>1</sup>	τ	Tau
Υ <sup>1</sup>	υ	Upsilon
Φ	φ, ϕ <sup>2</sup>	Phi
X <sup>1</sup>	χ	Chi
Ψ	ψ	Psi
Ω	ω	Omega

<sup>1</sup> Since these letters are equal to Latin letters, they are not used as mathematical symbols. The end-sigma is also not used.

<sup>2</sup> The typographic shape of these letters may vary depending on the fonts.

# 1 Mechatronic Systems

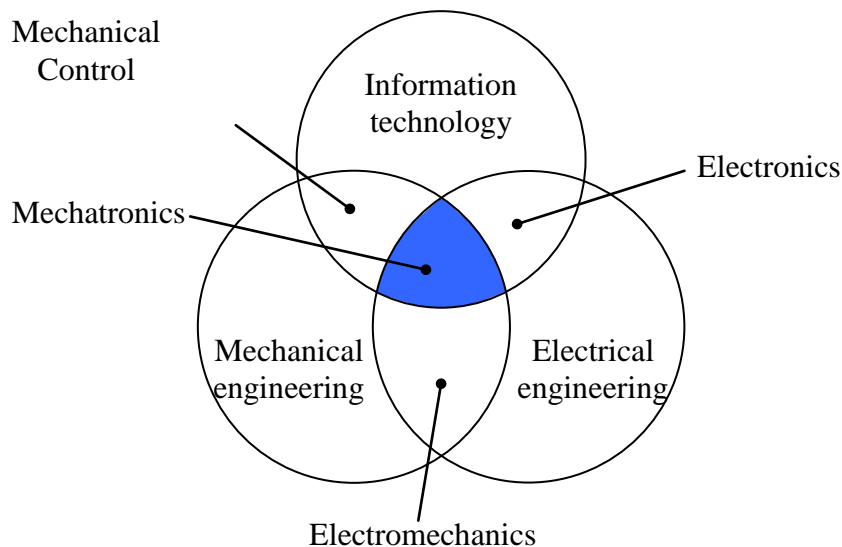


**Fig. 1-1:** Mechatronics as integration of mechanical and electrical engineering and information technology <sup>1</sup>

A system comprising electrical, mechanical and information processing components or subsystems is not necessarily of mechatronic nature. Important characteristics of a mechatronic system is the *integration*:

- A function is being established only by the *interaction* of the components of the three different areas.

*Example: Active cancellation of oscillations* of mechanic structures (satellite with large structure of photovoltaic panels) by means of closed-loop control and electromechanic actuators. The components (actuator, control system, sensors, mechanical structure) may be spatially separated. The intended function, however, is realized only by the interaction of all participating components.

and/or

<sup>1</sup> Though the first calculators and even the first universally programmable computer built by the German engineer *Zuse* were mechanical machines, digital mechanical information processing does not play any role today. However, there are construction elements in mechanical systems which can be seen to some extent as (analogue) mechanical information processing as, e.g., main shafts, cam disks, toothed belts and pitches, levers, cranks in order to transmit information of positions.

- Highly spatial or constructive integration

*Example: Movable read/write head of a hard disk drive.* Information processing components, actuator and mechanical parts are highly spatially integrated.

- Production integrations: The mechatronic system is no longer assembled with prefabricated electrical, mechanical and information processing components, but being produced in an integrated production process.

Further characteristics of mechatronic systems are the entangled *flows of power and information*.

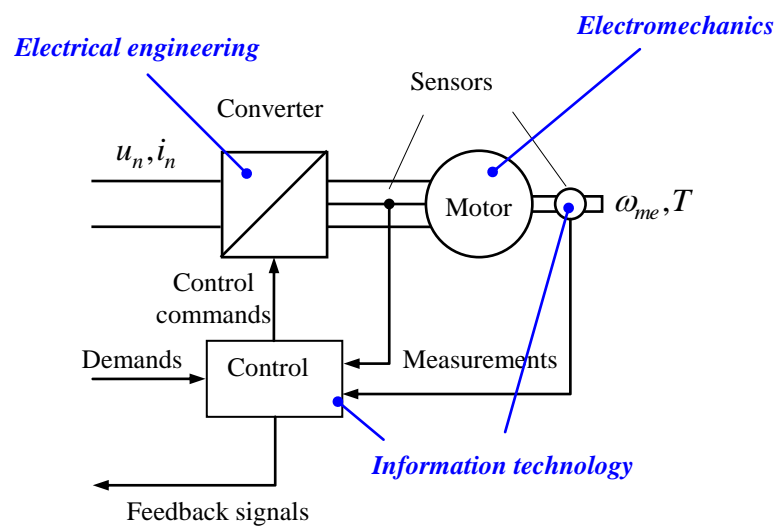


**Fig. 1-2:** Basic structure of an electric drive, the drive as mechatronic system

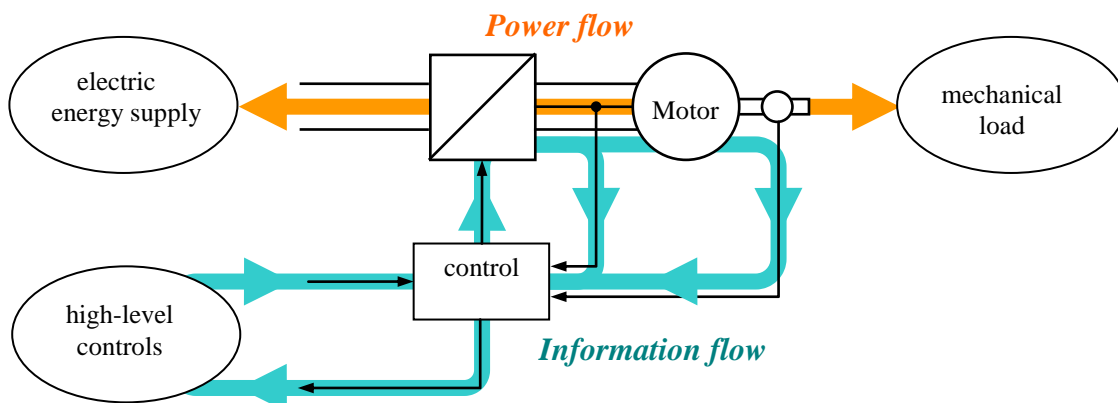


**Fig. 1-3:** Power and information flows

## 2 Magnetic Circuits

### 2.1 Magnetic Reluctance

Let us assume piecewise homogenous fields (magnetic field strength  $h_k$  and magnetic flux density  $b_k$ ) within geometric elements of length  $l_k$  and of cross section  $A_k$ . Magnetic voltage (magnetomotive force, MMF):

$$\theta_k = l_k h_k \quad (2.1)$$

Magnetic flux:

$$\phi_k = A_k b_k \quad (2.2)$$

With linear passive material it holds:

$$b_k = \mu_0 \mu_{rk} h_k \quad (2.3)$$

With that, the *magnetic reluctance* is defined as

$$R_k = \frac{\theta_k}{\phi_k} = \frac{l_k}{\mu_0 \mu_{rk} A_k} \quad (2.4)$$

as well as the *magnetic conductivity*

$$\Lambda_k = \frac{1}{R_k} = \frac{\mu_0 \mu_{rk} A_k}{l_k} \quad (2.5)$$

From the Maxwell's equations it follows for a single closed magnetic circuit

$$\sum_k \theta_k = \theta_0 = Ni \quad (2.6)$$

$$\phi_k = \phi = \text{const.} \quad (2.7)$$

The calculation of flux and magnetic voltage in a magnetic network is done by means of Kirchhoff's laws:

$$\phi = \frac{\theta_0}{R_\Sigma} = \frac{\theta_0}{\sum_k R_k} \quad (2.8)$$

With the multiple-linked magnetic flux (*flux linkage*)

$$\psi = N\phi \quad (2.9)$$

we can write:

$$\psi = \frac{N^2}{R_\Sigma} i = Li \quad (2.10)$$

where the inductance is

$$L = \frac{N^2}{R_\Sigma} \quad (2.11)$$

Measurement units of the considered quantities:

Quantity	Symbol	Unit
Electric Voltage	$u$	1V
Magnetic flux density	$b$	1T = 1Vs/m <sup>2</sup>
Magnetic flux	$\phi$	1Vs
Magnetic flux linkage	$\psi$	1Vs
Electric current	$i$	1A
Magnetic field strength	$h$	1A/m
Magnetic voltage, MMF <sup>2</sup>	$\theta$	1A
Inductance	$L$	1H = 1Vs/A
Magnetic conductance	$\Lambda$	1H = 1Vs/A
Reluctance	$R$	1A/Vs

## 2.2 Energy and Power

The *internal magnetic energy* of one element consisting of linear material with homogenous fields can be written in various representations:

---

<sup>2</sup> In literature, one finds the unit “Ampere-turns“, which is, though often repeated, wrong. Even if the magnetomotive force (MMF) is built up by several turns, the unit of the MMF is still only Ampere, because the number of turns is a pure number without physical dimension and unit. If that strange wording would be consequently applied also to the EMF, one must speak of its unit as “Volt-turns” because the EMF is also usually generated by several turns. That makes clear that “Ampere-turns” is nonsense.

$$\begin{aligned}
 E_{ki} &= \frac{1}{2} b_k h_k A_k l_k = \frac{1}{2 \mu_0 \mu_{rk}} b_k^2 A_k l_k = \frac{1}{2} \mu_0 \mu_{rk} h_k^2 A_k l_k \\
 &= \frac{1}{2} \phi_k \theta_k = \frac{1}{2} R_k \phi_k^2 = \frac{1}{2 R_k} \theta_k^2
 \end{aligned} \tag{2.12}$$

If the material is nonlinear, but still reversible (i.e. with an unambiguous characteristic curve without hysteresis), the internal energy can be calculated by means of integration along the nonlinear magnetization curve:

$$E_{ik} = A_k l_k \int_0^b h(\tilde{b}) d\tilde{b} \tag{2.13}$$

With materials that show a hysteresis, the differential

$$dW = A_k l_k h(b) db \tag{2.14}$$

is still the work supplied to the material, however, a part of which is being lost (irreversible losses, area of the hysteresis loop) and will not contribute the magnetic energy. It has to be accounted as inner losses. Thus, the differential  $dW$  is not a total differential and cannot be integrated to a functional of an internal energy.

The total energy is summed up through all components

$$E_i = \sum_k E_{ik} = \frac{1}{2} \sum_k \phi_k \theta_k = \frac{1}{2} \phi \theta_0 = \frac{1}{2} \psi i = \frac{1}{2} L i^2 = \frac{1}{2L} \psi^2 \tag{2.15}$$

With nonlinear materials it follows

$$E_i = \sum_k E_{ik} = \int_0^\phi \theta_0(\tilde{\phi}) d\tilde{\phi} = \int_0^\psi I(\tilde{\psi}) d\tilde{\psi} \tag{2.16}$$

### Magnetic systems with one kinematic degree of freedom

Let us assume that the reluctance  $R_\Sigma$  depends on a geometric parameter, e.g. of a varying displacement  $x$ :

$$R_\Sigma = R_\Sigma(x) \tag{2.17}$$

That could be, e.g., a varying air gap  $x = d$  or later with the reluctance motor the rotation angle  $x = \varepsilon$ . With that, the internal energy will be a function not only of the current, but also of that new variable

$$E_i = E_i(i, x) \tag{2.18}$$

or equivalently

$$E_i = E_i(\psi, x) \quad (2.19)$$

Let us consider the power balance

$$\dot{E}_i = p_e - p_d \quad (2.20)$$

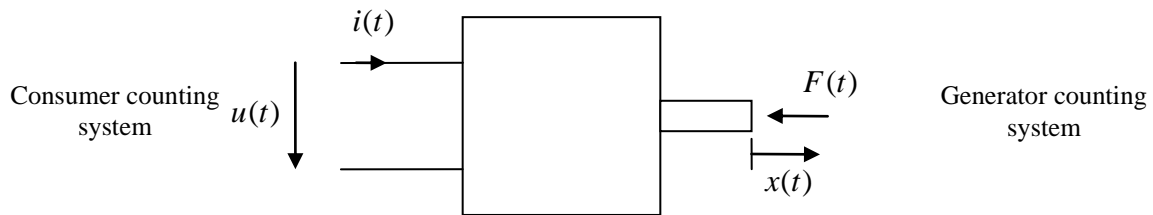


**Fig. 2-1:** a general electrically and mechanically cut-free electromechanic two-port

Supplied external power:

$$p_e = p_{el} - p_{me} = ui - vF \quad (2.21)$$

with

$$v = \dot{x}. \quad (2.22)$$

The signs are subject to arbitrary definition of the counting direction. For the electrical port the consumer counting system is chosen, for the mechanical port, the generator counting system.

The internal dissipated power is:

$$p_d = Ri^2 \quad (2.23)$$

$$p = p_e - p_d = ui - vF - Ri^2 = u_i i - vF \quad (2.24)$$

with the internal or induced voltage

$$u_i = u - Ri. \quad (2.25)$$

Let us calculate the total differential of the internal energy. First, a set of generalized coordinates have to be chosen. In principle, all possible coordinate sets are equivalent. Advantageously these coordinates should be chosen which appear already as time derivatives in the power term. These are  $x$  and  $\psi$  :

$$\dot{E}_i(\psi, x) = \dot{\psi} \frac{\partial E_i}{\partial \psi} + \dot{x} \frac{\partial E_i}{\partial x} \quad (2.26)$$

Faraday's induction law:

$$u_i = \dot{\psi} \quad (2.27)$$

Kinematics:

$$v = \dot{x} \quad (2.28)$$

Comparison with the power term yields:

$$i = \left. \frac{\partial E_i}{\partial \psi} \right|_{x=\text{const.}} \quad \text{and} \quad F = - \left. \frac{\partial E_i}{\partial x} \right|_{\psi=\text{const.}}$$

Thus, the resulting force at constant flux has been determined. Furthermore:

$$\dot{E}_i(\psi, x) = \psi \dot{i} - \dot{x} F \quad (2.29)$$

or as total differential

$$dE_i(\psi, x) = i d\psi - F dx \quad (2.30)$$

The force with respect to constant current can be determined from the so-called *co-* or *complementary energy*, which is introduced by a *Legendre transform* from the internal energy:

$$E_c(i, x) = \psi i - E_i(\psi, x) \quad (2.31)$$

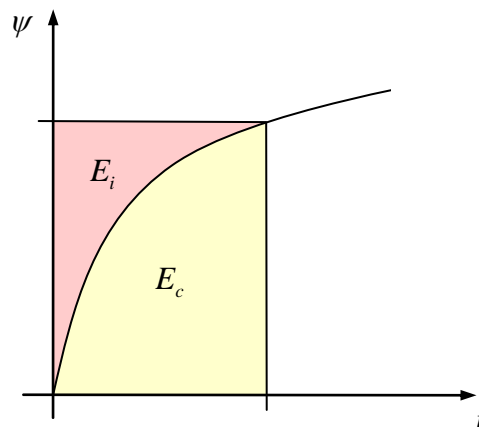


**Fig. 2-2:** Internal energy and co-energy

The time derivative of the co-energy is developed as follows:

$$\dot{E}_c(i, x) = \frac{d}{dt}(\psi i) - \dot{E}_i(\psi, x) = \psi \dot{i} + \dot{\psi} i - u_i i + v F = \dot{i} \psi + \dot{x} F \quad (2.32)$$

or, again as total differential:

$$dE_c = \psi di + F dx \quad (2.33)$$

From the mathematical viewpoint, the Legendre transform exchanges the chosen generalized coordinates, i.e. the independent variables of the energy functional. As both energies can be interpreted as geometreic areas under or left of the magnetization curve,  $\psi = \psi(i)$ , the energy and the co-energy complement each other to a rectangular  $\psi i$ . From a technical viewpoint, the term  $\psi i$  within the Legendre transform is the supplied electrical work through a mechanical movement while the electrical current is kept constant. So this ancillary condition is considered implicitly by the co-energy.

From the above power balance we can identify:

$$F = \left. \frac{\partial E_c}{\partial x} \right|_{i=\text{const.}} \quad \text{and} \quad \psi = \left. \frac{\partial E_c}{\partial i} \right|_{x=\text{const.}} \quad (2.34)$$

With linear materials, internal energy and co-energy are of the same values. However, in case of a nonlinear behavior, the derivative  $\partial E_i / \partial x|_{i=\text{const.}}$  will generally yield the wrong result for the force!

Interpretation of the energy balance and of the energy differential

$$dE_i(\psi, x) = i d\psi - F dx = dW_{el} - dW_{me} \quad (2.35)$$

Unlike the *total* differential  $dE_i$ , the differential of the right-hand side

$$dW_{el} = i d\psi = i u_i dt \quad (2.36)$$

$$dW_{me} = F dx = F v dt \quad (2.37)$$

are not *total* or *complete*. They are differentials of the electrical or mechanical *work* (not *energy* because they are not total or not complete). To represent this difference in the symbol, sometimes a struck-through  $d$  is used:  $\bar{d}W_{el}$ ,  $\bar{d}W_{me}$ .

The differential of the mechanic work can immediately be expressed by the change of the co-energy:

$$dW_{me} = F dx = dx \left. \frac{\partial E_c}{\partial x} \right|_{i=\text{const.}} = dE_c|_{i=\text{const.}} \quad (2.38)$$

These differentials can be graphically represented by a bundle of characteristic curves  $\psi = \psi(i, x)$ .

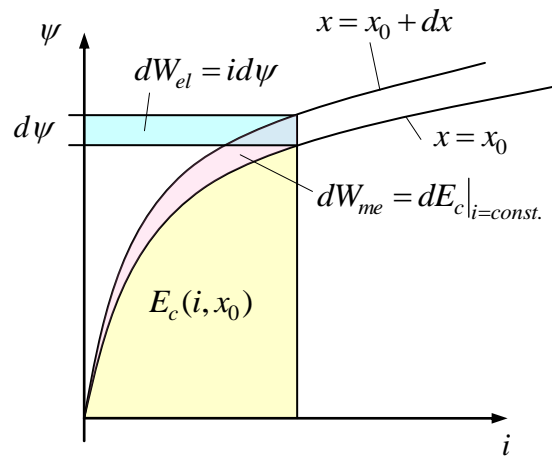


**Fig. 2-3:** Interpretation of work differentials

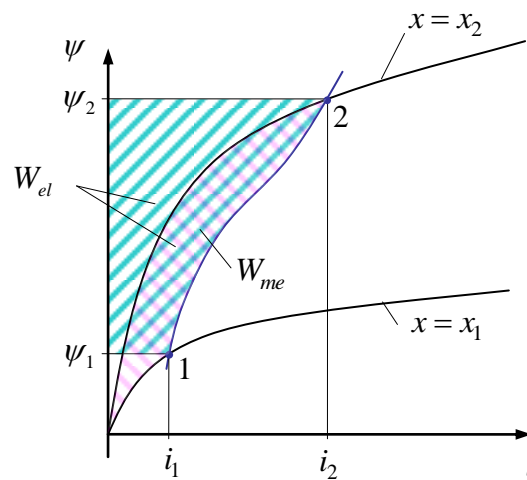


**Fig. 2-4:** Mechanic and electric works of the transition between two states

**The 2nd derivatives of the energy**

The energy functionals should be assumed to be two times continuously differentiable — which is usually the case with common technical system. Then, the sequence of derivations can be exchanged. Thus, the mixed 2nd-order derivatives of the energy

$$\frac{\partial^2 E_i}{\partial x \partial \psi} = \frac{\partial^2 E_i}{\partial \psi \partial x} \tag{2.39}$$

yield the reciprocal the *reciprocity law*

$$\frac{\partial i(\psi, x)}{\partial x} = - \frac{\partial F(\psi, x)}{\partial \psi} \quad (2.40)$$

Similarly, from the mixed derivatives of the co-energy

$$\frac{\partial^2 E_c}{\partial x \partial i} = \frac{\partial^2 E_c}{\partial i \partial x} \quad (2.41)$$

follows the reciprocity law

$$\frac{\partial \psi(i, x)}{\partial x} = \frac{\partial F(i, x)}{\partial i} \quad (2.42)$$

The (differential) magnetic *stiffness* is the derivative of the magnetic force with respect to the displacement. Due to the chosen generator counting system of the mechanical port, the stiffness is being introduced as negative derivative. This definition corresponds to the common definition of the stiffness of a conventional spring as a positive quantity.

With constant current, the magnetic stiffness results as

$$S_i = - \left. \frac{\partial F}{\partial x} \right|_{i=\text{const.}} = - \left. \frac{\partial^2 E_c}{\partial x^2} \right|_{i=\text{const.}} \quad (2.43)$$

However, the stiffness with constant magnetic flux is

$$S_\psi = - \left. \frac{\partial F}{\partial x} \right|_{\psi=\text{const.}} = \left. \frac{\partial^2 E_i}{\partial x^2} \right|_{\psi=\text{const.}} \quad (2.44)$$

Both stiffnesses  $S_i$  and  $S_\psi$  will have generally different values.

Accordingly, the differential inductance is being determined from the co-energy by

$$L = \left. \frac{\partial \psi}{\partial i} \right|_{x=\text{const.}} = \left. \frac{\partial^2 E_c}{\partial i^2} \right|_{x=\text{const.}} \quad (2.45)$$

Alternatively, that can be done with the internal energy

$$\frac{1}{L} = \left. \frac{\partial i}{\partial \psi} \right|_{x=\text{const.}} = \left. \frac{\partial^2 E_i}{\partial \psi^2} \right|_{x=\text{const.}} \quad (2.46)$$

## 2.3 Magnetic Materials

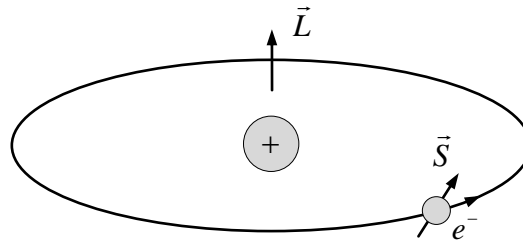


**Fig. 2-5:** Naïve Bohr's atomic model in order to explain the angular momentum and the magnetic momentum

The physical reason of magnetization of matter is the magnetic momentum of atoms, molecules, or crystal lattices. From the viewpoint of the naïve Bohr's atomic model, the electrons generate the magnetic momentum from their orbital angular momentum  $\vec{L}$ . However, that is completed by the intrinsic angular momentum  $\vec{S}$  of the electron, called *spin*, which cannot be explained by Bohr's orbital movement. According to the laws of quantum mechanics, the magnitude of the total angular momentum  $\vec{J} = \vec{L} + \vec{S}$  can only be a multiple of the *Planck's quantum of action*  $h = 6.626 \cdot 10^{-34}$  Js,

$$J = M_j \frac{h}{2\pi} \quad (2.47)$$

where  $M_j$  is an integer or half-integer (0, 1/2, 1, 3/2, usw.). The angular momentum is joined with a magnetic momentum which is

$$M = \frac{e}{m_e} J = M_j \frac{eh}{2\pi m_e} \quad (2.48)$$

Here,  $e = 1.602 \cdot 10^{-19}$  As is the elementary charge and  $m_e = 9.109 \cdot 10^{-31}$  kg is the mass of an electron.

To some extent, also the spins of the atomic nuclei will contribute to the total magnetic momentum of an atom. That effect is being exploited by magnetic resonance imaging (MRI). The common magnetic behavior of matter, however, is determined mainly by the atom's electron shell only. Depending on the type of participating atoms or crystal lattices, the magnetic momenta of neighbouring atoms are interacting so that they may align in parallel or anti-parallel to each other or to an external field. The different types of magnetism are distinguished as follows:

*Diamagnetism:* Even if the magnetic momentum of atoms in the basic state is zero, an external field will excite magnetic dipoles by quantum mechanical interference. The direction of the dipoles is opposite to that of the external field which is then attenuated. From a macroscopic view, it results  $\mu_r < 1$ . Examples: Water, carbon, copper, bismuth.

*Paramagnetism:* Atoms and molecules with a non-zero magnetic momentum will align in parallel to an external field so that the field is enhanced:  $\mu_r > 1$ . Alkali metals and rare earths show such paramagnetic behavior.

*Ferromagnetism:* The magnetic momenta of the atoms in a lattice are parallelly aligned within the *Weiß's domains* already without any external field. The direction of magnetization of neighbouring Weiß's domains will vary more or less randomly so that, in total, the overall magnetization is cancelled out. With an external field, however, the borders of the Weiß' domains, called *Bloch-walls*, will move. Domains with a magnetization in parallel to the external field will grow rapidly, while others are getting smaller. With further increasing external field, a Weiß's domain may also abruptly change the direction of its magnetization (*Barkhausen jump*). Unlike paramagnetism, the material reacts extremely strongly to external fields which results in  $\mu_r \gg 1$ . Another effect in ferromagnetic materials is the *residual magnetism (remanence)*, i.e. a magnetization is retained even after the external field is switched off. Best known representatives of ferromagnetic materials are iron, cobalt, and nickel.

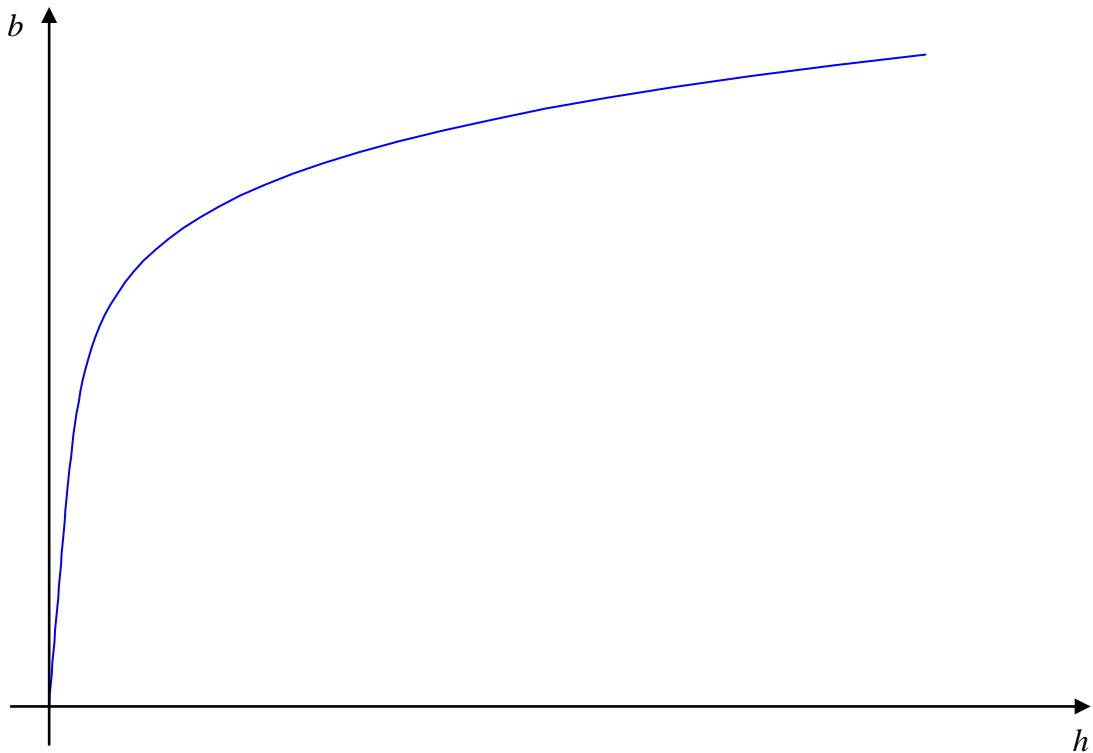
*Ferrimagnetism:* Within *ferrites*, the magnetizations of neighbored atoms are aligned anti-parallel so that the magnetisms is partly compensated.

Table of some magnetic materials

Material	$\mu_r$	$\frac{\hat{b}_{\max}}{\text{T}}$	$\frac{f_{\max}}{\text{kHz}}$
Ferrites ( <i>NiZn, MnZn</i> )	10-2000	0,1-0,5	10-100000
Dynamo sheets ( <i>Fe</i> )	1000-10000	1-1,5	0,5-20
Permalloy, Mumetall ( <i>FeNi</i> )	10000-50000	1	0,1-100
<i>Fe</i> powder cores	10-100	0,5-1,9	1000-350000
<i>FeNi</i> powder cores	20-300	1-1,5	100-2000
<i>FeSiAl</i> powder cores	25-120	1	200-10000

The maximal flux density  $\hat{b}_{\max}$  specified in the table is not a hard limit that could not be exceeded. It is only a specification of usual technical rating. However, above the maximal flux density and above the recommended frequency range the losses are expected to increase rapidly.

The characterization of ferromagnetic materials only by their permeability  $\mu_r$  is problematic, because that would give the impression of a linear relationship between field strength and flux density which may be approximately valid only for small values of the field strength. With increasing excitation, the material is getting more and more saturated. Thus, it is recommended to describe the material's behavior better with the magnetization characteristic curve rather than by a simple permeability number.



**Fig. 2-6:** Magnetization characteristics with saturation

A graphical consideration may be appropriate for nonlinear magnetic circuits with ferromagnetic materials. Let the magnetic circuit consists of a magnetomotive (MMF) source  $\theta_0 = Ni$ , an airgap reluctance  $R_L$ , and an ferromagnetic element. The result for flux and MMF can easily be determined by graphical intersection of the linear characteristic of the source with linear airgap and the nonlinear magnetization characteristic. If the material characteristic is given as  $b$  vs.  $h$ , simply rescaling would transform it to a curve of flux  $\phi$  vs. MMF  $\theta$ . Alternatively,  $\theta_0$  und  $R_L$  can be transferred to  $b$ - $h$ -*diagram*.

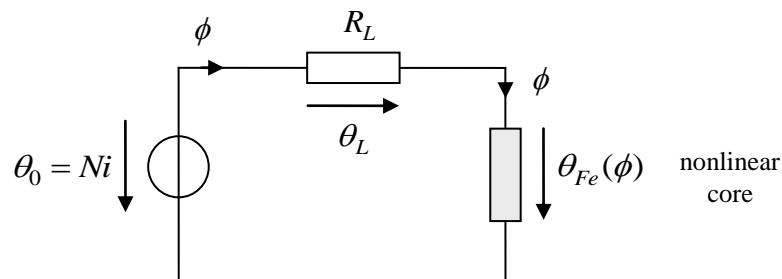


**Fig. 2-7:** Nonlinear magnetic circuit

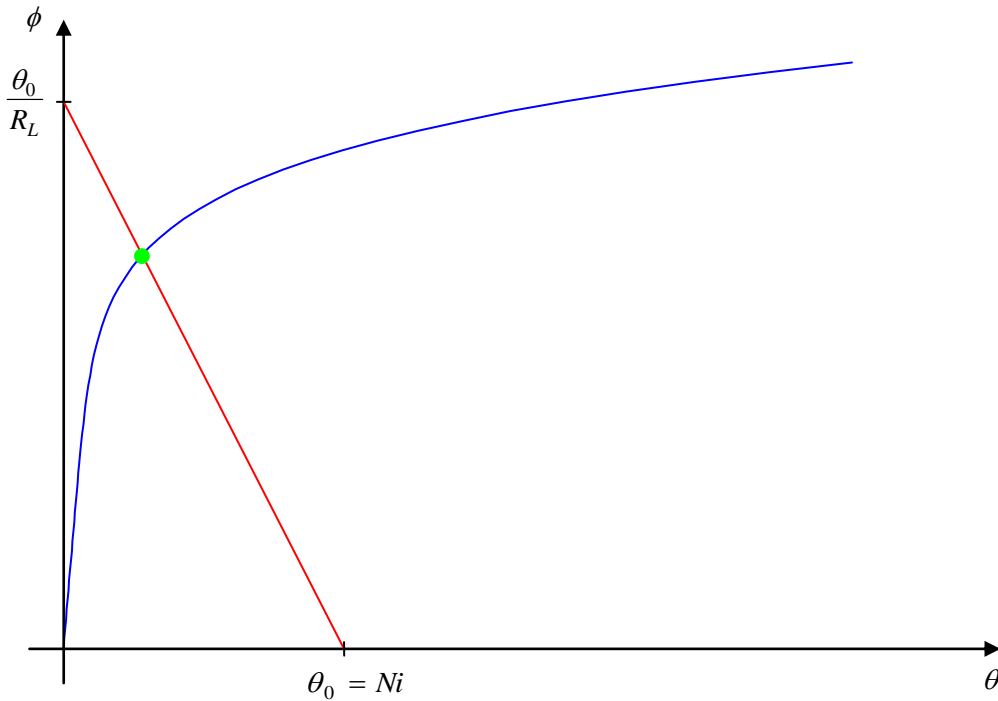


**Fig. 2-8:** Intersection of the characteristic of the magnetic source with a linear internal resistance and the nonlinear characteristic

Alternative way: Consider the total magnetomotive force

$$\theta = \theta_L + \theta_{Fe} = R_L\phi + \theta_{Fe}(\phi) \tag{2.49}$$

as new nonlinear characteristic. This new curve results from the original magnetization curve by shearing with the airgap line:

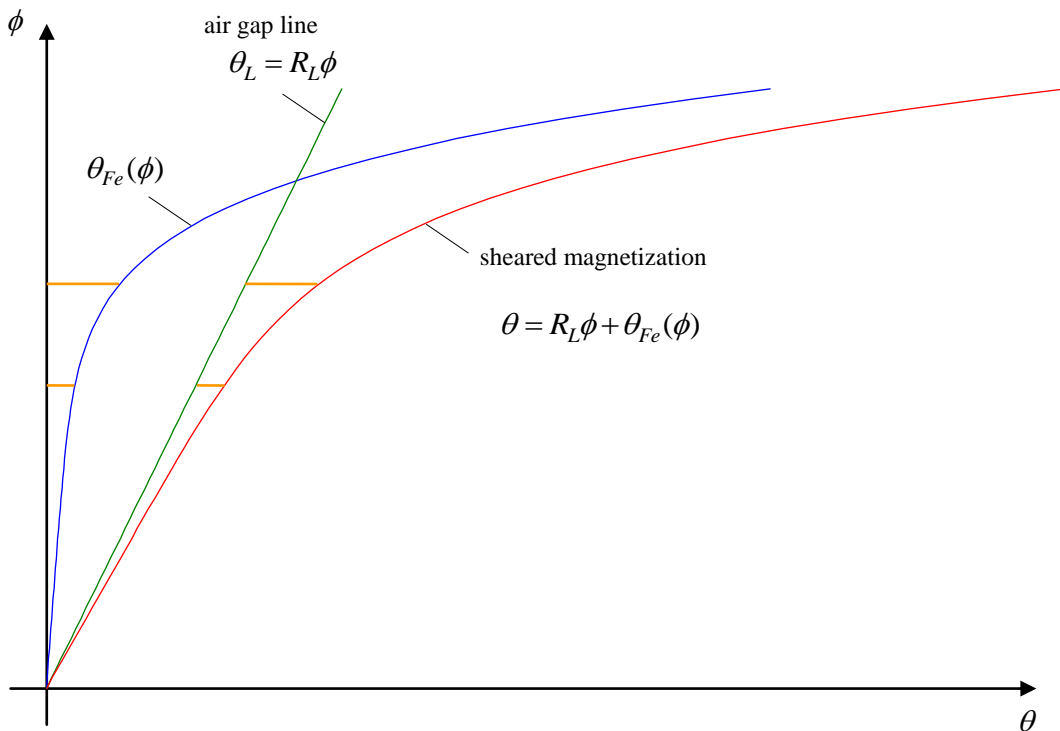


**Fig. 2-9:** Sheared magnetization curve

Besides saturation, a more or less strong hysteresis will be observed. In this case, there is no longer an *unambiguous* magnetization curve, but only a relation between field strength and flux density where the actual values depend on the previous history as well as on the momentary direction of change. Typically, symmetrical cycles are considered.

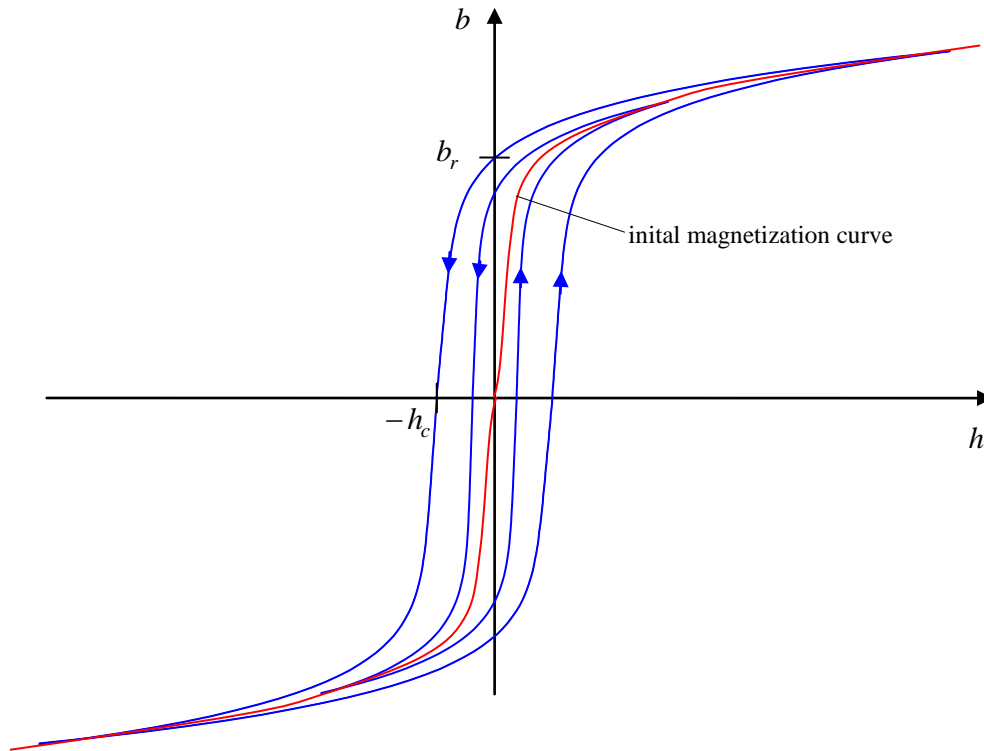


**Fig. 2-10:** Hysteresis

$b_r$ : remanence flux density, i.e. the flux density at zero field strength

$h_c$ : coercive field strength, i.e. the (negative) field strength at zero flux density

The curve connecting the reversal points of the hysteresis when varying the magnitude is called the *commutation curve*. The curve of the first magnetization starting from an unmagnetized condition is called *initial magnetization curve*.

The shape of the hysteresis depends on the previous history and on frequency. Further variations will result, if the cycle is not complete or asymmetrical.

In order to demagnetize such materials, AC fields with slowly decreasing magnitude are applied.

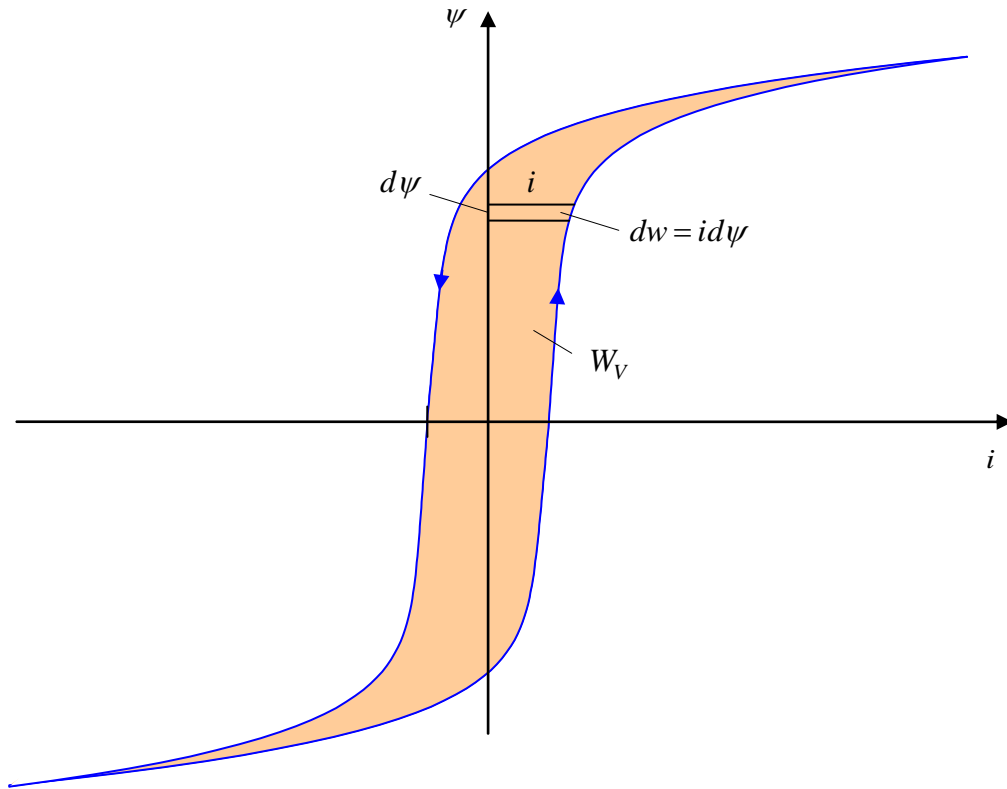


**Fig. 2-11:**

If there is no longer an unambiguous magnetization curve, the areas below or beside the curve can still be interpreted as work supplied to the material, but no longer as internal or co-energy. The work as integral of power is then dependent on the chosen path. The integral along one cycle,

$$W_V = \int dw = \int p(t) dt = \int u(t)i(t) dt = \int \dot{\psi}(t)i(t) dt = \int i(\psi) d\psi = \int \theta(\phi) d\phi \quad (2.50)$$

is the *hysteresis loss*.

If the operation is periodic with  $T$  as period of one cycle, then the loss relative to time can be taken as a mean power dissipation

$$P_V = \frac{W_V}{T} = f W_V \quad (2.51)$$

Thus, as a first-order approximation, the power dissipation is proportional to the frequency,

$$P_V \sim f \quad (2.52)$$

For higher frequencies, however, this relation will not describe the behavior well, because the shape of the hysteresis will also change. Typically, the losses rise more than linearly:

$$P_V \sim f^{e_f} \quad , \quad e_f \approx 1...2 \quad (2.53)$$

An approximative empiric law describing the dependency on the magnitude is

$$P_V \sim \hat{b}^{e_b} \quad ; \quad e_b \approx 2...3 \quad (2.54)$$

Both relations are brought together as the so-called *Steinmetz equation*

$$P_V = K f^{e_f} \hat{b}^{e_b} \quad (2.55)$$

The Steinmetz equation can be used to calculate losses, based on the above coefficients which are given in a datasheet for all other operations points (magnitude of flux density and frequency). Material loss data are usually provided in units of W/kg.

## 2.4 Permanent Magnets

Today's favoured permanent magnet materials are mainly

- Neodymium-iron-boron ( $NdFeB$ )
- Samarium-cobalt ( $SmCo$ ) or
- Ferrites ( $BaFeO$  or  $SrFeO$ )

The first two materials are alloys from rare earths (neodymium  $Nd$  or samarium  $Sm$ ) which are paramagnetic by themselves, and ferromagnetic materials. They are called rare-earth-magnets. Today,  $NdFeB$  is the best performing magnetic material. The prices for raw material of rare earths have performed some capriols in the last years. The largest mineral deposits are located in China.

Permanent magnets from rare earths corrode rather quickly. Therefore, they must be protected by a surface coating. Ferrites are favoured even now due to their reasonable cost unless highest energy density is required.

The production process of high performing magnets is very complex. The powdered magnet material is compressed in the desired form and sintered at a well defined temperature and duration. As a result, the powder particles were cemented, but not melted which retains the fine crystalline structure. After sintering the material is magnetized with the help of a strong electromagnet.

In principle, the behavior of permanent magnets is similar to those of ferromagnetic materials with hysteresis. The shape of the hysteresis, however, is rather different. In general, the relation between flux density  $b$ , magnetic field strength  $h$ , and magnetization<sup>3</sup>  $m$  is

$$b = \mu_0 h + m \quad (2.56)$$

With permanent magnets, the magnetization  $m$  is during common operation nearly completely saturated and constant,

$$m = m_{sat} = const. \quad (2.57)$$

Then, in such operation area, the differential permeability follows as

$$\mu_r = \frac{1}{\mu_0} \frac{db}{dh} = 1 \quad (2.58)$$

i.e., the permanent magnet behaves with respect to its magnetic reluctance like air or vacuum.

---

<sup>3</sup> Please note that in literature the term magnetization is not used uniformly. For the magnetization as used here,  $m = b - \mu_0 h$ , you will find also the symbol  $j$  and the term *magnetic polarization*. As magnetization, the definition  $m = b / \mu_0 - h$  is also common.

Typical values of the saturated magnetization are:

$$m_{sat} \approx \begin{cases} 1,2 - 1,4 \text{ T with } NdFeB \\ 0,9 \text{ T with } SmCo \\ 0,4 \text{ T with ferrites} \end{cases}$$

From this, the remanence flux density results directly as

$$b_r = m_{sat} \tag{2.59}$$

and the coercive field strength as

$$h_c = \frac{m}{\mu_0} \tag{2.60}$$

where this point is assumed to lie within the reversible area.

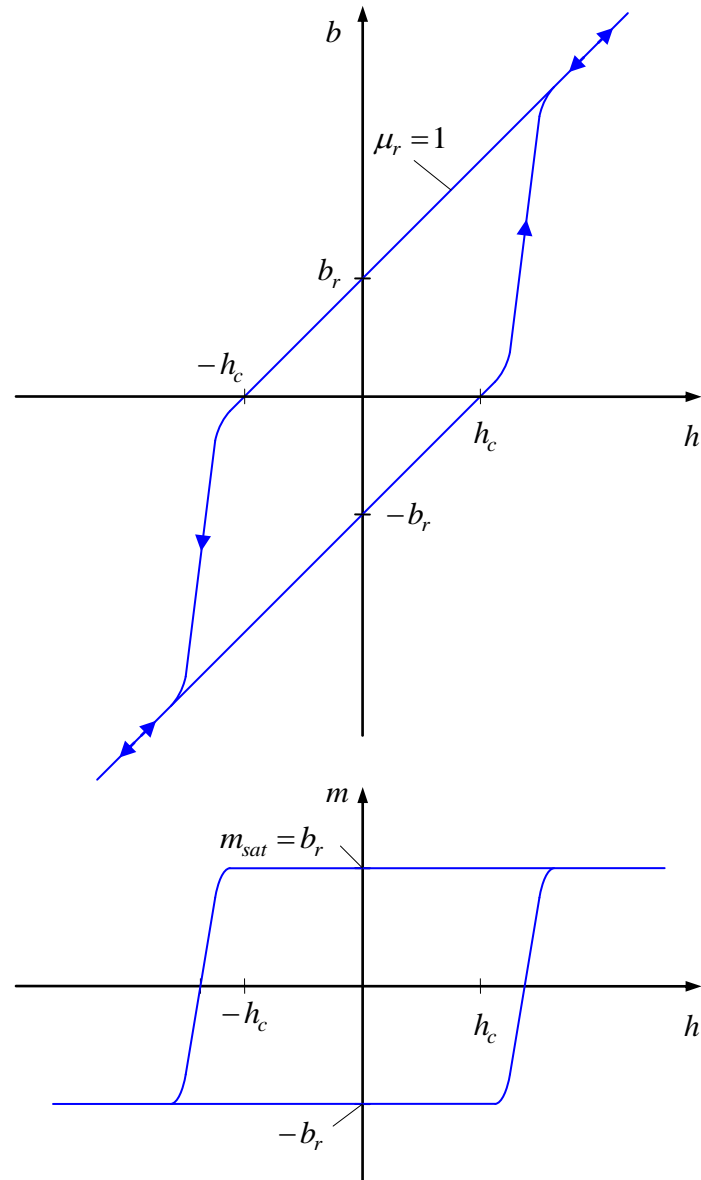


**Fig. 2-12:** Typical magnetization curves of a permanent magnet material

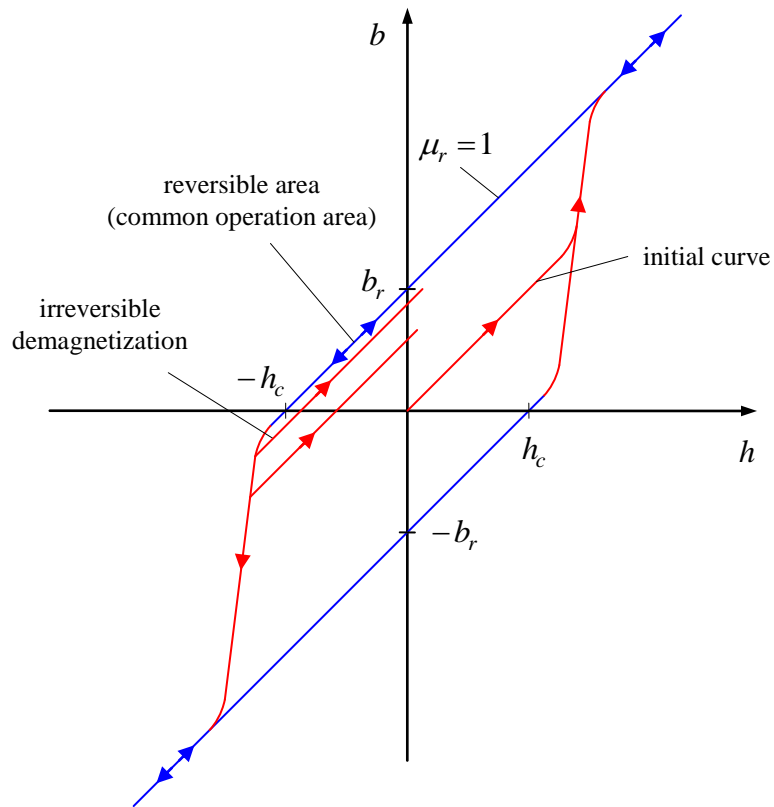
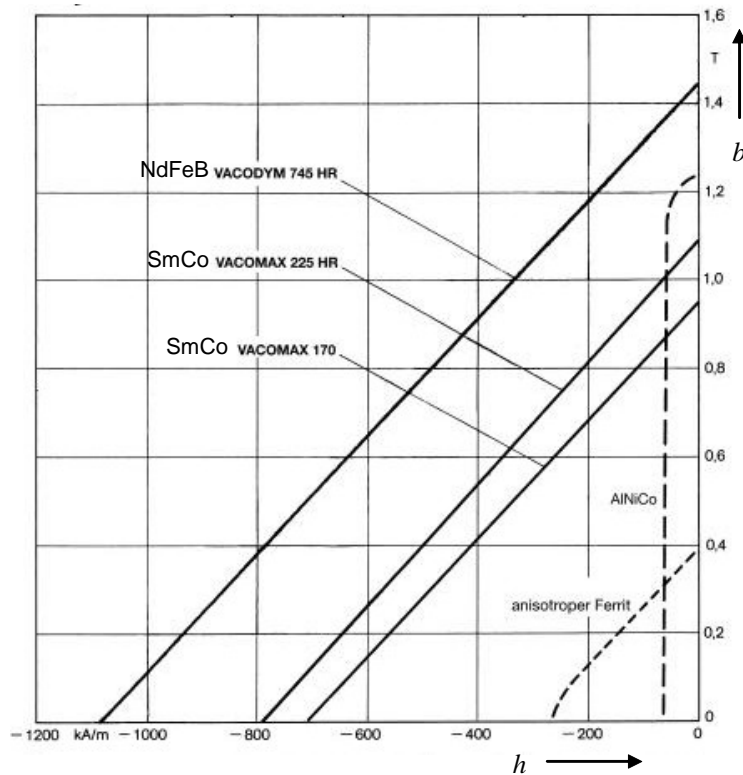
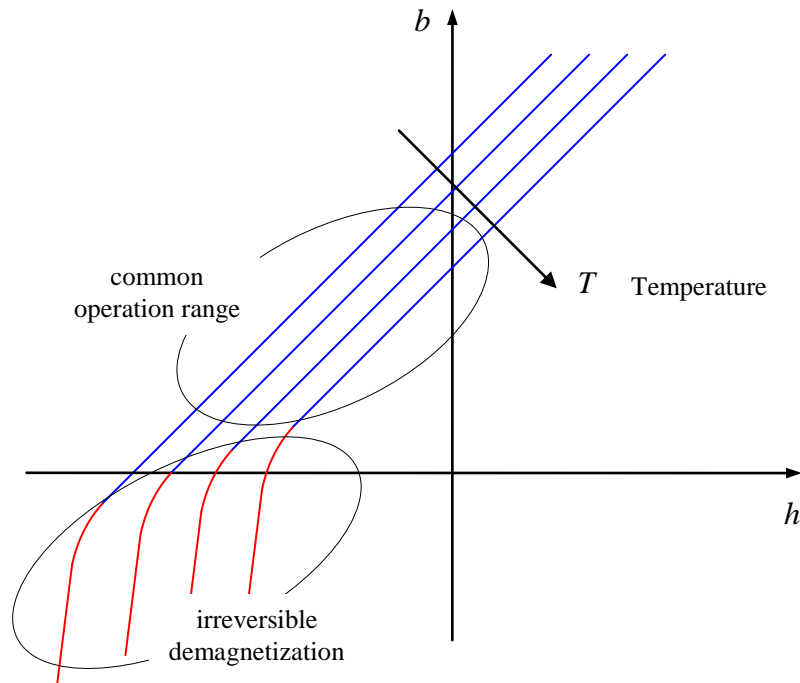


Fig. 2-13: Reversible and irreversible demagnetization



Characteristics of various permanent magnet materials within the reversible operation area (source: Vacuumschmelze)

The magnetization curve depends considerably on the temperature. The magnetization decreases with increasing temperature. If a maximum temperature is not exceeded, the initial magnetization will return after cooling down. With increasing temperature, however, the “knee” of the irreversible magnetization will be shifted towards right and upwards so that the danger of irreversible demagnetization grows.



**Fig. 2-14:** Variation of the magnetization curve vs. temperature

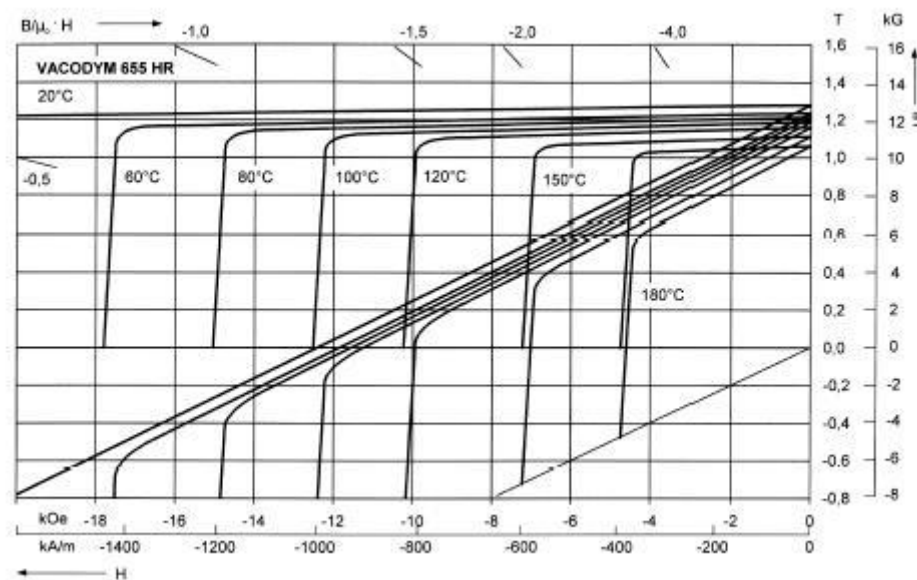


**Fig. 2-15:** Characteristics of flux density and magnetization vs. field strength of NdFeB-material in dependency on the temperature (source: Vacuumschmelze)

Assume homogeneous fields in a straight prismatic element of permanent material of cross section  $A_{PM}$  and length  $l_{PM}$ . Then flux and magnetomotive force are immediately obtained from flux density and field strength via

$$\phi = A_{PM}b \quad , \quad \theta = l_{PM}h$$

Similarly, we can define a remance flux and coercive magnetomotive force as

$$\phi_r = A_{PM}b_r \quad , \quad \theta_c = l_{PM}h_c .$$

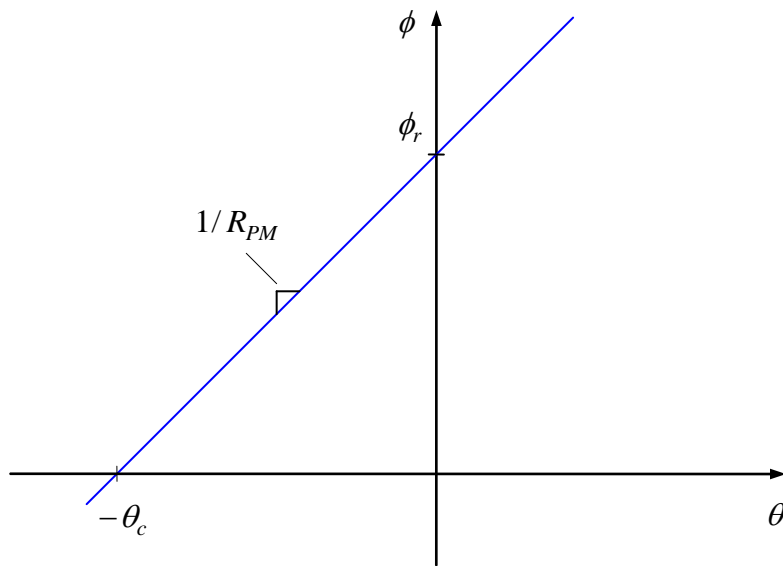


**Fig. 2-16:** Characteristics of the magnetic flux vs. magnetomotive force for a magnetic element

In the reversible operation area, the relation between flux and magnetomotive force can be written as

$$\theta = R_{PM}(\phi - \phi_r) \tag{2.61}$$

or

$$\phi = \frac{\theta + \theta_c}{R_{PM}} \tag{2.62}$$

Here,

$$R_{PM} = \frac{\theta_c}{\phi_r} = \frac{l_{PM}}{\mu_0 A_{PM}} \tag{2.63}$$

is the magnetic reluctance of the magnet. These equations can also be interpreted as equivalent circuit diagrams, either with a flux source and an internal parallel resistance as shown in figure part (a), or with a MMF source with internal resistance in series (b).

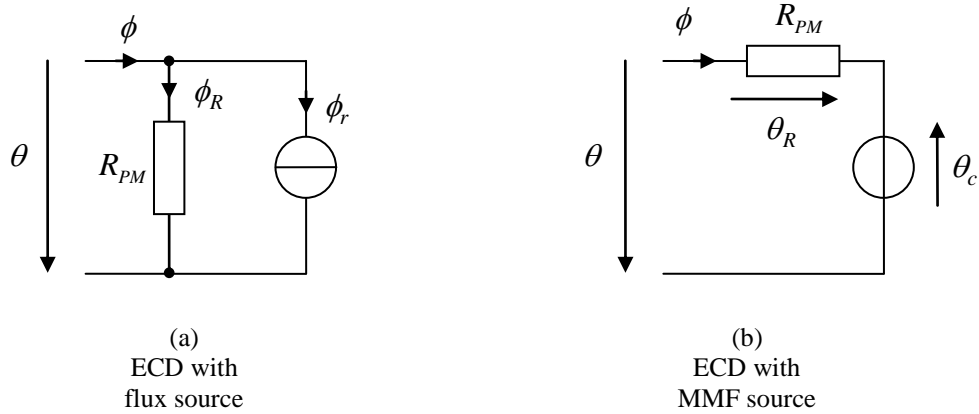


**Fig. 2-17:** Equivalent circuit diagrams of a magnet

**Equivalent models for magnetized materials from a local field consideration**

Consider Maxwell's equations in vector form:

$$\begin{aligned} \nabla \cdot \vec{b} &= 0 & \nabla \cdot \vec{d} &= \rho_e \\ \nabla \times \vec{h} &= \vec{j} + \frac{\partial \vec{d}}{\partial t} & \nabla \times \vec{e} &= -\frac{\partial \vec{b}}{\partial t} \end{aligned}$$

The magnetic material is described by the equation

$$\vec{b} = \mu_0 \vec{h} + \vec{m} \tag{2.64}$$

with magnetization  $\vec{m}$ . Let us write

$$\vec{h} = \frac{\vec{b}}{\mu_0} - \frac{\vec{m}}{\mu_0} = \vec{h}_0 - \frac{\vec{m}}{\mu_0} \tag{2.65}$$

The new introduced quantity  $\vec{h}_0$  can be understood as magnetic field strength that results from a given flux density  $\vec{b}$  if vacuum is assumed instead of magnetized material. Let us insert this representation into Oersted's law:

$$\nabla \times \vec{h} = \nabla \times \vec{h}_0 - \nabla \times \frac{\vec{m}}{\mu_0} = \vec{j} + \frac{\partial \vec{d}}{\partial t} \tag{2.66}$$

With

$$\vec{j}_m = \nabla \times \frac{\vec{m}}{\mu_0} \quad (2.67)$$

it follows

$$\nabla \times \vec{h}_0 = \vec{j} + \vec{j}_m + \frac{\partial \vec{d}}{\partial t} \quad (2.68)$$

This representation can be understood in such a way that the original magnetized material is being substituted by vacuum and an additional electrical current of density  $\vec{j}_m$  that is calculated from the curls of the original magnetization. That is rather demonstrative: If homogeneously magnetized material is considered,  $\vec{m} = \text{const.}$ , then  $\vec{j}_m$  is equal zero within the material as well as outside. On the surface, however, there is a step-like change between constant and zero magnetization. Thus, via differentiation, we will get an equivalent surface current density of  $m/\mu_0$ . The direction of this current density is orthogonal to the surface normal and also orthogonal to the original magnetization. To verify that this equivalent current is really a physically correct electrical current, the divergence must be zero as it is acknowledged by

$$\nabla \cdot \vec{j}_m = -\nabla \cdot \nabla \times \frac{\vec{m}}{\mu_0} = 0 \quad (2.69)$$

So, the current will circulate within the surface and is called *surface current*. The value of this surface current is the same as the coercive field strength and can be directly obtained from the material characteristics. With rare earth materials it is in the range of

$$\frac{m}{\mu_0} = h_c \approx 1000 \text{ kA/m} = 1000 \text{ A/mm} \quad (2.70)$$

In reality, a surface current can be realized with an electric coil only approximatively, because a coil would require non-zero thickness for its wires. Assuming a technical current density in copper of  $10 \text{ A/mm}^2$  (that requires already a good cooling), a thickness of the coil of 100 mm would result in order to allow the above mentioned current. The filling factor is even not considered in that calculation. This comparison shows the enormous strength of modern magnet materials. In practice, it is nearly impossible to replace magnets of size of some millimeters by realistic electric coils.

Instead of substitution by equivalent currents it is possible to derive an alternative equivalent representation. Let us write the material relation as

$$\vec{b} = \mu_0 \vec{h} + \vec{m} = \vec{b}_0 + \vec{m} \quad (2.71)$$

Here,  $\vec{b}_0$  is the flux density that would result from a field strength  $\vec{h}$  in vacuum. This equation is inserted into the equation of vanishing magnetic sources:

$$0 = \nabla \cdot \vec{b} = \nabla \cdot \vec{b}_0 + \nabla \cdot \vec{m} \tag{2.72}$$

or

$$\nabla \cdot \vec{b}_0 = \rho_m, \tag{2.73}$$

where

$$\rho_m = -\nabla \cdot \vec{m} \tag{2.74}$$

can be seen as an equivalent magnetic charge density. With a material with constant magnetization,  $\nabla \cdot \vec{m} = 0$  holds within the material. So, equivalent magnetic sources will result only on the surface of the material. The magnitude of the charge density results directly from the original magnetization  $\vec{m}$ . Since the equivalent flux density field  $\vec{b}_0$  is no longer free of magnetic sources, the lines of the stationary field are no longer closed as it is common with the original magnetic field, but starting from a positive magnetic charge and ending in a negative charge. This equivalent model has no technical or physical relevance<sup>4</sup>. However, that method could be beneficial for the purpose of numerical field computation. The fields introduced by this equivalent model

$$\vec{h}_0 = \vec{h} - \frac{\vec{m}}{\mu_0} = \frac{\vec{b}}{\mu_0} \quad \text{and} \quad \vec{b}_0 = \vec{b} - \vec{m} = \mu_0 \vec{h}$$

differ from the original fields  $\vec{h}$  and  $\vec{b}$ , respectively, only within the magnetized material. Outside they equal the original fields, since  $\vec{m} = 0$  holds outside of the material.

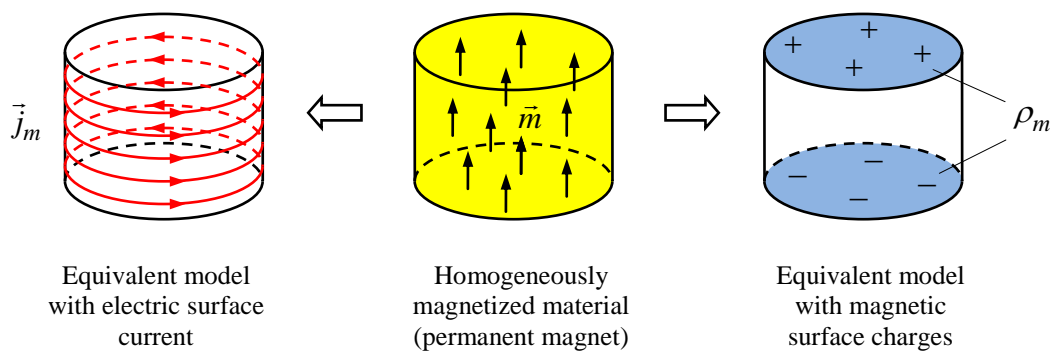


**Fig. 2-18:** Equivalent models for magnetized material

<sup>4</sup> Some theorists consider magnetic single charges possibly existent. So far, such particles have not been detected.

## Energy

With a hysteresis, the areas given by the magnetization curve can be seen as work to or from the system, however, these areas have no longer the meaning of an energy which is the path-independent integral of power. With a complete cycle of the hysteresis, the total work is dissipated as magnetic loss. However, if the consideration is restricted to the reversible part of the magnet, the magnetization curve is unambiguous and an energy can be defined. The reference point, a zero level or integration constant, can be chosen arbitrarily. The internal energy is then

$$E_i = \frac{1}{2}(\phi - \phi_r)\theta = \frac{R_{PM}}{2}(\phi - \phi_r)^2. \quad (2.75)$$

For the co-energy, a modified definition is advantageous

$$E_c = \phi\theta - E_i + \frac{1}{2}\phi_r\theta_c, \quad (2.76)$$

where an additional constant  $\phi_r\theta_c/2$  changes only the reference point, which can be done without consequences, because only the derivatives of the energy functions are relevant. That yields

$$E_c = \phi\theta - E_i + \frac{1}{2}\phi_r\theta_c = \frac{1}{2}(\phi + \phi_r)\theta + \frac{1}{2}\phi_r\theta_c = \frac{1}{2}\phi(\theta + \theta_c), \quad (2.77)$$

where the relation

$$\phi = \phi_r + \frac{\phi_r}{\theta_c}\theta \quad (2.78)$$

was used. The geometric interpretation is given in the following figure.

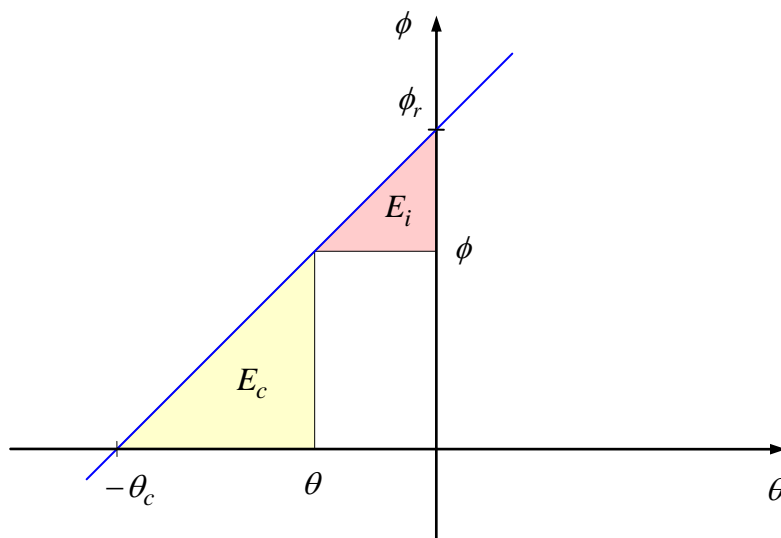


**Fig. 2-19:** Internal energy and co-energy with a permanent magnet

If the representation of these energies is compared with the equivalent circuit diagrams, variants (a) and (b), one finds that the internal energy

$$E_i = \frac{1}{2}(\phi - \phi_r)\theta = \frac{1}{2}\phi_R\theta = \frac{\theta^2}{2R_{PM}} \quad (2.79)$$

can be interpreted as magnetic energy of the paralleled internal resistance  $R_{PM}$  in case (a). In case (b), the co-energy is equivalent to the magnetic energy of the series-connected internal resistance  $R_{PM}$ :

$$E_c = \frac{1}{2}\phi(\theta + \theta_c) = \frac{1}{2}\phi\theta_R = \frac{1}{2}R_{PM}\phi^2 \quad (2.80)$$

### Magnetic circuit with permanent magnets

If a magnetic circuit consists of a permanent magnet, an airgap, and a high-permeable core, the reluctance of the core can usually be neglected compared with the reluctance of the airgap and the magnet. This leads to the equivalent circuit shown below. The resulting magnetic condition can be easily sketched graphically. It should be noted that the characteristics of the permanent magnet are commonly given in a consumer counting direction so that the counting system of the other part of the circuit, i.e. the airgap should be the generator counting system resulting in a negative sign in the equation

$$\theta = -R_L\phi, \quad (2.81)$$

then, the airgap line results with a negative slope as depicted in the figure. The graphical construction can be done in a diagram  $\phi$  vs.  $\theta$  as well as directly in the material's characteristic curve of the permanent magnet vs.  $h$ . In the first case, the slopes of the lines are given by the magnetic reluctances. In the second case, it is appropriate to introduce first a *permeance ratio*

$$\alpha = \frac{R_{PM}}{R_L} = \frac{A_L l_{PM}}{A_{PM} l_L}, \quad (2.82)$$

which is the ratio of the reluctances or the ratio of the slopes of the materials' characteristic lines.

Extreme cases:

- No airgap, i.e.  $\alpha = \infty$ : Then, the flux is  $\phi = \phi_r$  and the magnetomotive force is  $\theta = 0$ .
- Large airgap compared to the size of the magnet, i.e.  $\alpha = 0$ : Then, MMF is  $\theta = \theta_c$  and the flux  $\phi = 0$ .

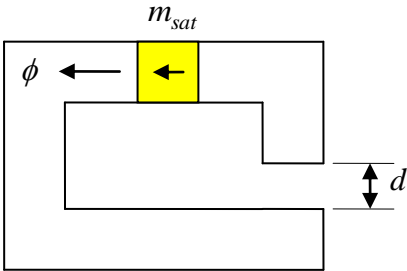


Fig. 2-20: Magnetic circuit with permanent magnet

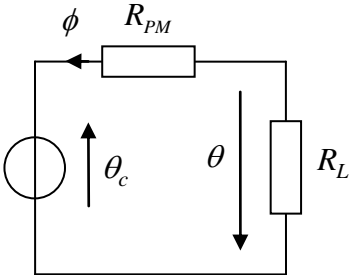


Fig. 2-21: Equivalent magnetic circuit with permanent magnet and airgap

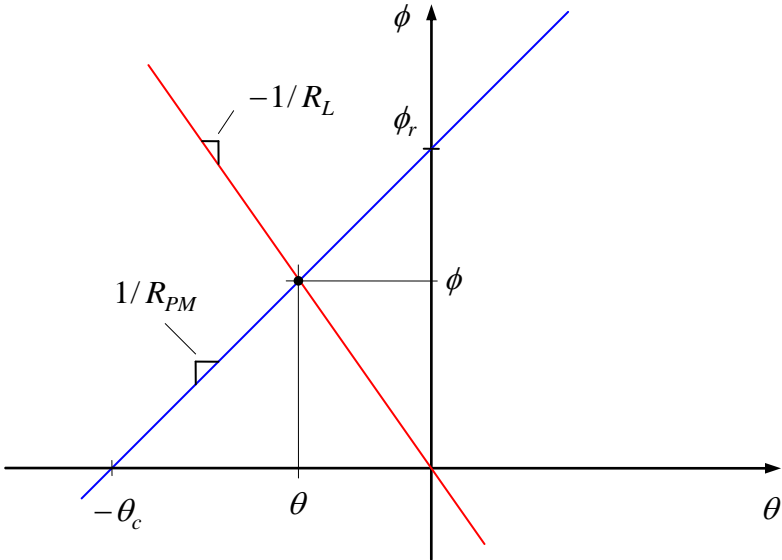
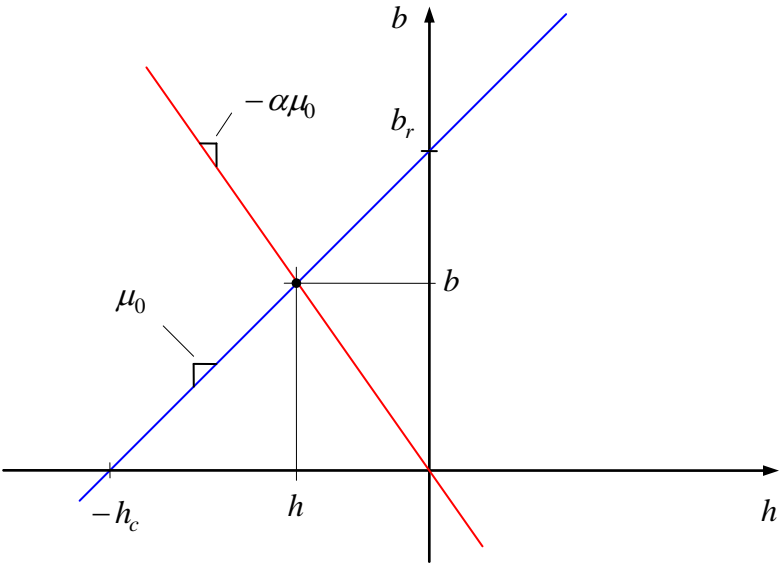


Fig. 2-22: Intersection of the characteristic lines of magnet and airgap



**Fig. 2-23:** Intersection of the characteristic materials' lines of magnet and air

### 3 Magnetic Bearing

#### 3.1 Magnetic Yoke

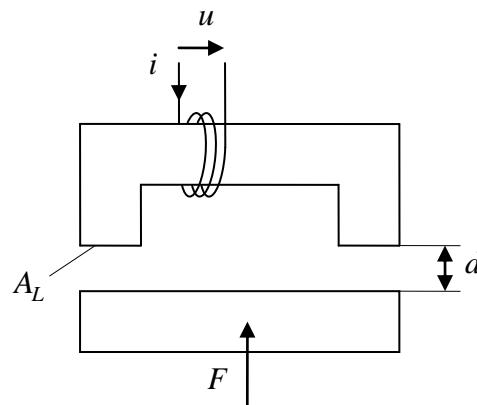


**Fig. 3-1:** Principle diagram of an electromagnetic actuator

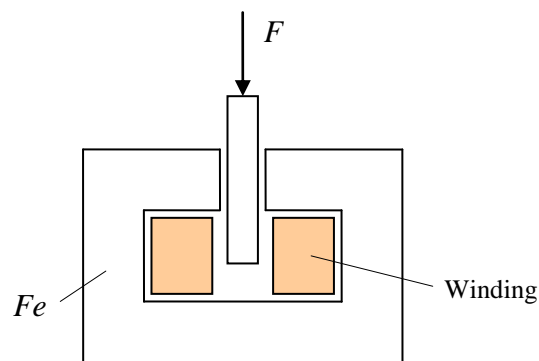


**Fig. 3-2:** Possible technical construction of a linear actuator

Apply the general equation to a system as represented. Assume

$$R_{Fe} \ll R_L, \tag{3.1}$$

which is ensured if

$$l_{Fe} \ll \mu_{rFe} l_L \tag{3.2}$$

The magnetomotive force and thus also the energy within the iron core is neglected. The total airgap length is

$$l_L = 2d. \tag{3.3}$$

The magnetomotive force of the electric coil is

$$\theta_0 = Ni \quad (3.4)$$

It results

$$E_c(i, d) = \psi i - \frac{1}{2} \psi i = \frac{1}{2} \psi i = \frac{1}{2} \phi \theta_0 = \frac{1}{2} \frac{\theta_0^2}{R_L} = \frac{N^2 i^2 A_L \mu_0}{4d} \quad (3.5)$$

$$F(i, d) = \frac{\partial E_c}{\partial d} = -\frac{N^2 i^2 A_L \mu_0}{4d^2} = -\frac{1}{2d} \phi \theta_0 = -\frac{1}{2} 2A_L b_L h_L = -p_L 2A_L \quad (3.6)$$

with the *magnetic pressure*

$$p_L = \frac{1}{2} b_L h_L = -\frac{F}{2A_L} \quad (3.7)$$

Stiffness:

$$S_i(i, d) = -\frac{\partial F}{\partial d} = -\frac{N^2 i^2 A_L \mu_0}{2d^3} = \frac{2F(i, d)}{d} = -\frac{4p_L A_L}{d} < 0 \quad (3.8)$$

The Stiffness is negative, i.e. unstable.

Flux linkage:

$$\psi(i, d) = \frac{N^2 i A_L \mu_0}{2d} \quad (3.9)$$

Inductance:

$$L(i, d) = \frac{N^2 A_L \mu_0}{2d} \quad (3.10)$$

### 3.2 Construction with two Yokes

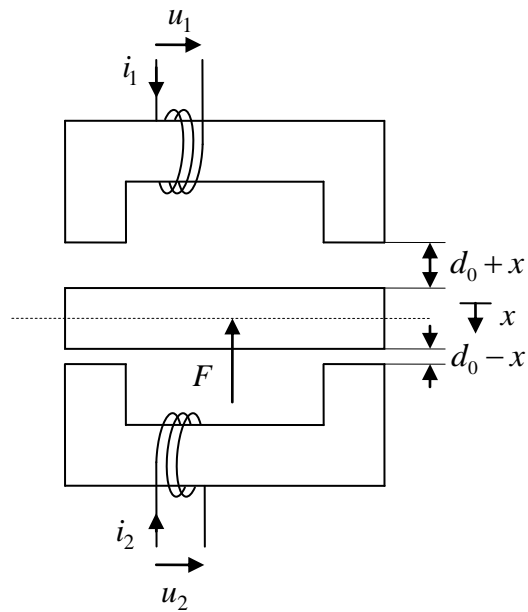


**Fig. 3-3:** Magnetic bearing with two yokes

$$\begin{aligned} d_1 &= d_0 + x \\ d_2 &= d_0 - x \end{aligned} \quad (3.11)$$

$$\begin{aligned} F_1(i_1, x) &= -\frac{N^2 i_1^2 A_L \mu_0}{4(d_0 + x)^2} \\ F_2(i_2, x) &= \frac{N^2 i_2^2 A_L \mu_0}{4(d_0 - x)^2} \\ F(i_1, i_2, x) &= F_1(i_1, x) + F_2(i_2, x) \\ &= -\frac{N^2 A_L \mu_0}{4} \left[ \frac{i_1^2}{(d_0 + x)^2} - \frac{i_2^2}{(d_0 - x)^2} \right] \\ S_i(i_1, i_2, x) &= -\frac{N^2 A_L \mu_0}{2} \left[ \frac{i_1^2}{(d_0 + x)^3} + \frac{i_2^2}{(d_0 - x)^3} \right] < 0 \end{aligned} \quad (3.12)$$

### 3.3 Control of a Magnetic Bearing with Bias Excitation by a Separate Winding

Idea: Apply a bias current  $I_0$  to both coils and superimpose a differential mode current  $\Delta i$  :

$$\begin{aligned} i_1 &= I_0 + \Delta i \\ i_2 &= I_0 - \Delta i \end{aligned} \quad (3.13)$$

This superposition of a constant common mode DC current and a varying differential mode current can be carried out directly by the winding scheme as shown in the figure:

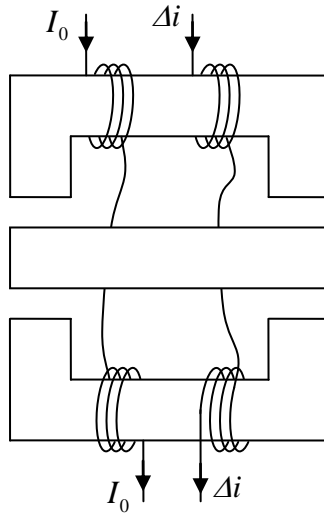


**Fig. 3-4:** Magnetic bearing with separate windings for constant bias current and a “control current”

$$F(\Delta i, x) = -\frac{N^2 A_L \mu_0}{4} \left[ \frac{(I_0 + \Delta i)^2}{(d_0 + x)^2} - \frac{(I_0 - \Delta i)^2}{(d_0 - x)^2} \right] \quad (3.14)$$

Linearization at the operation point  $x = 0$  and  $\Delta i = 0$  :

$$\begin{aligned} F(\Delta i, x) &= \Delta i \left. \frac{\partial F}{\partial \Delta i} \right|_{\substack{\Delta i=0 \\ x=0}} + x \left. \frac{\partial F}{\partial x} \right|_{\substack{\Delta i=0 \\ x=0}} \\ &= -\frac{N^2 A_L \mu_0 I_0}{d_0^2} \Delta i + \frac{N^2 A_L \mu_0 I_0^2}{d_0^3} x = -C \Delta i - S_i x \end{aligned} \quad (3.15)$$

with

$$C = \frac{N^2 A_L \mu_0 I_0}{d_0^2} \quad \text{and} \quad S_i = -\frac{N^2 A_L \mu_0 I_0^2}{d_0^3} \quad (3.16)$$

The constant  $C$  is the force-to-current ratio. With rotating machines this constant is well known as the *motor constant*.

The total flux of the winding carrying the current  $\Delta i$  results as

$$\psi_{\Delta}(\Delta i, x) = \frac{N^2(I_0 + \Delta i)A_L\mu_0}{2(d_0 + x)} - \frac{N^2(I_0 - \Delta i)A_L\mu_0}{2(d_0 - x)} \quad (3.17)$$

The inductance of this coil is

$$L_{\Delta}(x) = \frac{\partial \psi_{\Delta}}{\partial \Delta i} = N^2 A_L \mu_0 \left[ \frac{1}{2(d_0 + x)} + \frac{1}{2(d_0 - x)} \right] \quad (3.18)$$

For small  $x$ , the first-order approximation is simply a constant which is determined by the value at  $x=0$  :

$$L_{\Delta}(0) = \frac{N^2 A_L \mu_0}{d_0} \quad (3.19)$$

**Control idea:**

$$\Delta i = Kx \quad (3.20)$$

Resulting total stiffness:

$$S = -\frac{dF}{dx} = S_i + KC = \frac{N^2 A_L \mu_0 I_0}{d_0^2} \left( K - \frac{I_0}{d_0} \right) \quad (3.21)$$

If it is chosen

$$K > K_{\min} = -\frac{S_i}{C} = \frac{I_0}{d_0} \quad (3.22)$$

the total stiffness  $S$  results as positive.

More detailed investigation of the control behavior: The displacement  $x$  must be measured by a sensor. A real sensor has a limited bandwidth and can be modeled as a low pass filter with time constant  $\tau_s$  :

$$G_s(s) = \frac{\hat{x}(s)}{x(s)} = \frac{1}{1 + \tau_s s} \quad (3.23)$$

Similarly, the desired current cannot be impressed momentarily. The transfer behavior between desired current and actual current can also be modelled as low pass with time constant  $\tau_i$  :

$$G_i(s) = \frac{\Delta i(s)}{\Delta i^*(s)} = \frac{1}{1 + \tau_i s} \quad (3.24)$$

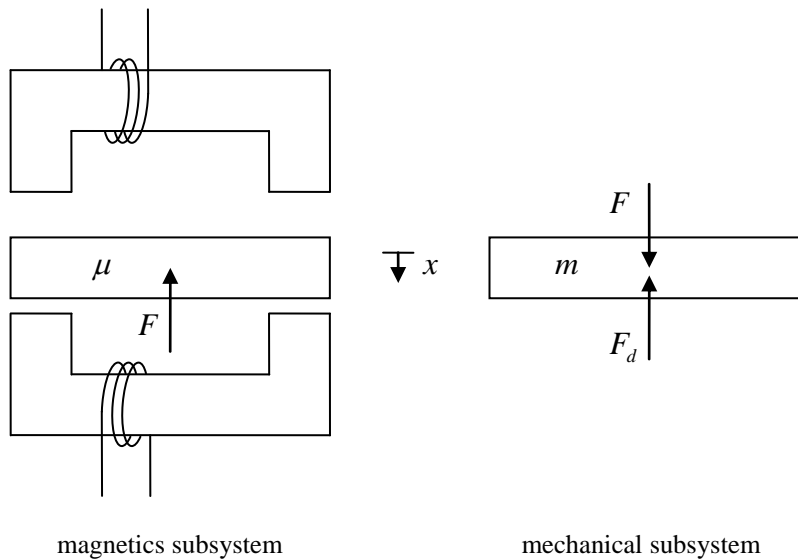


**Fig. 3-5:** Cut-free diagrams in order to separate the magnetic and the inertial behavior of the materials

Behavior of the mechanical inertia:

$$G_m(s) = \frac{x(s)}{F(s) - F_d(s)} = \frac{1}{ms^2} \quad (3.25)$$

In steady state,  $\ddot{x} = 0$ , it follows

$$F = F_d \quad (3.26)$$

The transfer function  $G_m(s)$  is to be merged with the feedback via  $S_i$  :

$$G'_m(s) = \frac{1}{S_i + ms^2} \quad (3.27)$$

Let us introduce also:

$$G'_i(s) = G_i(s)C \quad (3.28)$$

As a first approach, a  $P$ -type controller is used:

$$G_c(s) = \frac{\Delta i^*(s)}{\Delta x(s)} = -K \quad (3.29)$$

The negative sign is due to correct action of the controller. This sign can be compensated with the negative sign before the motor constant  $C$  so that the control law can be written as

$$G'_c(s) = -G_c(s) = \frac{-\Delta i^*(s)}{\Delta x(s)} = K \quad (3.30)$$

with a common positive gain.

Control error:

$$\Delta x = x^* - x \quad (3.31)$$

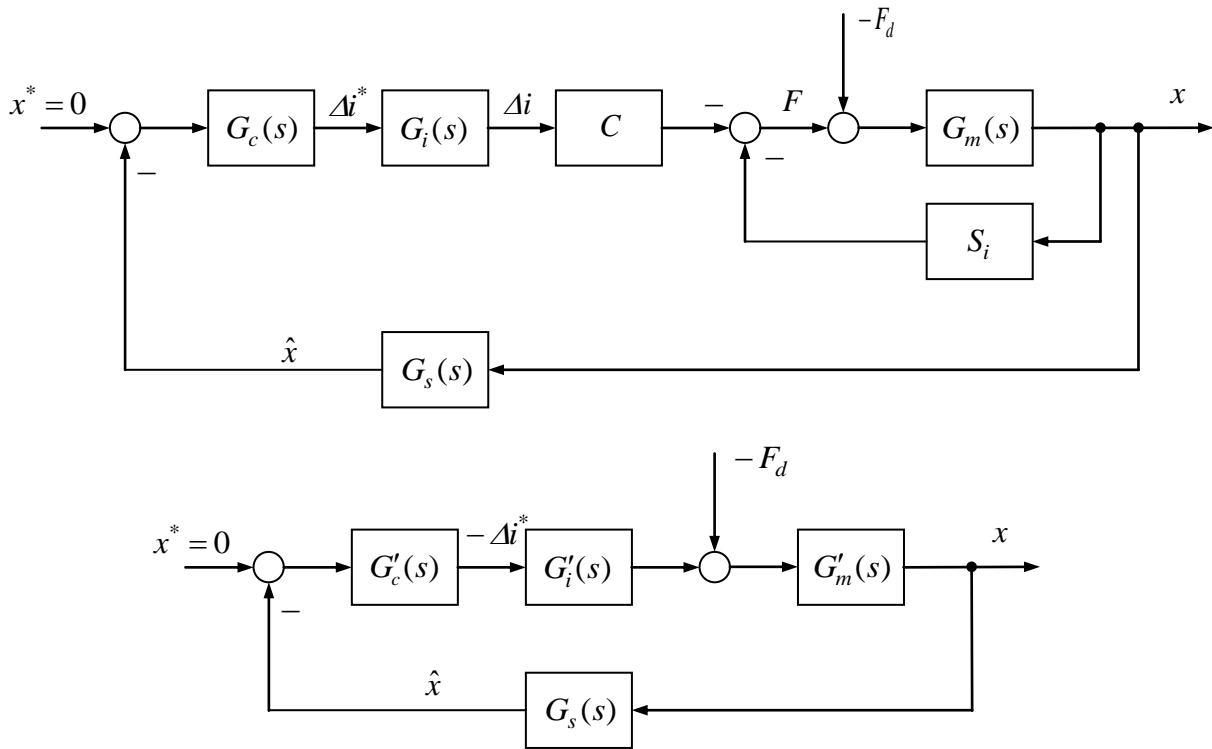


**Fig. 3-6:** Tracking transfer function:

$$\begin{aligned} T(s) &= \frac{x(s)}{x^*(s)} = \frac{G'_c(s)G'_i(s)G'_m(s)}{1 + G'_c(s)G'_i(s)G'_m(s)G_s(s)} \\ &= \frac{G'_c(s)G'_i(s)G'_m(s)}{1 + L(s)} \\ &= \frac{(1 + \tau_s s)KC}{(S_i + ms^2)(1 + \tau_s s)(1 + \tau_i s) + KC} \end{aligned} \quad (3.32)$$

Disturbance transfer function

$$\begin{aligned}
 T_d(s) &= \frac{x(s)}{-F_d(s)} = \frac{G'_m(s)}{1 + G'_c(s)G'_i(s)G'_m(s)G_s(s)} \\
 &= \frac{G'_m(s)}{1 + L(s)} \\
 &= \frac{(1 + \tau_s s)(1 + \tau_i s)}{(S_i + ms^2)(1 + \tau_s s)(1 + \tau_i s) + KC}
 \end{aligned} \tag{3.33}$$

where

$$L(s) = G'_c(s)G'_i(s)G'_m(s)G_s(s) \tag{3.34}$$

is the loop transfer function. The reciprocal of the disturbance transfer function can be interpreted as dynamical stiffness:

$$S(s) = \frac{-F_d(s)}{x(s)} = \frac{1}{T_d(s)} \tag{3.35}$$

The transfer function of the mechanical subsystem

$$G'_m(s) = \frac{1}{S_i + ms^2} \tag{3.36}$$

exhibits the poles

$$s_1 = \sqrt{-\frac{S_i}{m}}, \quad s_2 = -\sqrt{-\frac{S_i}{m}} \tag{3.37}$$

Both poles are real (please note that  $S_i < 0$ ). One pole lies in the right complex half-plane. All other subsystem transfer functions are stable and show poles with negative real parts.

Thus, for principle reasons, a  $P$ -type controller cannot stabilize the system.

*Control engineering reasoning:*  $D$ -type compensation is required in order to increase the phase margin (in Bode plot) or to shift the poles to the left half plane (root locus method).

*Mechanical engineering reasoning:* Introduce damping (which is, in the end, the same result as a  $D$ -type compensator). An additional  $I$ -action can be introduced in order to ensure a stationary zero control error (i.e. infinite stationary stiffness). Thus, new approach with  $PID$ -controller:

$$G'_c(s) = K \left( 1 + \frac{1}{sT_n} \right) \frac{1+sT_v}{1+sT_r} = K \frac{(1+sT_n)(1+sT_v)}{sT_n(1+sT_r)} \quad (3.38)$$

The transfer function of an PI controller is now augmented by an differential action  $1+sT_v$  with rate time  $T_v$ . It was also considered that a realistic differentiator has only limited bandwidth, represented by the additional low pass  $1/(1+sT_r)$ .

Outline of control design procedure in frequency domain: One pole of the loop gain transfer function  $L(s)$  has a positive real part (contribution of  $G'_m(s)$ ). In case of an  $I$ -action in the controller, an additional pole is located on the imaginary axis. The Nyquist locus curve  $1+L(j\omega)$  must then show a wrapping of  $+3\pi/2$  (for positive  $\omega$ ) in order to stabilize the closed-loop control. Without integral controller action, i.e. with a  $PD$ -controller, the wrapping must be only  $+\pi$ . In case of  $PD$ -control, the minimum stabilizing controller gain can be directly deduced, because the wrapping of  $+\pi$  is only possible, if the starting point of the Nyquist locus satisfies the condition

$$L(0) < -1 \quad (3.39)$$

From this follows

$$\frac{KC}{S_i} < -1 \quad (3.40)$$

or

$$K > K_{\min} = -\frac{S_i}{C} \quad (3.41)$$

Please note again  $S_i < 0$ . This result is consistent with the consideration of a positive total stiffness.

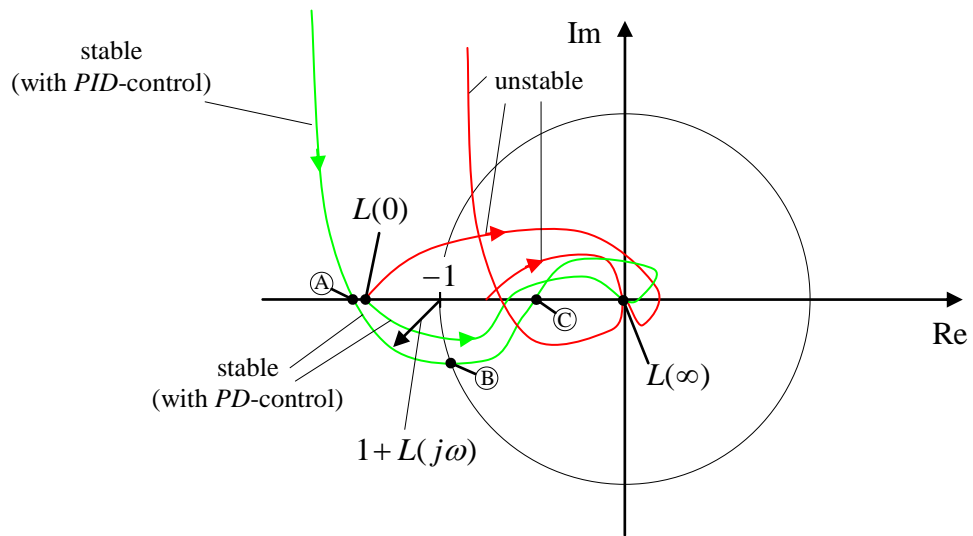


**Fig. 3-7:** Nyquist locus curves

With frequency response diagrams (Bode plots) the control design is usually more convenient rather than with Nyquist loci. However, a normalization of the subsystem transfer functions is recommended first:

$$G_m''(s) = -S_i G_m'(s) = -\frac{1}{1 + \frac{m}{S_i} s^2} \quad (3.42)$$

$$G_c''(s) = -\frac{C}{S_i} G_c'(s) \quad (3.43)$$

$$K'' = -\frac{C}{S_i} K' \quad (3.44)$$

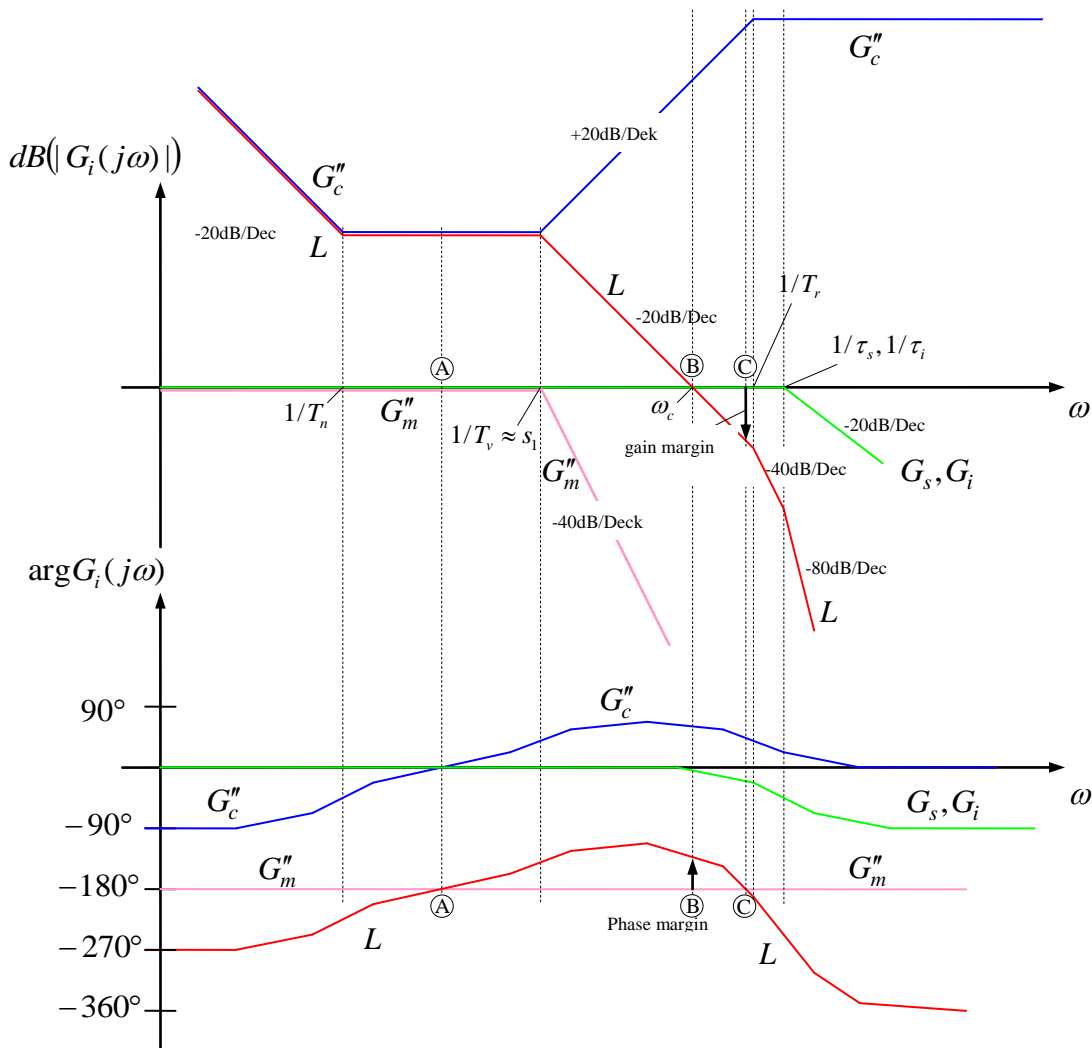
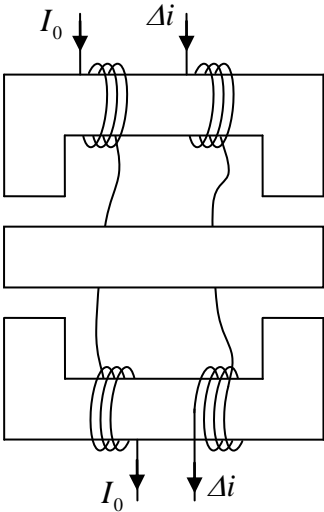


**Fig. 3-8:** Frequency response diagrams for control design

Few notes for control design:

- $D$ -action increases the phase margin of  $L(j\omega)$  in the area of the cut-off frequency  $\omega_c$ .
- Controller rate time  $T_v$  can be chosen equal to or in the range of  $1/s_1 = -1/s_2$ .
- Controller gain and thus overall gain of  $L(j\omega)$  is chosen in such a way that the cut-off frequency  $\omega_c$  (or bandwidth, resp.) results as desired.
- Controller reset time  $T_n$  should be chosen as small as possible, i.e. the frequency  $1/T_n$  as large as possible, as far as the phase margin at  $\omega_c$  is not too much decreased.
- Corner frequencies of the sensor and the current source  $1/\tau_s, 1/\tau_i$  and the real differential action  $1/T_r$  must be large enough above the desired cut-off frequency  $\omega_c$ . All three time constants together may cause a considerable decrease of the phase margin, even if they are not that close-by to  $\omega_c$ .

Detailed control design as exercise!



### 3.4 Magnetic Bearing with Permanent Magnets Magnetlager mit Permanentmagneten

As we learnt from equations (3.15) and (3.16), a bias magnetisation by a DC current  $I_0$  is necessary in order to get a linearisation with non-zero current-to-force constant  $C$ .

However, the magnetisation bias can also be achieved by permanent magnets as the following consideration will show.

Wie wir aus den Gleichungen (3.15) und (3.16) gesehen haben, ist eine Vormagnetisierung durch einen Gleichstrom  $I_0$  notwendig, damit in der Linearisierung die Kraft-Strom-Konstante  $C$  nicht null wird.

Eine Vormagnetisierung kann alternativ aber auch durch Permanentmagnete erreicht werden, wie im Folgenden gezeigt wird.

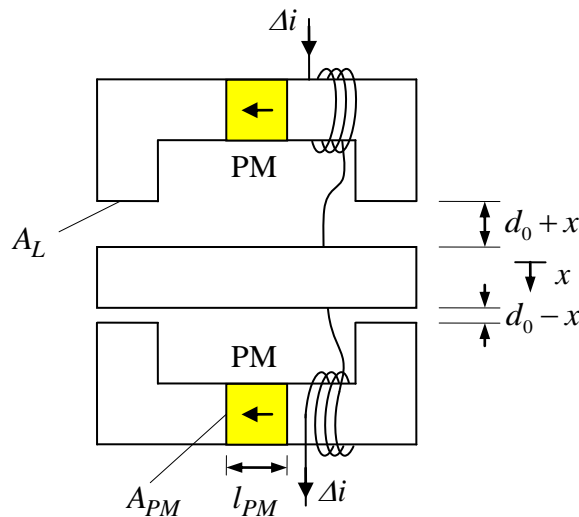


**Fig. 3-9:** Magnetic bearing with permanent magnets / Magnetlager mit Permanentmagneten

A principal sketch is shown in the above figure. The upper yoke should be investigated first. In order to represent the permanent magnet in an equivalent magnetic circuit, we use the right-hand-side diagram of Fig. 2-17, augmented by the airgap reluctance and the MMF source  $\theta_0 = N\Delta i$ . The reluctance of the ferromagnetic core is neglected.

Das Prinzip ist im obigen Bild dargestellt. Zunächst soll nur das obere Joch untersucht werden. Um den Permanentmagneten in einem magnetischen Ersatzschaltbild wiederzugeben, bedienen wir uns der rechten Darstellung aus Fig. 2-17 und ergänzen die Luftspalt-Reluktanz und die Durchflutungsquelle  $\theta_0 = N\Delta i$ . Die Reluktanz des ferromagnetischen Kerns wird vernachlässigt.

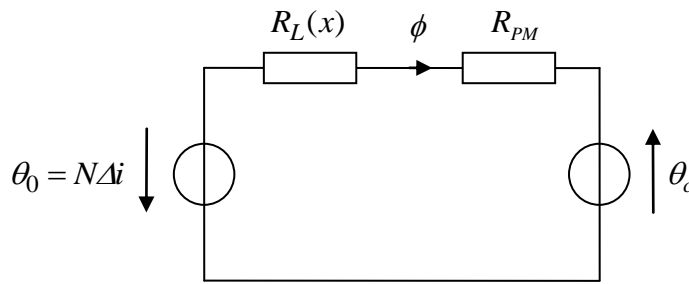


**Fig. 3-10:** Magnetic ECD of the upper yoke / Magnetisches ESB des oberen Jochs

Now, the circuit comprises two MMF series-connected sources. The magnetic flux results as

Nun enthält der magnetische Kreis zwei Spannungsquellen in Reihe. Der magnetische Fluss folgt zu

$$\phi = \frac{\theta_0 + \theta_c}{R_{PM} + R_L(x)} \tag{3.45}$$

with the reluctances

mit den Reluktanzen

$$R_L(x) = \frac{2(d_0 + x)}{\mu_0 A_L} \quad , \quad R_{PM} = \frac{l_{PM}}{\mu_0 A_{PM}} = \frac{l_{PM} A_L}{\mu_0 A_{PM} A_L} = \frac{l'_{PM}}{\mu_0 A_L} \tag{3.46}$$

In case of different cross sections areas of the permanent magnet and the airgap, it is advantageous to introduce a normalised magnet length  $l'_{PM}$  as it is done above.

Für den Fall unterschiedlicher Querschnittsflächen von Magnet und Luftspalt empfiehlt sich die Einführung einer normalisierte Magnetlänge  $l'_{PM}$  wie oben erfolgt.

According to (2.80), the co-energy of the system is

Gemäß (2.80) ist die Koenergie des Systems

$$E_c(x) = \frac{1}{2} (R_{PM} + R_L(x)) \phi^2 = \frac{1}{2} \frac{(\theta_0 + \theta_c)^2}{R_{PM} + R_L(x)} = \frac{\mu_0 A_L}{2} \frac{(N\Delta i + \theta_c)^2}{2(d_0 + x) + l'_{PM}} = \frac{\mu_0 A_L}{4} \frac{(N\Delta i + \theta_c)^2}{d'_0 + x} \tag{3.47}$$

with

mit

$$d'_0 = d_0 + \frac{1}{2} l'_{PM} = d_0 + \frac{1}{2} l_{PM} \frac{A_L}{A_{PM}} \tag{3.48}$$

The resulting formula has got exactly the same form as (3.5) with the exception that  $\theta_c$  takes over the role of bias magnetisation and that the magnet length contributes to the

Die resultierende Formel hat genau die gleiche Form wie (3.5), wobei jetzt  $\theta_c$  die Rolle der Vormagnetisierung übernimmt und die Magnetlänge bei der gesamten

total airgap length.

Luftspatllänge zu berücksichtigen ist.

For the System with upper and lower yokes, similar formulae result to those of Section 3.3 as

Für das System mit oberem und unterem Joch ergeben sich ähnliche Formeln zu denen des Abschnitts 3.3:

$$E_c(\Delta i, x) = \frac{\mu_0 A_L}{4} \left[ \frac{(\theta_c + N\Delta i_c)^2}{d'_0 + x} + \frac{(\theta_c - N\Delta i_c)^2}{d'_0 - x} \right]. \quad (3.49)$$

$$F(\Delta i, x) = \frac{\partial E_c}{\partial x} = -\frac{\mu_0 A_L}{4} \left[ \frac{(I_0 + N\Delta i)^2}{(d'_0 + x)^2} - \frac{(I_0 - N\Delta i)^2}{(d'_0 - x)^2} \right] \quad (3.50)$$

$$S_i(\Delta i, x) = -\frac{\partial F}{\partial x} = -\frac{\mu_0 A_L}{2} \left[ \frac{(\theta_c + N\Delta i)^2}{(d'_0 + x)^3} + \frac{(\theta_c - N\Delta i)^2}{(d'_0 - x)^3} \right] \quad (3.51)$$

That applies also for the linearisation around the operating point  $\Delta i = 0, x = 0$ :

Das gilt ebenso für die Linearisierung um den Arbeitspunkt  $\Delta i = 0, x = 0$ :

$$F(\Delta i, x) = \Delta i \left. \frac{\partial F}{\partial \Delta i} \right|_{\substack{\Delta i=0 \\ x=0}} + x \left. \frac{\partial F}{\partial x} \right|_{\substack{\Delta i=0 \\ x=0}} = -C \Delta i - S_i x \quad (3.52)$$

with

mit

$$C = \frac{A_L \mu_0 \theta_c}{d'_0{}^2}, \quad S_i = -\frac{A_L \mu_0 \theta_c^2}{d'_0{}^3} \quad (3.53)$$

The advantages of a permanent bias magnetisation over a bias current are obvious: There is no need of an electrical supply to feed the bias winding. Additionally, it turns out that a permanent magnet results in a much stronger magnetisation than it is possible with an electric winding of comparable geometric size.

Die Vorteile einer Vormagnetisierung durch Permanentmagnete sind offensichtlich: Es wird keine elektrische Stromversorgung für die Vormagnetisierungs-Spule benötigt. Außerdem stellt sich heraus, dass mit einem Permanentmagneten eine viel stärkere Magnetisierung möglich ist als mit einer elektrischen Spule vergleichbarer geometrischer Größe.

### 3.5 Sensors

In order to measure the displacement optical or inductive measurement principles can be applied.

Inductive measurements utilize the variation of the inductance of a sensor coil depending on the displacement. AC signals are applied to measure the inductance. Usually several sensors are configured in a bridge circuit in order to compensate for offsets.

### 3.6 Current Converters

In order to feed the windings of a magnetic bearing with appropriate current, linearly operating power amplifiers could be used. However, due to the high losses of such type of amplifiers, switched-mode converters are usually applied (see figure below). The current of a winding can be positive as well as negative. As well, both voltage polarities are required in order to control the current dynamically. Thus, all four quadrants in the voltage-current-area have to be governed by the converter.

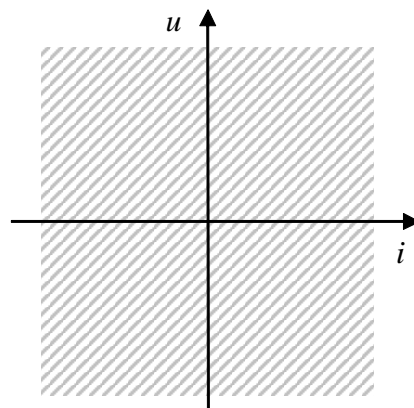


**Fig. 3-11:** Required current voltage area (all four quadrants)

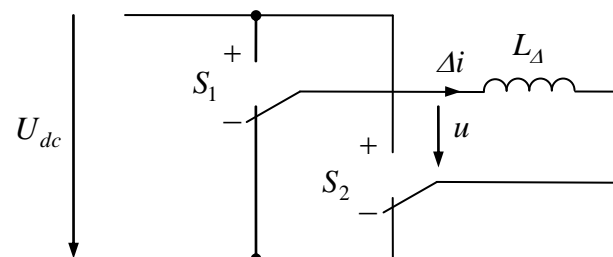


**Fig. 3-12:** Principle circuit diagram of the required converter depicted with ideal switches (4-quadrant converter, 4QC)

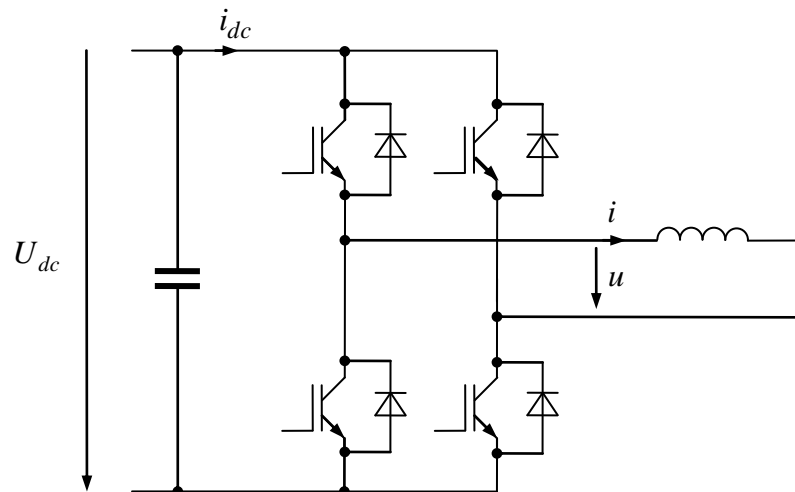


**Fig. 3-13:** 4-quadrant converter circuit diagram with power electronic devices

$S_1$	$S_2$	$u$
+	-	$+U_{dc}$
-	+	$-U_{dc}$
-	-	0
+	+	0

**Fig. 3-14:** Table: Output voltage vs. switching state

### 3.7 Pulse Width Modulation

The purpose of the pulse width modulation (PWM) is to approximate a given continuous value

$$s^* \in [-1,1] \tag{3.54}$$

by a discrete-valued function in time

$$s(t) \in \{-1;1\} \tag{3.55}$$

so that the average value within a *switching period*  $T_s$  is equal to the desired continuous value:

$$\bar{s} = \frac{1}{T_s} \int_{kT_s}^{(k+1)T_s} s(t) dt = s^* \tag{3.56}$$

The principle is shown in the following figures.

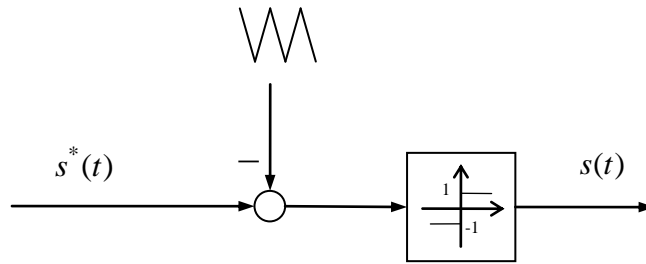


**Fig. 3-15:** Realization of the pulse width modulation via triangular modulation carrier and a comparator

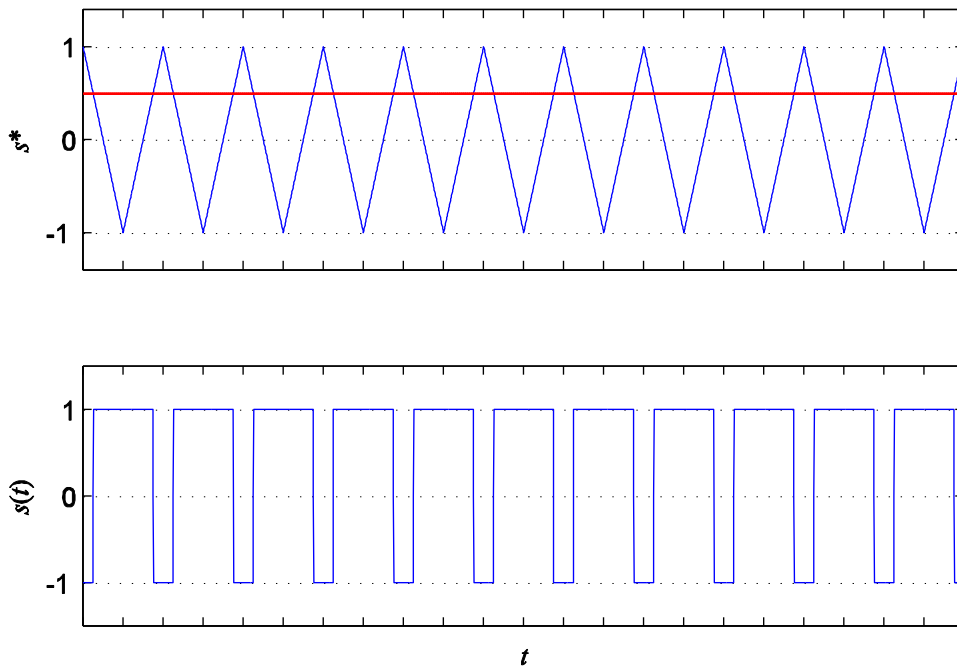


**Fig. 3-16:** Principle of the pulse width modulation

The PWM is applied in order to realize continuous-valued voltage demands, at least in an averaged consideration, even with the switched-mode 4-quadrant converter. First, the desired voltage reference value  $u^*$  is normalized as input to the PWM,

$$s^* = \frac{u^*}{U_{dc}} \tag{3.57}$$

Best practise is to use for the two switches of the 4QC two modulation carriers with phase shift of  $180^\circ$  as shown in the next figure. In this manner, the effective pulse frequency is doubled as well as the output voltage steps are divided by half.

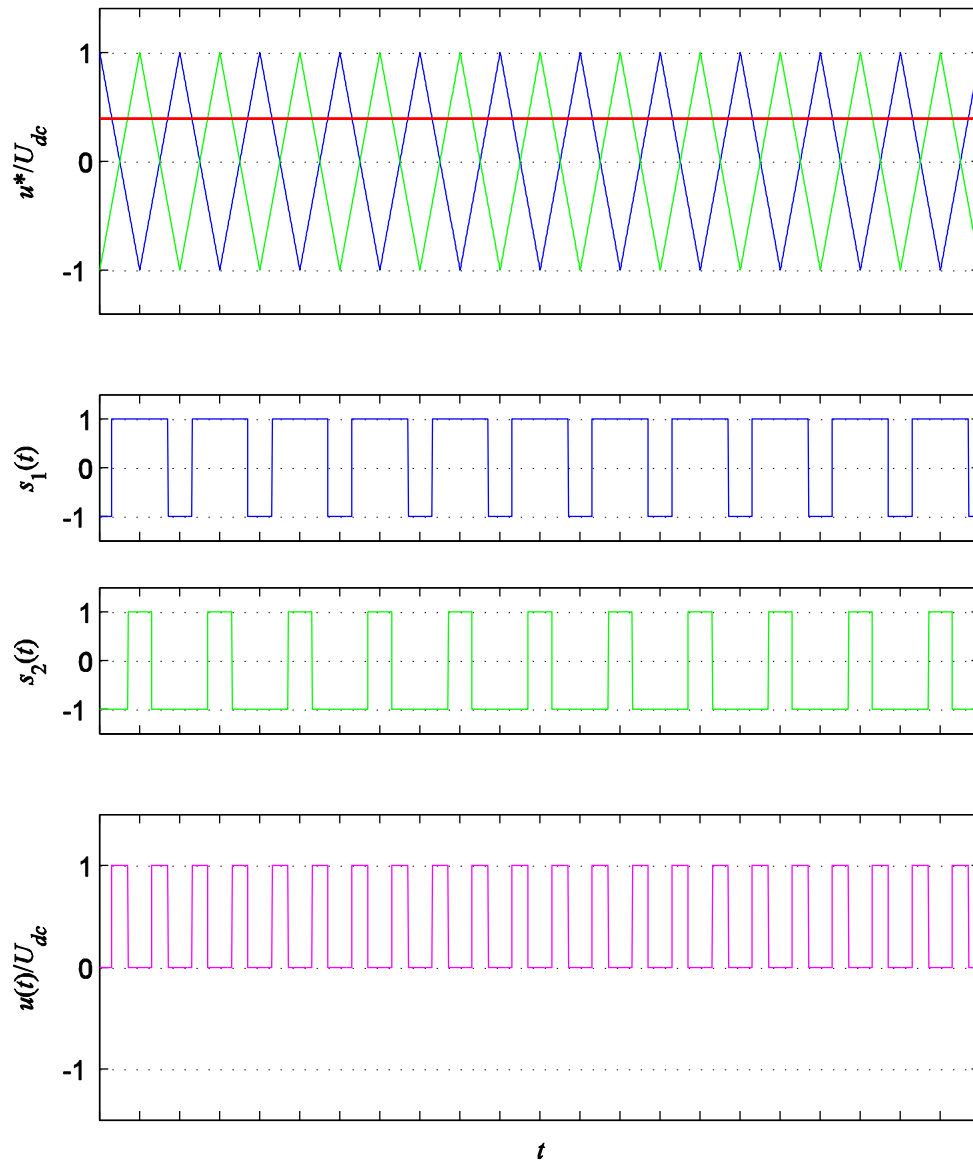


**Fig. 3-17:** Pulse width modulation for the 4QC with phase-shifted modulation carriers

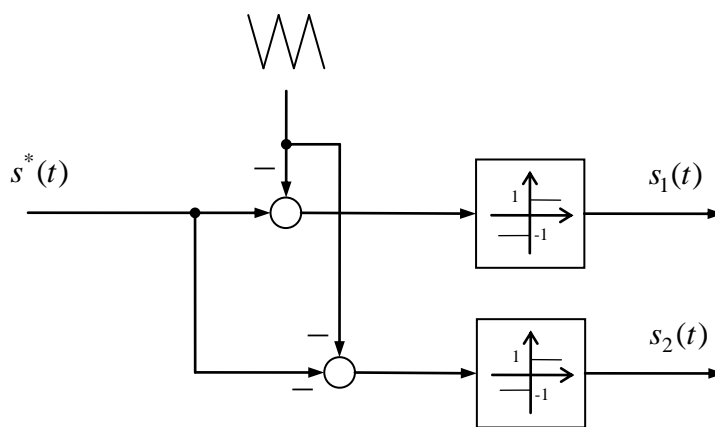


**Fig. 3-18:** Realization of the phase-shifted PWM for 4-quadrant converter

The 4-quadrant converter is a voltage source topology. For the magnetic bearing, however, a current source is needed. This is achieved by employing a subordinate current control.

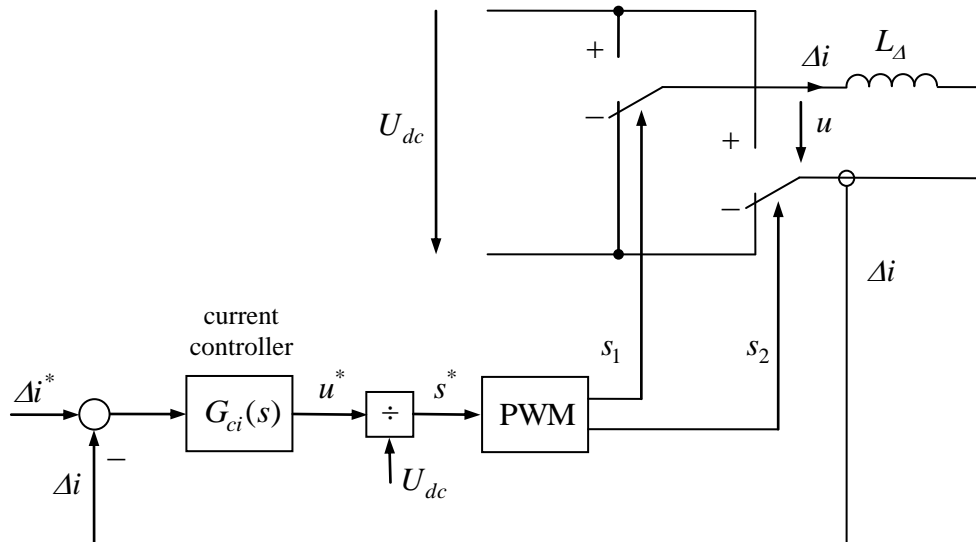


**Fig. 3-19:** Current control structure for the 4-quadrant converter

From the viewpoint of control design, the harmonics of voltage and current that are due to the pulse frequency of the converter can be neglected. That means, the actual pulsating voltages are substituted by their locally averaged values, which are just the input to the PWM:

$$u(t) \approx u^*(t) \tag{3.58}$$

In doing so, a rather simplified control structure results, where the PWM has to be no longer considered.<sup>5</sup>

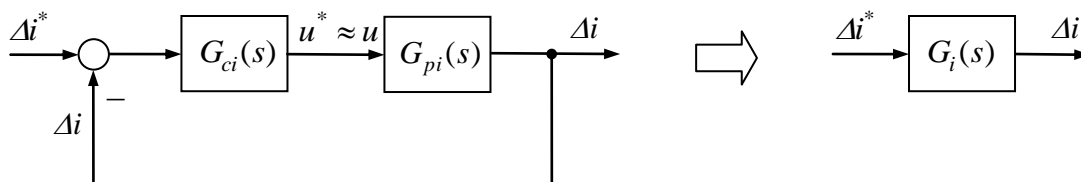


**Fig. 3-20:** Simplified current control structure for the 4QC

The plant transfer function is determined by the inductance  $L_\Delta$ , and, if necessary, by an internal winding resistance:

<sup>5</sup> The fundamentals of this approach are provided by the *dynamical averaging method* which is not subject of this lecture.

$$G_{pi}(s) = \frac{1}{sL_{\Delta} + R_{\Delta}} \quad (3.59)$$

The tracking transfer function results as

$$G_i(s) = \frac{G_{ci}(s)G_{pi}(s)}{1 + G_{ci}(s)G_{pi}(s)} \quad (3.60)$$

As controller, *PI* as well as *P*-types can be applied. The latter cannot guarantee a stationary zero control error. That can be accepted, however, because the integral action of an overlaid position control would compensate for this error. With

$$G_{ci}(s) = K_i \quad (3.61)$$

it follows

$$G_i(s) = \frac{K_i}{K_i + R_{\Delta} + sL_{\Delta}} = \frac{V_i}{1 + s\tau_i} \quad (3.62)$$

where

$$V_i = \frac{1}{1 + R_{\Delta}/K_i}, \quad \tau_i = \frac{L_{\Delta}}{K_i + R_{\Delta}}$$

For small winding resistance or high controller gain  $V_i$  is close to 1 and the above mentioned delay behavior of the controlled current source results.

### 3.8 Magnetic Bearing with Two Degrees of Freedom

The above mentioned systems with one degree of freedom can be extended to control two orthogonal axes of spatial movements. That would result in 4 windings in total, where two of them are connected in parallel, if a magnetic bias with a permanent magnet is applied (compare Section **Fehler! Verweisquelle konnte nicht gefunden werden.**). So, also two 4-quadrant converters would be needed with 8 transistors and 8 diodes in total.

In contrast, the coils can be arranged with a spatial shift of 120°, resulting in three coils that can be connected as star or delta. The converter expense thus reduces to only 6 transistors and 6 diodes. The number of electrical terminals and windings from 4 to 3.

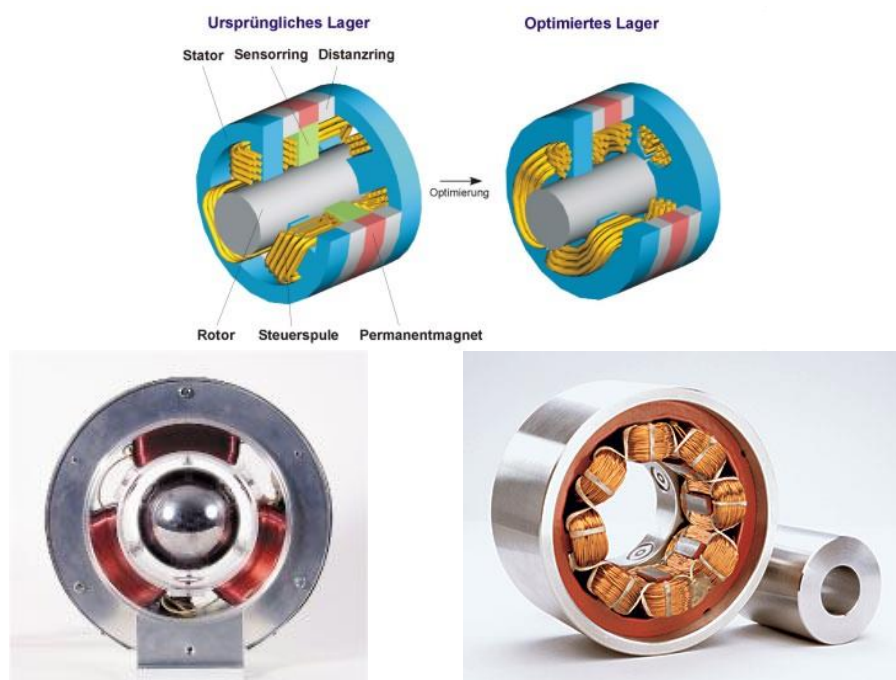


**Fig. 3-21:** Various constructions of magnetic bearings

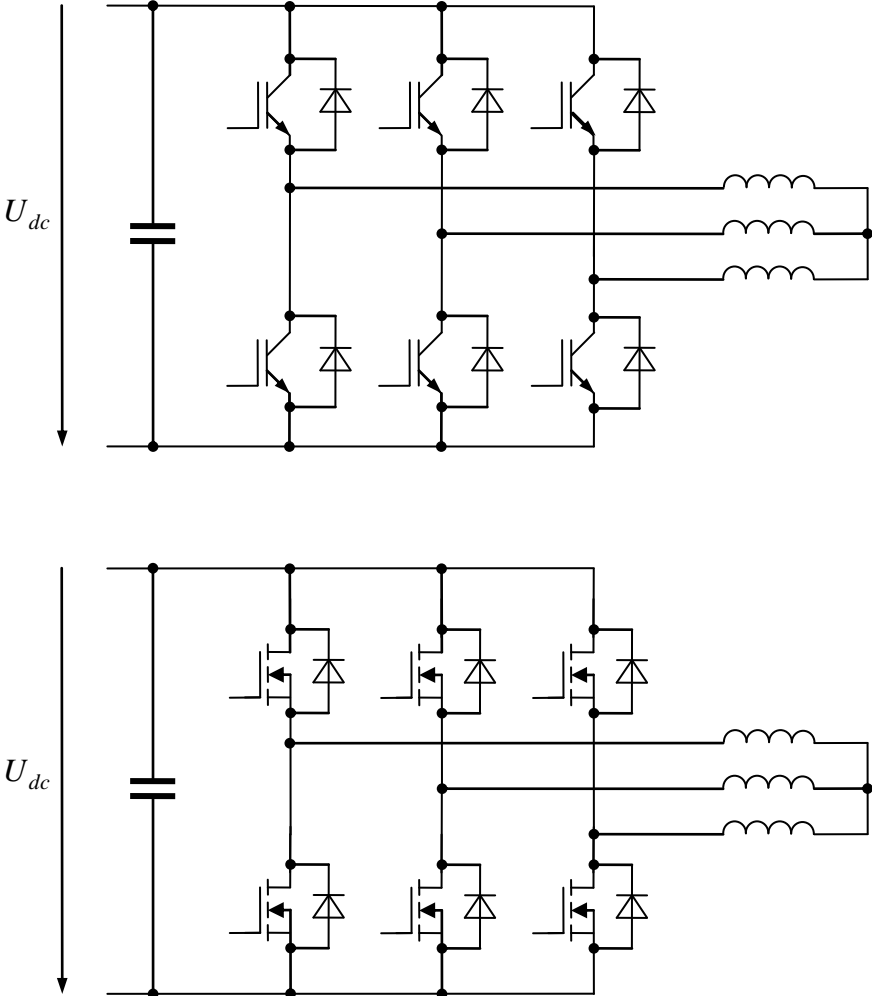
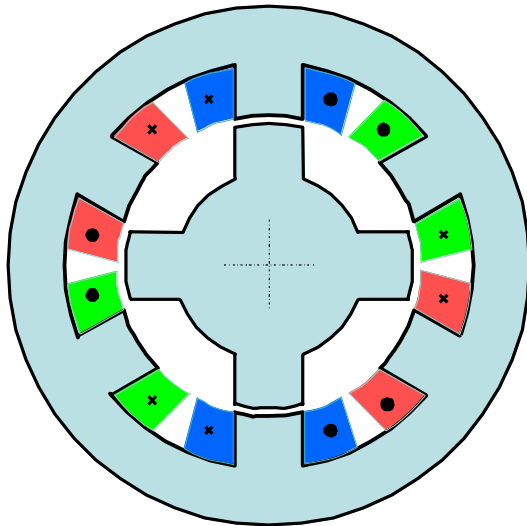


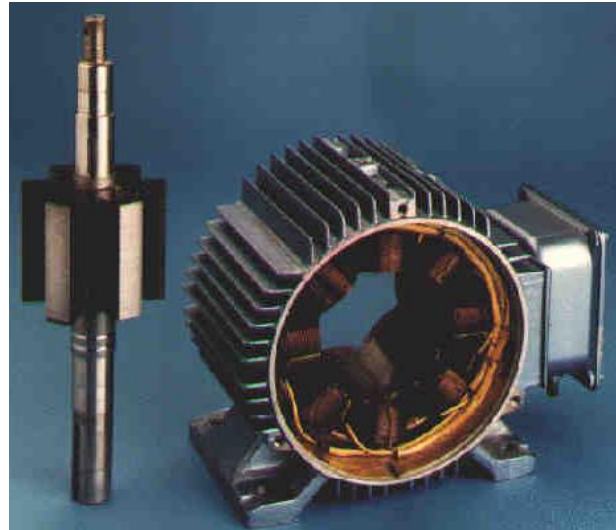
**Fig. 3-22:** Converter for magnetic bearing with three windings, circuit with IGBT (above) or MOSFET (below)

## 4 Switched Reluctance Motor

### 4.1 Construction



6/4-SRM



8/6-SRM

**Fig. 4-1:**

Characteristic of a switched reluctance motor (SRM) is the saliency of the rotor. This leads to a magnetic reluctance which depends on the angular position. The windings of the stator are constructed as concentrated pole windings. Opposite windings belong to the same phase and are connected in parallel or in series. The motor can be constructed with different numbers of stator and rotor poles. Common combinations of stator and rotor pole numbers are 6/8, 8/6, 8/10. However, even single-phase 2/2-machines are possible.

The shape of the phase currents is usually block-like with a phase shift between the phases so that only one phase is turned on at a time. The polarity of the currents is not important which simplifies the required converter topology.

The principle of the switched reluctance motor is already known since 1838. However, only in the last one or two decades this motor could gain a larger market share because the motor control is more complicated compared with other motor types and could not be realized with reasonable effort in former times.

The switched reluctance motor itself can be manufactured at reasonable cost. The pole windings can be manufactured separately. Then, they are mounted as ready-made coils on the poles. Construction of stator and rotor is very simple and robust. Therefore, the motor is dedicated also for high speed applications. Efficiency and torque-to-volume ratio are reasonable.

A drawback is the generation of noise, which is caused by pulsating radial forces. So, the mechanical construction is a very crucial point to handle these forces and thus the noise emission.

The SRM is not adequate for fine positioning tasks with accuracy below a pole pitch, and also not for smooth running at low speed. However, sophisticated control would be needed to cope with such requirements.

### 4.2 Functional principle

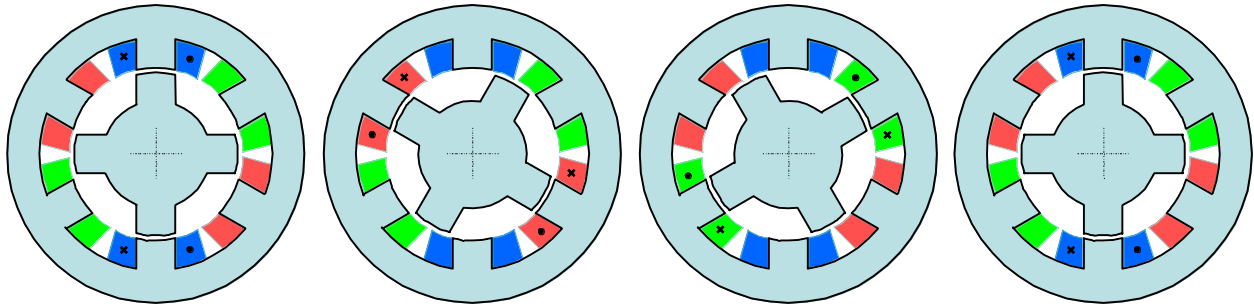


**Fig. 4-2:** Functional principle of a switched reluctance motor:  
The phases are turned on phase-by-phase

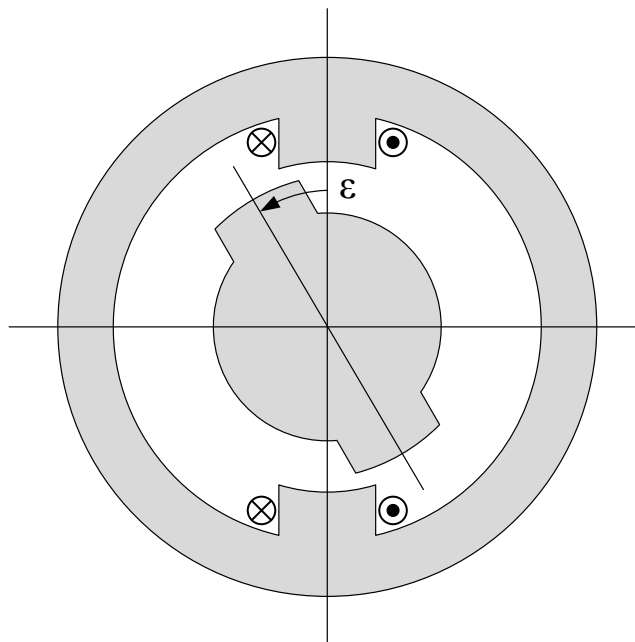


**Fig. 4-3:** Single-phase motor (2/2-SRM)

In order to investigate the operation behavior, only a single phase should be considered first. The modeling is done with a simple magnetic circuit consisting of a nonlinear magnetic reluctance,

$$\phi = \phi_{Fe}(\theta_{Fe}) \quad \text{or} \quad \theta = \theta_{Fe}(\phi), \text{ respectively,}$$

and the linear reluctance of the airgap,

$$\theta_L = R_L(\varepsilon)\phi \quad (4.1)$$

which depends on the angular position  $\varepsilon$ . At the aligned positions  $\varepsilon=0$  and  $\varepsilon=\pi$ , the magnetic reluctance  $R_L$  is at its minimum. The magnetomotive force of the winding is  $\theta_0 = Ni$ , where  $N$  is number of turns of all windings connected in series.

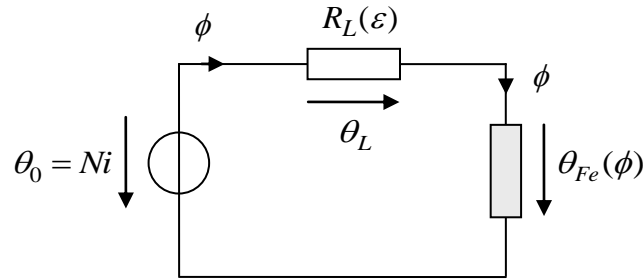


**Fig. 4-4:** Simple magnetic circuit of a single-phase SRM

$$Ni = \theta_0 = \theta_L + \theta_{Fe} = R_L(\varepsilon)\phi + \theta_{Fe}(\phi) \quad (4.2)$$

$$\psi = N\phi \quad (4.3)$$

The representation of the phase current depending on the flux linkage  $\psi = N\phi$  and position angle yields

$$i = i(\psi, \varepsilon) = \frac{R_L(\varepsilon)}{N^2}\psi + \frac{1}{N}\theta_{Fe}\left(\frac{\psi}{N}\right) \quad (4.4)$$

It should be assumed this equation can be solved for the flux so that magnetization curve results as

$$\psi = \psi(i, \varepsilon) \quad (4.5)$$

As it was shown in Section 2.2, the flux and the torque can be derived from the co-energy via

$$\psi(i, \varepsilon) = \frac{\partial E_c}{\partial i}, \quad T(i, \varepsilon) = \frac{\partial E_c}{\partial \varepsilon}$$

With the magnetization curves, the functional principle of the SRM can be demonstrated graphically. For means of simplification, saturation is not considered at first, i.e. the magnetization curves are assumed as straight lines. The gradient of such a line is the inductance that depends on the angular position.

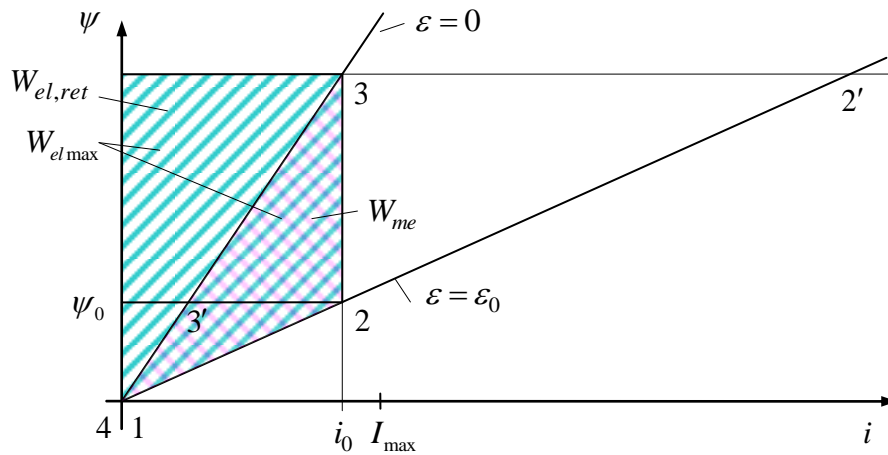


**Fig. 4-5:** Cycle of energy conversion of the SRM with linear magnetic material

The conversion of energy is discussed with an idealized cycle. Particularly, we will investigate the differentials of work

$$dW_{el} = i d\psi \quad (4.6)$$

and

$$dW_{mech} = T d\varepsilon = \frac{\partial E_c}{\partial \varepsilon} d\varepsilon \quad (4.7)$$

which can be interpreted as areas left from and below the magnetization curve (cf. Section 2.2). Let us begin in ...

- State 1:  $i = 0$ ,  $\varepsilon = \varepsilon_0$

The rotor is in an unaligned position  $\varepsilon = \varepsilon_0$ . The winding is turned off, the current is zero. Then, the current is increased from zero to the final value  $i = i_0$ . During this time of magnetizing the rotor is assumed not to move or to be fixed by a brake. As a result, the next state is ...

- State 2:  $i = i_0$ ,  $\varepsilon = \varepsilon_0$

Until now, the electric work supplied to the motor is

$$W_{el1,2} = \int_1^2 i d\psi \quad (4.8)$$

which is the triangular area between the line 1-2 and the  $\psi$ -axis. During the transition between state 1 and state 2 no mechanical work is done.

Now, the rotor is released so that it can move to the aligned position. During that movement, the current is kept constant, resulting in the new state

- State 3:  $i = i_0$ ,  $\varepsilon = 0$

The rotor has now aligned to the stator poles. Until now, the electrical work fed into the motor is

$$W_{el\max} = W_{el1,3} = \int_1^3 i d\psi \quad (4.9)$$

which is the area between the curve 1-2-3 and the  $\psi$ -axis. During the transition from position 2 and 3, the motor provides the mechanical work

$$W_{me} = \int_1^3 \frac{\partial E_c}{\partial \varepsilon} d\varepsilon \quad (4.10)$$

This is the area of the triangle 1-2-3, i.e. the change of the area below the magnetization curve.

In the aligned position, the rotor is assumed to be fixed again and then the current is turned off, resulting in ...

- State 4:  $i = 0$ ,  $\varepsilon = 0$

During this demagnetization, the stored magnetic energy of the winding is returned to the electrical energy supply:

$$W_{el\,ret} = -\int_3^4 i d\psi \quad (4.11)$$

This is the area of the triangle between line 3-4 and the  $\psi$ -axis.

Neglecting ohmic voltage drops and hysteresis losses, the total balance results as

$$W_{me} = W_{el} = W_{el\max} - W_{el\,ret} \quad (4.12)$$

However, because the electrical supply must provide the full peak value  $W_{el\max}$  before a part of the work is returned, it is reasonable to introduce a power factor similar to that of common one-phase or three-phase AC systems like

$$\gamma = \frac{W_{me}}{W_{el\max}} = 1 - \frac{W_{el\,ret}}{W_{el\max}} \tag{4.13}$$

Using linear materials, this power factor cannot be better as 0.5 by principle as it can be seen directly from the graphical representation:

$$\gamma < 0.5 \tag{4.14}$$

A better power factor could be achieved running a modified cycle like 1, 2', 3, 4. However, that would exceed a maximum current limit  $I_{\max}$  so that it is not possible. The modified cycle 1, 2, 3', 4 would improve the power factor as well, but the result of converted work per cycle is smaller. So, the cycle 1, 2, 3, 4 provides really the best work exploitation within a given current limit. For operation at partial load, however, cycle 1, 2, 3', 4 is an alternative.

Curiously, the power factor improves in case of magnetic saturation as it is shown in the following figure. In this case values  $\gamma > 0.5$  are possible.

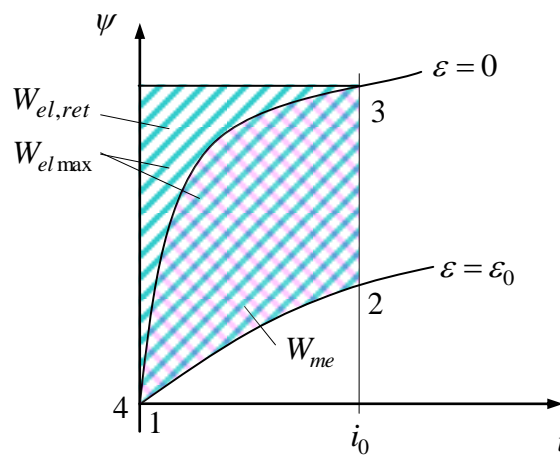


**Fig. 4-6:** Cycle of energy conversion of the switched reluctance motor with consideration of iron saturation

Naturally, the motor is not always in charge to operate at full load. Partial load is realized if either the current magnitude  $i_0$  is reduced and/or the switch-on and switch-off positions are changed.

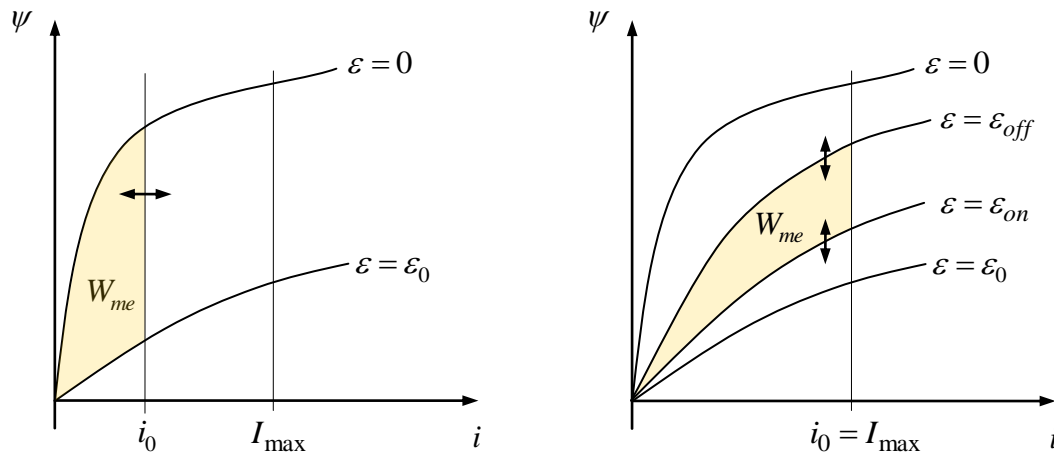


**Fig. 4-7:** Changing the converted energy and the mean torque by variation of the current magnitude or of the switch-on and switch-off positions

Usually, the torque of a switched reluctance motor will change more or less in one period. However, for the effect on the mechanical load, we are particularly interested in the averaged torque over one period  $\tau_0$  which corresponds with the 2/2-SRM to half of a mechanical revolution, i.e. an angle of  $180^\circ = \pi$ ,

$$\bar{T} = \frac{1}{\tau_0} \int_0^{\tau_0} T(t) dt = \frac{1}{\tau_0} \int_0^{\pi} \frac{T(t)}{\omega(t)} d\varepsilon = \frac{1}{\tau_0 \omega} \int_0^{\pi} T(t) d\varepsilon = \frac{W_{me}}{\pi} \quad (4.15)$$

The above derivation assumed the speed  $\omega(t)$  constant due to a sufficiently large inertia so that  $\omega$  can be pulled out of the integral resulting in  $\tau_0 \omega = \pi$ . The remaining integral yields the mechanical work of one period. Thus, the averaged torque is equal to the work except for a factor of  $\pi$ . Please note that also the units of the quantities *work* and *torque* are matching.

With a motor of rotor pole number  $N_r$ , the rotor rotates within a full electrical period (when all stator phases  $N_s$  have completed one cycle) only by the angle  $\Delta\varepsilon = \pi / N_r$ . Additionally, each of the  $N_s$  stator phases (or stator pole pairs) contribute with the same amount of work  $W_{me}$ , resulting in the total work balance

$$\Delta\varepsilon \bar{T} = N_s W_{me} \quad (4.16)$$

This yields the mean torque of a  $2N_s / 2N_r$ -Motors as

$$\bar{T} = N_s N_r \frac{W_{me}}{\pi} \quad (4.17)$$

Let the commutation frequency be  $f_K$  (the frequency of turning the current from one phase to the next). Then the resulting speed is

$$\omega = \frac{\Delta\varepsilon}{N_s / f_T} = \frac{\pi f_K}{N_s N_r} \quad (4.18)$$

and the averaged power is

$$\bar{P} = \omega \bar{T} = f_K W_{me} \quad (4.19)$$

### 4.3 Dynamic Behavior

So far, the energy conversion was discussed without considering the dynamic behavior. In reality, the transition between the idealized states require time, and during this time, the motor continues its rotation.

Starting point is Faraday's law:

$$\dot{\psi} = u - Ri \quad (4.20)$$

With

$$\psi = \psi(i, \varepsilon) \quad (4.21)$$

The time derivative of the flux follows as

$$\dot{\psi} = i \frac{\partial \psi}{\partial i} + \dot{\varepsilon} \frac{\partial \psi}{\partial \varepsilon} \quad (4.22)$$

and then the voltage

$$u = Ri + i \frac{\partial \psi}{\partial i} + \dot{\varepsilon} \frac{\partial \psi}{\partial \varepsilon} \quad (4.23)$$

Solving this equation for the derivative of the current yields

$$\dot{i} = \frac{u - Ri - \omega \frac{\partial \psi}{\partial \varepsilon}}{\frac{\partial \psi}{\partial i}} = \frac{u - Ri - \omega \frac{\partial^2 E_c}{\partial \varepsilon \partial i}}{L(i, \varepsilon)} = \frac{u - Ri - \omega \frac{\partial T}{\partial i}}{L(i, \varepsilon)}, \quad (4.24)$$

with

$$\omega = \dot{\varepsilon} \quad (4.25)$$

and the differential inductance

$$L(i, \varepsilon) = \frac{\partial \psi}{\partial i} = \frac{\partial^2 E_c}{\partial i^2} \quad (4.26)$$

In stationary case with constant current  $i = I = \text{const.}$  the required stationary voltage results as

$$U_0 = RI + \omega \frac{\partial \psi}{\partial \varepsilon} = RI + \omega \frac{\partial^2 E_c}{\partial \varepsilon \partial i} \quad (4.27)$$

For means of simplicity, the magnetic material is assumed as linear with a constant reluctance  $R_{Fe}$  in the following section. With this assumption, the inductance no longer depends on the current, but on the rotation angle only:

$$L(\varepsilon) = \frac{N^2}{R_{Fe} + R_L(\varepsilon)} \quad (4.28)$$

The flux is then

$$\psi = L(\varepsilon) i \quad (4.29)$$

The internal energy and the co-energy result as

$$E_i(\psi, \varepsilon) = \frac{\psi^2}{2L(\varepsilon)}, \quad (4.30)$$

$$E_c(i, \varepsilon) = \frac{1}{2} L(\varepsilon) i^2. \quad (4.31)$$

The torque is

$$T = \frac{\partial E_c}{\partial \varepsilon} = \frac{1}{2} L'(\varepsilon) i^2 \quad (4.32)$$

where

$$L'(\varepsilon) = \frac{dL(\varepsilon)}{d\varepsilon}. \quad (4.33)$$

The generation of torque relies essentially on the angle-dependent change of the inductance. However, the sign of the current is irrelevant. In order to reverse the torque and to operate the machine as a generator, the current has to be switched on in the area of decreasing inductance (while still positive speed is assumed). The resulting operation is then just the inverse cycle as mentioned above for the driving case.

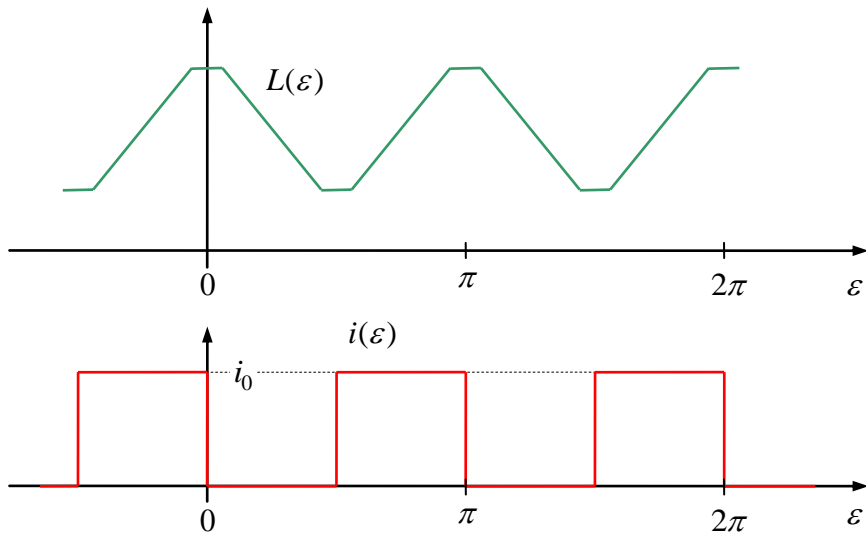


**Fig. 4-8:** Idealized shapes of inductance and current vs. position (driving operation)

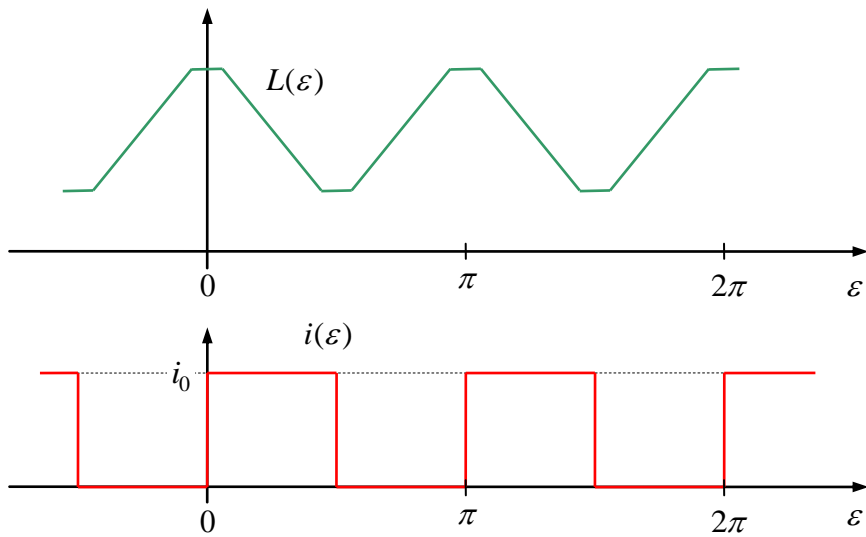


**Fig. 4-9:** Idealized shapes of inductance and current vs. position (regenerative operation)

Deviating from the idealized current shapes in the figure above, the current cannot be switched on and off instantaneously. The current obeys the differential equation

$$\dot{i} = \frac{u - Ri - \omega L'(\varepsilon)i}{L(\varepsilon)}. \tag{4.34}$$

For constant current the required voltage is

$$U_0 = (R + \omega L'(\varepsilon))I. \tag{4.35}$$

These equations remind us of DC motor's armature voltage, consisting of a ohmic voltage drop, a inductive voltage drop, and speed-varying electromagnetic force (EMF).

The time behavior in a working cycle should now be discussed in detail for various cases of the speed. The feeding electrical supply is considered as a freely controllable voltage source within the limits  $-U_{\max} < u(t) < U_{\max}$ .

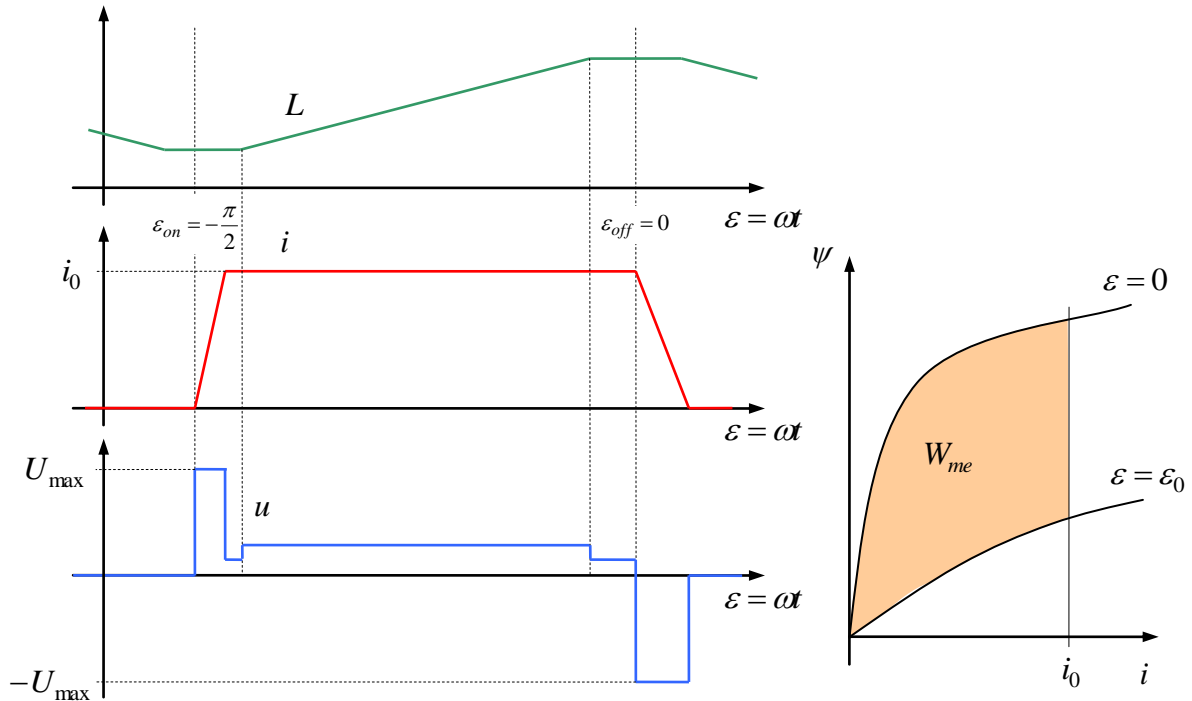


**Fig. 4-10:** Behavior at small speed

At small speed, the current is switched on at the position with smallest inductance and switched off at the aligned position. In order to switch-on and to switch-off the current as quickly as possible, maximum and minimum voltages are applied. The current rise is quicker as the decay, because the inductance in the aligned position is larger as at switch-on. If rise and decay of current are finished within the intervals of approximately constant inductance, the amount of converted energy is really that from the idealized view (left figure).

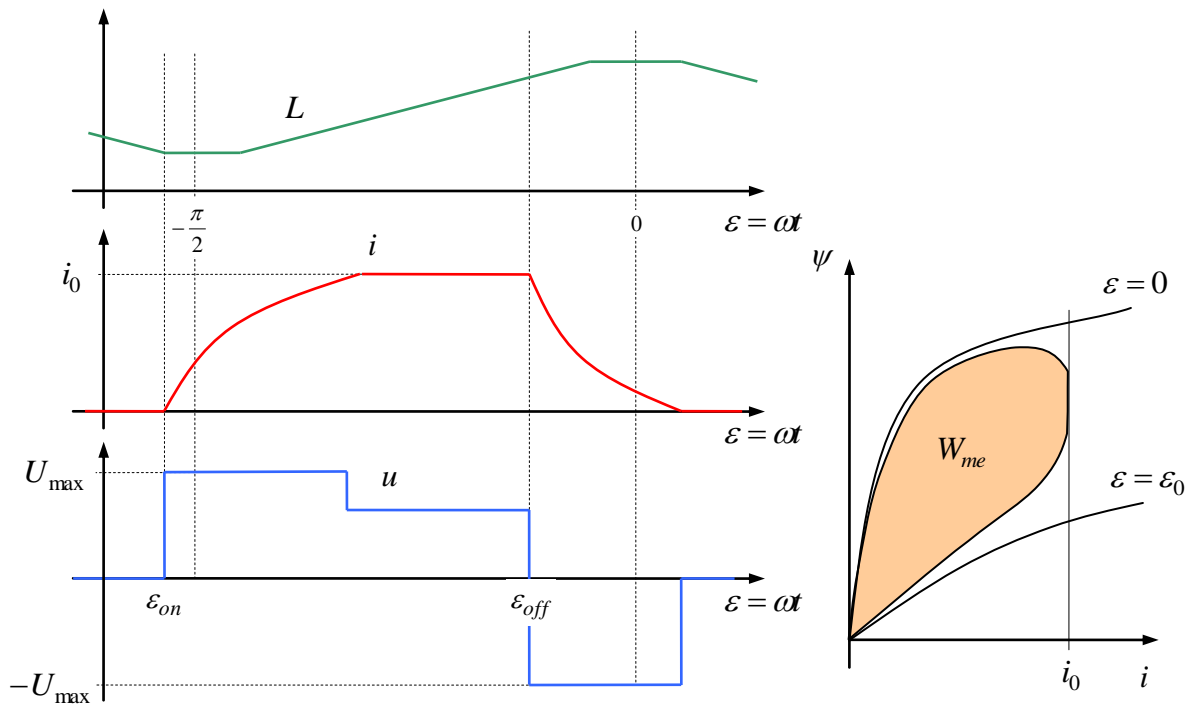


**Fig. 4-11:** Behavior at medium speed

At higher speed, the current rise takes more time because of the increased countervoltage. It must also be considered that the angle is passed through faster at higher speed, also contributing to a flatter shape of the current vs. angle. The countervoltage, however, helps during the demagnetization phase. Switch-on and switch-off should be triggered earlier compared to the case of small speed in order to increase the torque as quickly as possible and to bring it down before the inductance decreases again and would generate negative torque. Due to the rounded shape of the current a cut back of the converted work and also of the torque has to be taken into account compared to the idealized cycle.

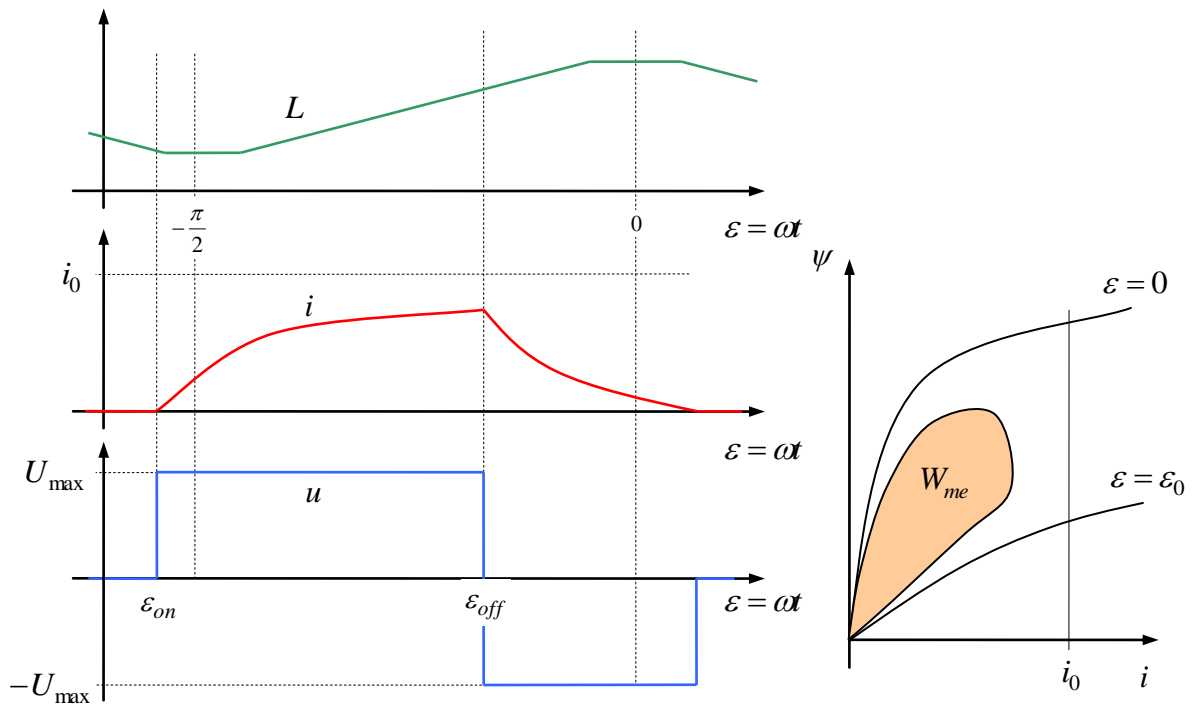


**Fig. 4-12:** Behavior at high speed

At high speed, switch-on and switch-off angles have to be pulled ahead. The countervoltage is now so large that current will no longer reach its previous peak value. The exploitation of work and torque decreases distinctly. As an approximation, the torque decreases inversely proportional to speed.

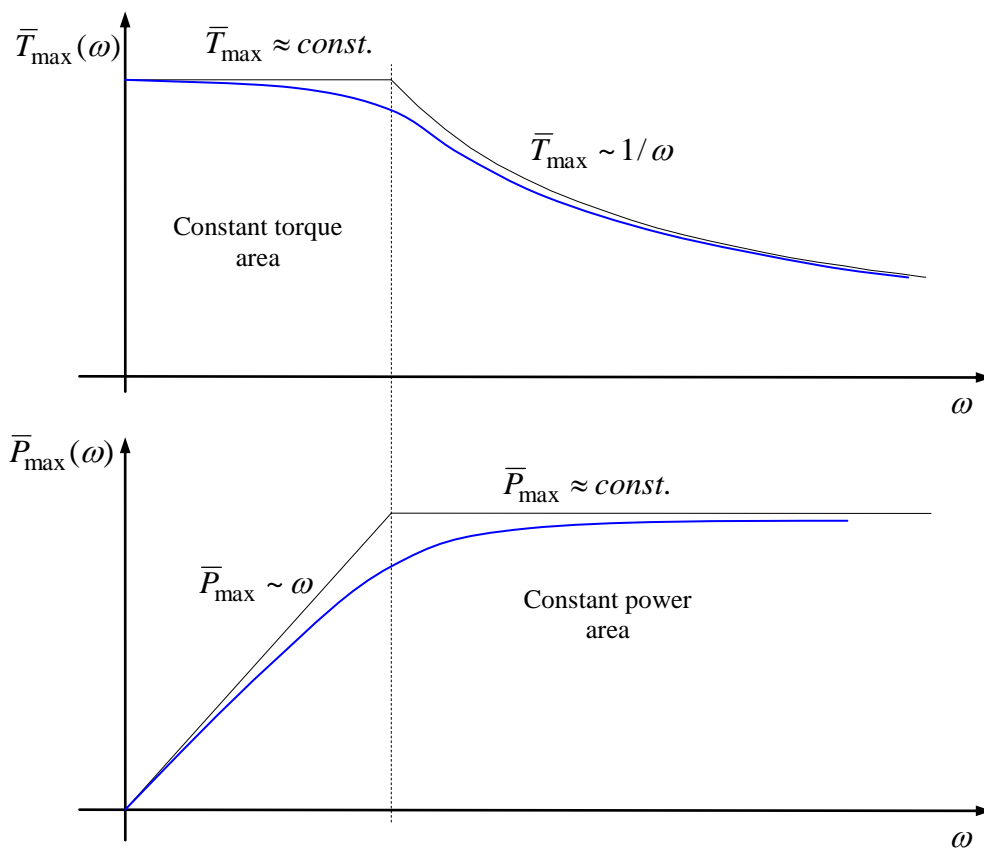


**Fig. 4-13:** Maximal torque and maximal power vs. speed

#### 4.4 Converter

The torque of a switched reluctance motor does not depend on the sign of the current. That is why the converter can be designed for only one current polarity. However, both voltage polarities are required since negative voltage is needed to quickly demagnetize the phases. The specified converter is then a 2-quadrant converter.

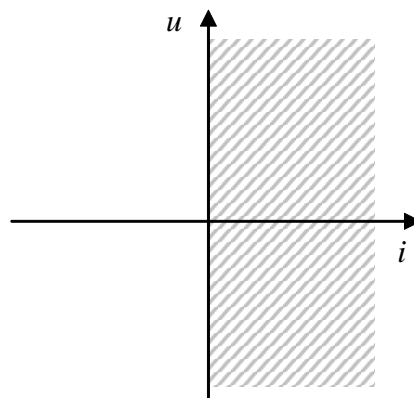


**Fig. 4-14:** Required current-voltage-area of a SRM phase

The specified converter can be derived from the 4-quadrant converter that is already known from Section 3.6. Removing all devices which are not necessary for the positive current polarity yields the 2-quadrant converter which is depicted in the following figure. It is also known as asymmetrical half-bridge.

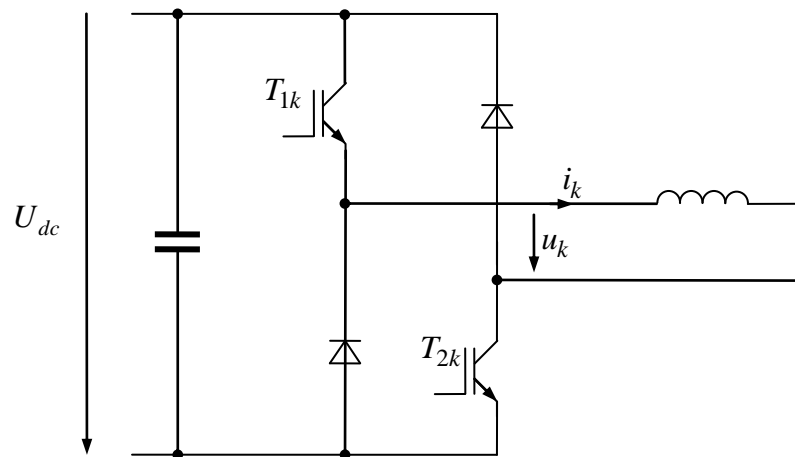


**Fig. 4-15:** 2-quadrant converter (half-bridge) as converter in order to supply one phase of a switched reluctance motor

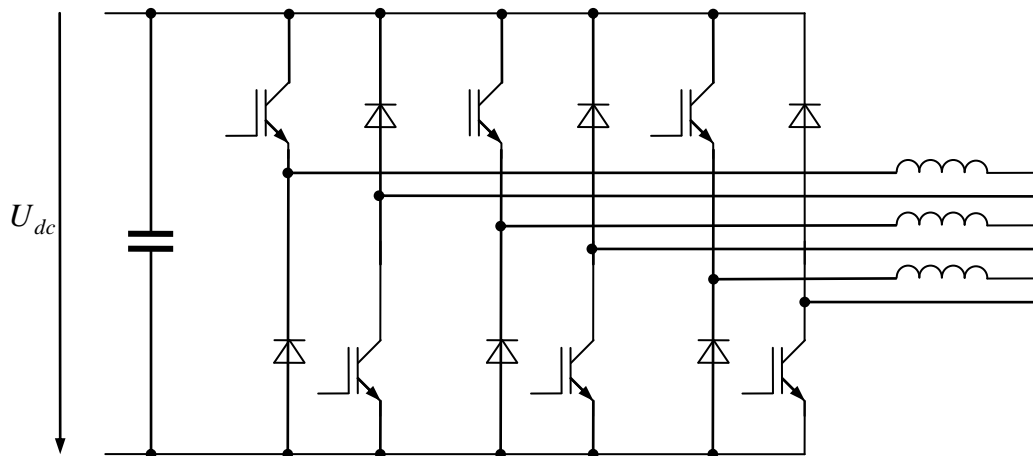


**Fig. 4-16:** Converter for a three-phase switched reluctance motor

Both endings of each phase winding of a switched reluctance motor have to be provided as external terminals. They are not allowed to be connected as star or delta circuit as in the cases of normal AC motors or a magnetic bearing. The wiring effort is thus larger as with AC motors. The converter consists of the same number of transistors and diodes as the AC motor converter. However, the converter topology is different so that standard AC modules cannot be used.

The voltage of a winding results from the following switching table. In the states marked with stars \*, only diodes are conducting. So, the declared voltage is only valid, if a current is actually flowing, i.e.  $i_k > 0$ . After end of conduction, the voltage is determined by load itself.

$T_{1k}$	$T_{2k}$	$u_k$
off	off	$-u_{dc}$ *
off	on	0 *
on	off	0 *
on	on	$+u_{dc}$

The transistors are chopped with the help of a pulse width modulation or a suitable current hysteresis or peak mode control. The approach of Section 3.7 can be applied also here.

## 5 Stepping Motors

Stepping motors are characterized by the fact that they are operated usually without any position sensor. Rather, an adequate electrical command (often block-shaped currents) should ensure that the motor moved by a certain increment so that the actual position can be determined by counting the electrical cycles.

Switched reluctance motors or brushless electronically commutated DC motors could be operated, in principle, as stepping motors. Both motor types do not generate any holding force or torque when the current is zero. The motor can move during the switched-off mode depending on the applied load so that the position may be unknown when starting next time. If the application requires to retain a definite position even in switched-off state, so-called hybrid motors are preferred, i.e. the varying reluctance is combined with permanent magnets.

Fig. 5-1 shows the example of a linear two-phase stepping motor. The simplest operation mode is to apply block-shaped currents so that the motor can be positioned with an accuracy of one pole pitch of the passive stator. Using current overlapping of both phases or sinusoidally shaped currents, even a finer positioning can be achieved.

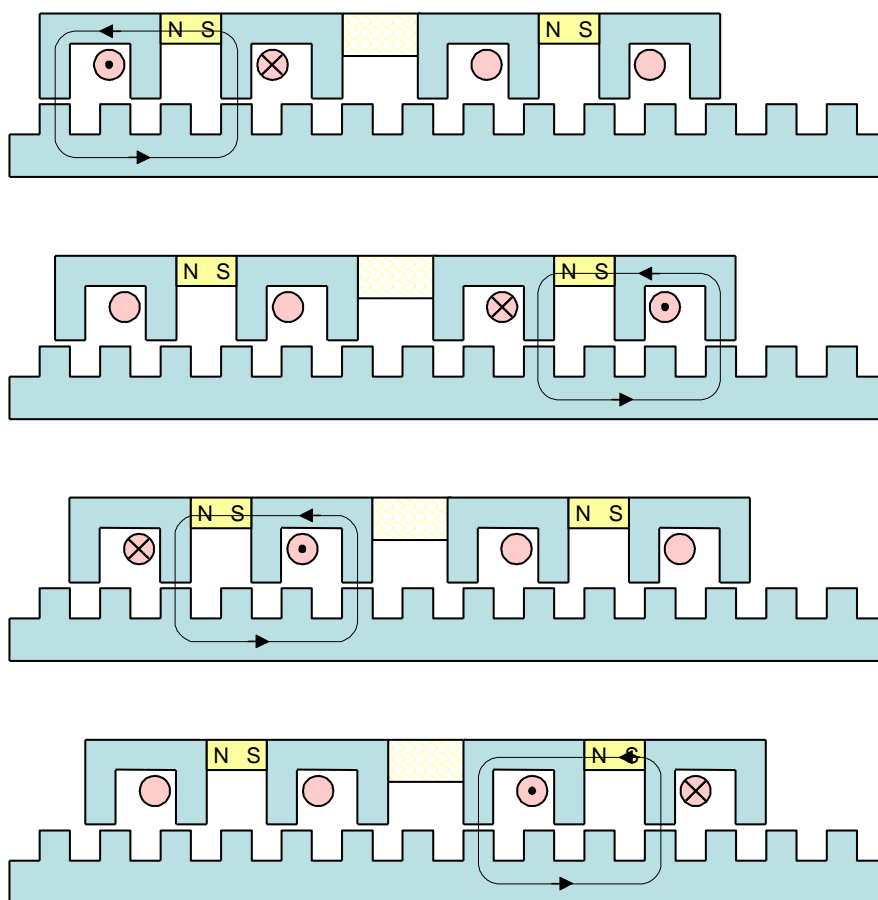


**Fig. 5-1:** Linear hybrid stepping motor

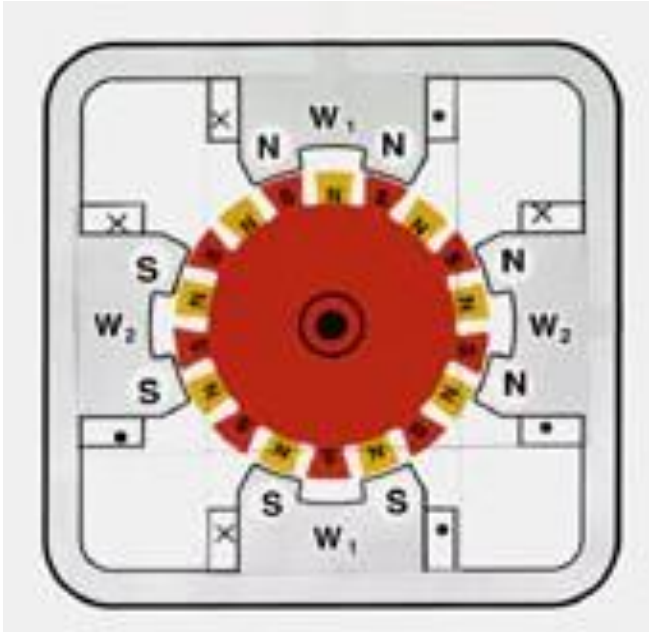
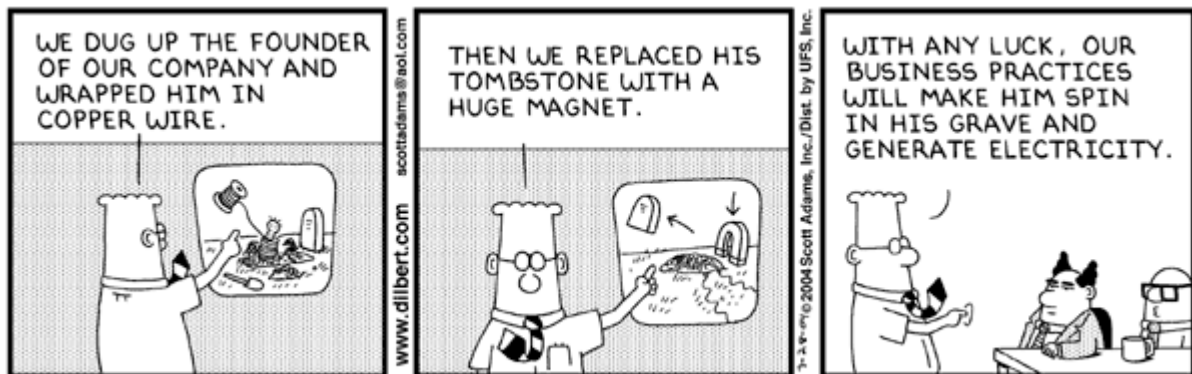


Fig. 5-2: Hybri stepping motor

## 6 Gleichstrommotor<sup>6</sup>



© UFS, Inc.

Fig. 6-1:

### 6.1 Wirkprinzip

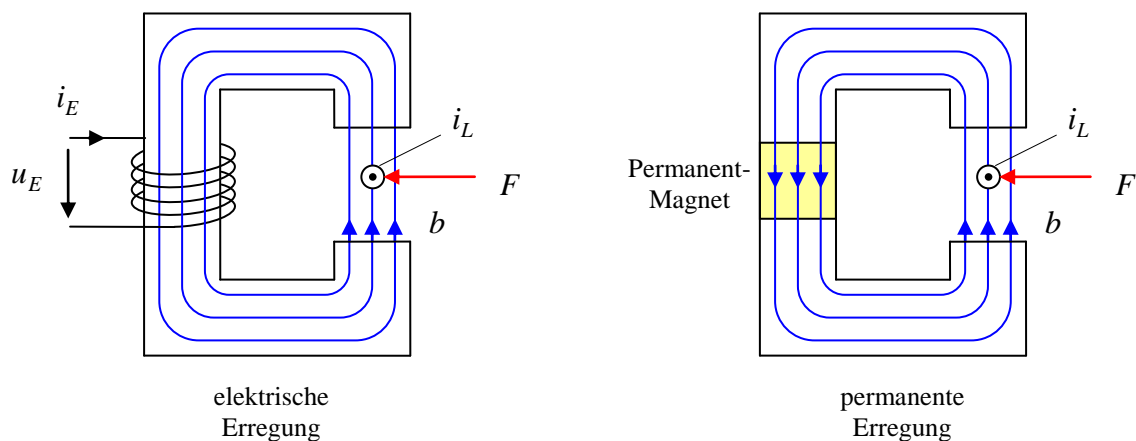


Fig. 6-2: Wirkprinzip

Kraftwirkung auf den stromdurchflossenen Leiter (*Lorentzkraft*):

$$F = i_L b l \tag{6.1}$$

$l$ : Länge des Leiters

<sup>6</sup> The following pages are particularly only a repetition of a chapter of the basic bachelor course „basics of electrical engineering. The pages are provided here only for reasons of completeness. As the basics of DC motors can be learnt from many textbooks, an English translation is only provided starting from Chapter 6.12.

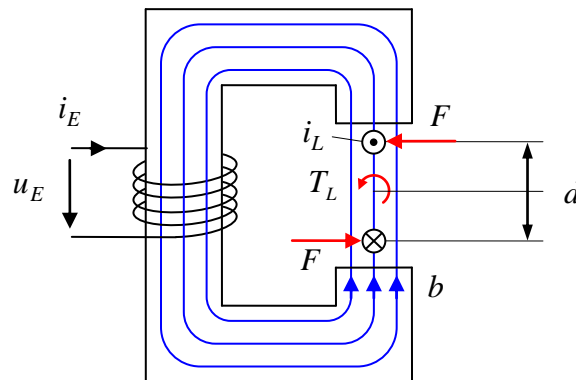


**Fig. 6-3:** Drehmoment auf Leiterschleife

*Drehmoment (torque):*

$$T_L = 2F \frac{d}{2} = Fd = i_L b d l \quad (6.2)$$

Induzierte Spannung in der Leiterschleife, entweder aus Induktionsgesetz:

$$u_L = \dot{\psi}_L = 2b \frac{d}{2} \omega l = b d l \omega \quad (6.3)$$

oder aus der Leistungsbilanz:

$$p_{el} = p_{mech} \quad (6.4)$$

$$u_L i_L = T_L \omega = i_L b d l \omega \quad (6.5)$$

$$u_L = b d l \omega \quad (6.6)$$

Der Term

$$\phi_0 = b d l \quad (6.7)$$

lässt sich als der magnetische Fluss deuten, der die Leiterschleife bei senkrechter Ausrichtung und bei homogener Flussdichte durchdringen würde. Hiermit:

$$u_L = \dot{\phi}_0 \omega \quad (6.8)$$

$$T_L = \phi_0 i_L \quad (6.9)$$

## 6.2 Aufbau

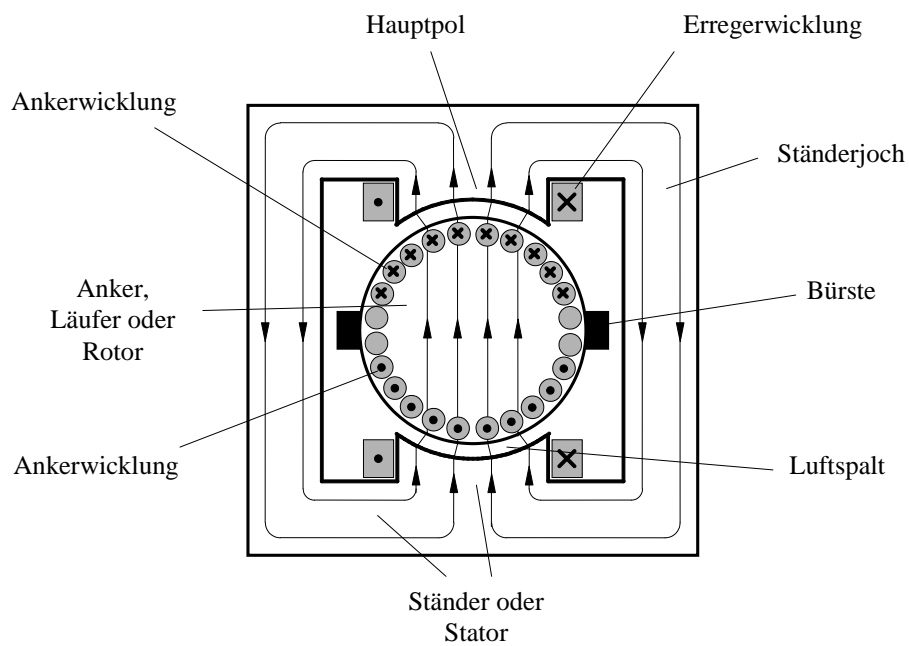


**Fig. 6-4:** Schnittskizze eines Gleichstrommotors

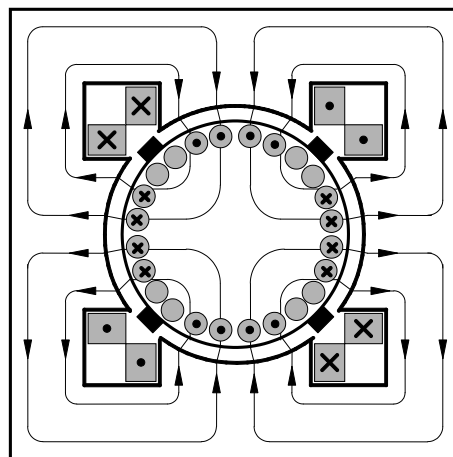


**Fig. 6-5:** Gleichstrommotor mit zwei Polpaaren,  $p = 2$

### 6.3 Kommutator und Ankerwicklungsschemata

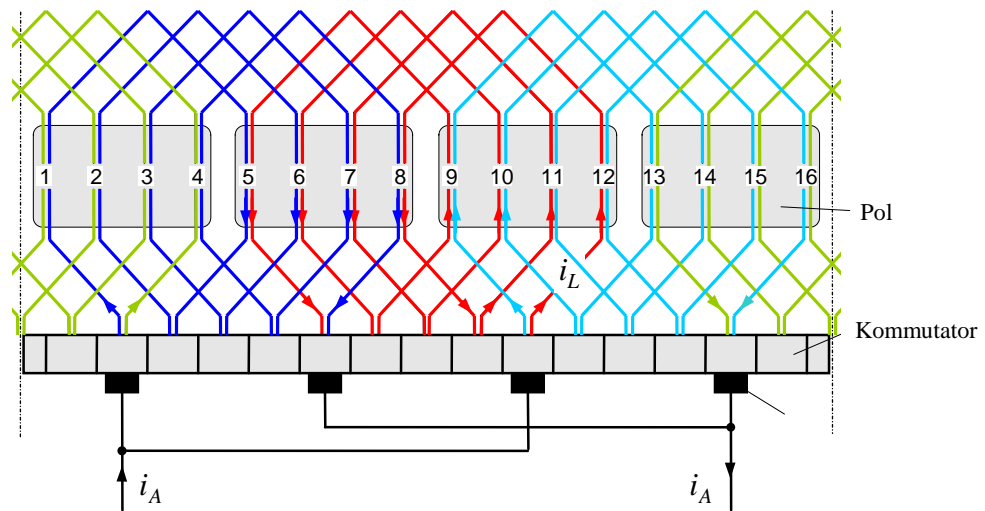


**Fig. 6-6:** Wicklungsschema des Ankers  
 Schleifenwicklung, hier für  $p = 2$ ,  
 Zahl der parallelen Zweige  $2a = 2p$

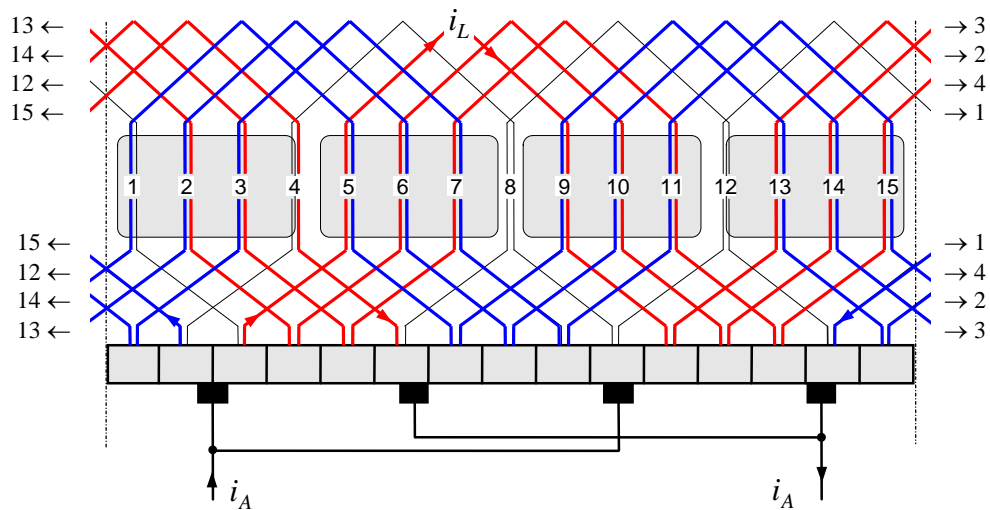


**Fig. 6-7:** Wicklungsschema des Ankers  
 Wellenwicklung, hier für  $p = 2$ ,  
 Zahl der parallelen Zweige  $2a = 2$

### 6.4 Kommutierung und Wendepolwicklung

Stichworte:

Kurzschluss der zu kommutierenden Leiterschleife durch den Kommutator.

Kurzgeschlossene Leiterschleife friert den Fluss ein:

$$i_L = u_L = 0 \Rightarrow \psi_L = const. \tag{6.10}$$

Daher vor dem Kurzschluss dafür sorgen, dass Leiterschleife frei vom Fluss des Ankerfeldes wird -> Einführung der Wendepolwicklung -> dadurch natürliche Stromkommutierung

Magnetische Durchflutung der Wendepolwicklung muss derjenigen der Ankerstromwicklung entsprechen.

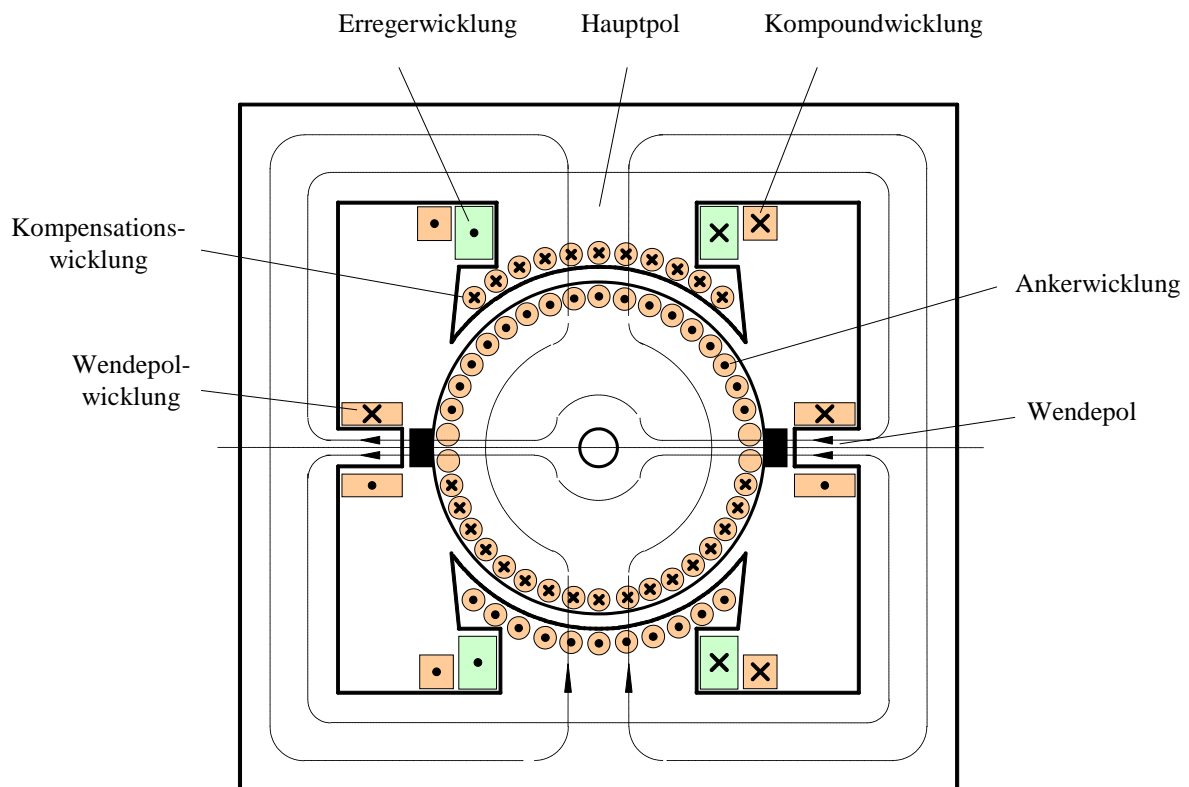


**Fig. 6-8:** Gleichstrommotor mit Erreger-, Anker-, Wendepol-, Kompound- und Kompensationswicklung

## 6.5 Ankerrückwirkung, Kompensations- und Kompoundwicklung

Stichworte:

Ankerfeld verursacht Feldverzerrung in den Erregerpolen. Bei linearem Material wäre dies kein Nachteil. Die einseitige magnetische Sättigung im Erregerpol führt jedoch zur Erhöhung des gesamten magnetischen Widerstands im Erregerkreis und somit zur Schwächung des Erregerflusses.

Gegenmaßnahmen

- Erhöhung der magnetischen Spannung im magnetischen Erregerkreis durch Kompoundwicklung, welche vom Ankerstrom durchflossen wird
- Einführung der Kompensationswicklung zur Kompensation der Ankerrückwirkung, ebenfalls vom Ankerstrom durchflossen.

## 6.6 Mathematische Modellierung

Bezeichnungen:

$T_L$	Drehmoment einer Leiterschleife
$T$	gesamtes Drehmoment des Ankers (Luftspaltdrehmoment)
$N_A$	Zahl der Anker-Leiterschleifen
$N_E$	Gesamtzahl aller Erregerwindungen
$2a$	Zahl der parallelen Ankerstromzweige
$p$	Polpaarzahl
$\alpha$	Polbedeckung, Verhältnis der aktiven Polflächen zur Ankeroberfläche
$\phi_E$	Erregerfluss
$b_E$	Erregerflussdichte
$l$	aktive Länge des Ankers
$d$	Ankerdurchmesser
$\delta$	Luftspalt
$A_{pol}$	Polfläche

Resultierendes auf den Anker wirkendes Drehmoment:

$$T = N_A T_L \alpha = N_A \phi_0 \alpha i_L = N_A b_E d l \alpha i_L \quad (6.11)$$

Ankerstrom  $i_A$  teilt sich auf  $2a$  Zweige auf:

$$i_L = \frac{1}{2a} i_A \quad (6.12)$$

$$\phi_E = b_E A_{pol} = \frac{\pi d l \alpha}{2p} b_E \quad (6.13)$$

Damit:

$$T = \frac{p N_A}{a \pi} \phi_E i_A = c \phi_E i_A = \psi'_E i_A \quad (6.14)$$

wobei

$$c = \frac{p N_A}{a \pi} \quad , \quad \psi'_E = c \phi_E$$

Die induzierte Spannung (*elektromotorische Kraft, EMK*) folgt wieder aus der Leistungsbilanz,

$$u_i = c \phi_E \omega = \psi'_E \omega, \quad (6.15)$$

oder alternativ durch Summation der induzierten Spannungen der in Reihe geschalteten Leiterschleifen.

Spannungsgleichung des Ankerkreises unter Berücksichtigung des Ankerwiderstands  $R_A$ , der Ankerinduktivität  $L_A$  und des Bürstenspannungsabfalls  $u_B$ :

$$u_A = u_i + L_A \dot{i}_A + R_A i_A + 2u_B \quad (6.16)$$

Mit guter Genauigkeit kann der Bürstenspannungsabfall  $u_B$  also eine konstante, vom Ankerstrom unabhängige Spannung von etwa 1 V angesetzt werden.

Erregerstromkreis:

$$u_E = L_E \dot{i}_E + R_E i_E \quad (6.17)$$

Beachte: Im Allgemeinen sind zwischen zwei Wicklungen Gegeninduktivitäten zu berücksichtigen. Die Flüsse von Erreger- und Ankerwicklung sind aber durch die zueinander senkrechte Anordnung nicht miteinander verkettet, so dass die Gegeninduktivität zwischen diesen Wicklungen Null ist.

Magnetischer Kreis der Erregung:

Magnetische Leitfähigkeit des Erregerkreises

$$\Lambda_E = \frac{1}{R_{magE}} = \frac{\mu_0 A_{Pol}}{2\delta} = \frac{\mu_0 \alpha \pi d l}{2\delta \cdot 2p} = \frac{\mu_0 \alpha \pi d l}{4p\delta} \quad (6.18)$$

Induktivität:

$$L_E = \Lambda_E \frac{N_E^2}{p} = \Lambda_E \frac{N_E^2}{p} \quad (6.19)$$

Erregerfluss:

$$\phi_E = \Lambda_E \frac{N_E}{p} i_E = \frac{L_E}{N_E} i_E = \frac{\mu_0 \alpha \pi d l N_E}{4p^2 \delta} i_E \quad (6.20)$$

$$\psi'_E = c \phi_E = \frac{c L_E}{N_E} i_E = L'_E i_E, \quad L'_E = \frac{c L_E}{N_E} = \frac{\mu_0 \alpha d l N_E N_A}{4a p \delta}$$

Zusammenfassung der wichtigsten Gleichungen:

$$T = \psi'_E i_A$$

$$\psi'_E = L'_E i_E$$

$$u_A = \psi'_E \omega + L_A \dot{i}_A + R_A i_A + 2u_B \quad (6.21)$$

$$u_E = L_E \dot{i}_E + R_E i_E \quad (6.22)$$

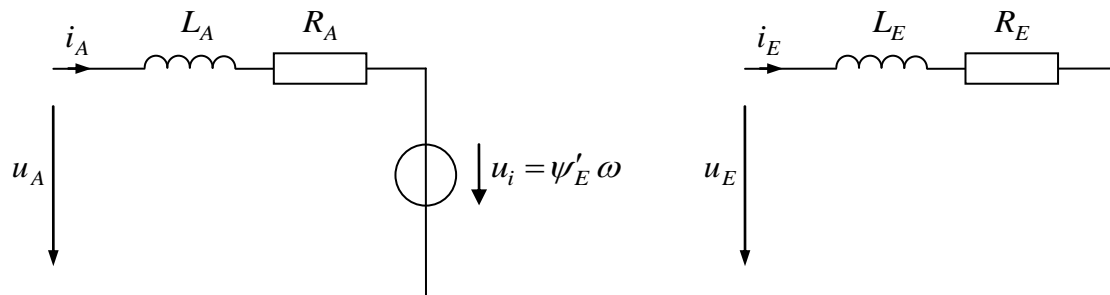


**Fig. 6-9:** Ersatzschaltbilder des Anker- und des Erregerkreises

### Dynamisches Verhalten

Das dynamische Verhalten des Anker- bzw. Erregerstroms entspricht dem einer  $RL$ -Glieder, die maßgeblichen Anker- und Erregerzeitkonstanten sind

$$\tau_A = \frac{L_A}{R_A} \quad \text{und} \quad \tau_E = \frac{L_E}{R_E}$$

## 6.7 Elektrische und mechanische Leistung, Wirkungsgrad

Elektrische Leistung (Verbraucherzählpeilsystem):

$$P_{el} = P_{elA} + P_{elE} = u_A i_A + u_E i_E \quad (6.23)$$

Mechanische Leistung (Erzeugerzählpeilsystem):

$$P_{mech} = \omega T \quad (6.24)$$

Energiebilanz:

$$P_{el} = \dot{w}_A + \dot{w}_E + P_V + P_{mech} \quad (6.25)$$

Verlustleistung:

$$P_V = P_{VA} + P_{VE} = R_E i_E^2 + R_A i_A^2 \quad (6.26)$$

Innere Energien:

$$w_A = \frac{1}{2} L_A i_A^2, \quad w_E = \frac{1}{2} L_E i_E^2$$

*Wirkungsgrad* des Ankerkreises (Vernachlässigung der Erregerverluste) im stationären Zustand für den motorischen Betrieb:

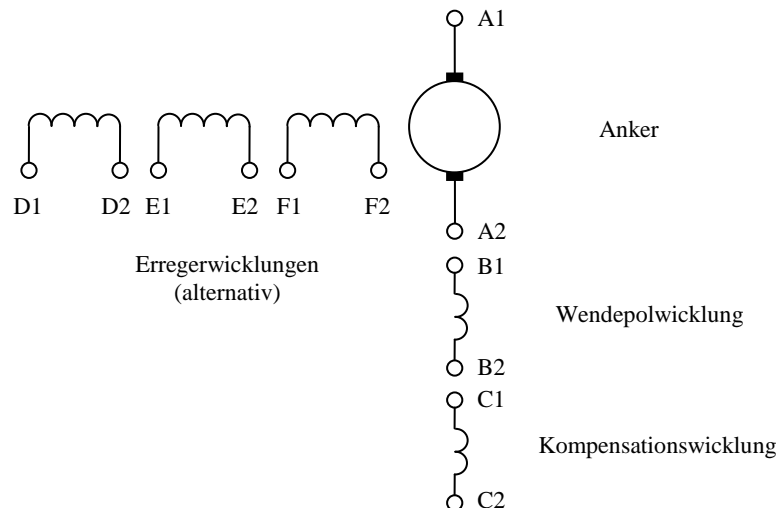
$$\eta = \frac{P_{mech}}{P_{elA}} = \frac{\omega T}{U_A I_A} = \frac{\omega T}{(R_A I_A + \psi'_E \omega) I_A} = \frac{\omega T}{\left( R_A \frac{T}{\psi'_E} + \psi'_E \omega \right) \frac{T}{\psi'_E}} = \frac{\omega}{\omega + \frac{R_A}{\psi'^2_E} T} = \frac{1}{1 + \frac{R_A}{\psi'^2_E} \frac{T}{\omega}} \quad (6.27)$$

## 6.8 Schaltungsarten, Klemmenbezeichnungen und Schaltzeichen

Man unterscheidet verschiedene Schaltungsarten:

- *Fremderregung*: Erreger- und Ankerkreis werden aus verschiedenen elektrischen Quellen gespeist
- *Nebenschluss*: Erreger- und Ankerkreis sind parallel geschaltet
- *Reihenschluss*: Erreger- und Ankerkreis sind in Reihe geschaltet

Wicklung	Klemmen
Ankerwicklung	A1, A2
Wendepolwicklung	B1, B2
Kompensationswicklung	C1, C2
Erregerwicklung für Reihenschlusschaltung	D1, D2
Erregerwicklung für Nebenschlusschaltung	E1, E2
Erregerwicklung für Fremderregung	F1, F2


**Fig. 6-10:**

## 6.9 Fremderregter und permanent erregter Motor

Beim fremderregten Betrieb werden Erreger- und Ankerwicklung unabhängig voneinander gespeist. Typischerweise wird der Erregerstrom und damit der Erregerfluss konstant gehalten,

$$i_E = \text{const.} \quad \Rightarrow \quad \phi_E = \text{const.} \quad \text{bzw.} \quad \psi'_E = \text{const.}, \quad (6.28)$$

Dies gelingt durch Aufschaltung einer konstanten Erregerspannung  $u_E$  allerdings nur unvollkommen, da sich der Strom aufgrund des temperaturabhängigen Widerstands  $R_E$  verändern kann. Ggf. wird eine Erregerstromregelung vorgesehen.

Beim permanent erregten Motor wird der Erregerfluss von einem Permanentmagneten erzeugt. Sein Verhalten gleicht dem des fremderregten Motors mit konstantem Erregerstrom.

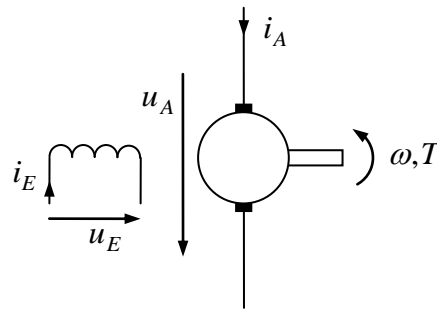


**Fig. 6-11:** Fremderregter Gleichstrommotor

**Stationäres Strom-Spannungs-Verhalten bei konstanter Drehzahl**

$$U_A = \psi'_E \omega + R_A I_A \tag{6.29}$$

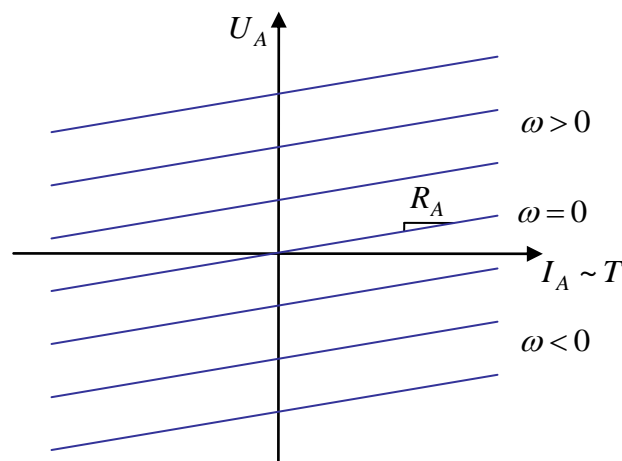


**Fig. 6-12:** Stationäre Kennlinien von Ankerstrom und -spannung

**Stationäres Drehmoment-Drehzahl-Verhalten bei konstanter Spannung**

Einsetzen der Drehmomentbeziehung in die Spannungsgleichung:

$$U_A = \frac{R_A}{\psi'_E} T + \omega \psi'_E \tag{6.30}$$

Auflösen nach  $\omega$  ergibt das stationäre Drehmoment-Drehzahlverhalten für konstante Ankerspannung:

$$\omega = \frac{U_A}{\psi'_E} - \frac{R_A T}{\psi'^2_E} \tag{6.31}$$

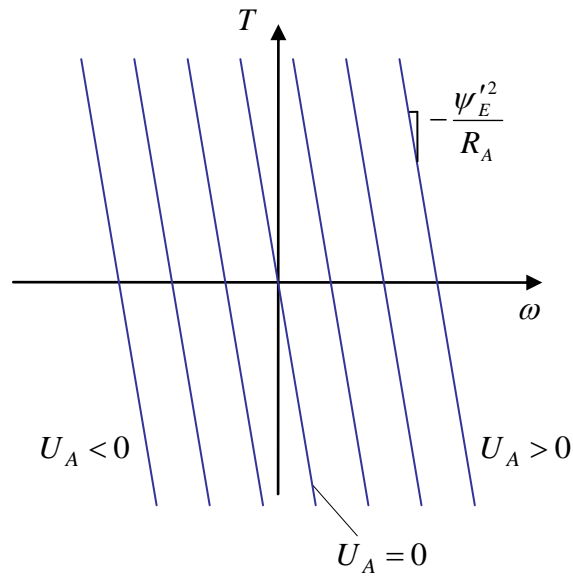


**Fig. 6-13:** Stationäre Kennlinien von Drehmoment und Drehzahl bei konstanter Ankerspannung

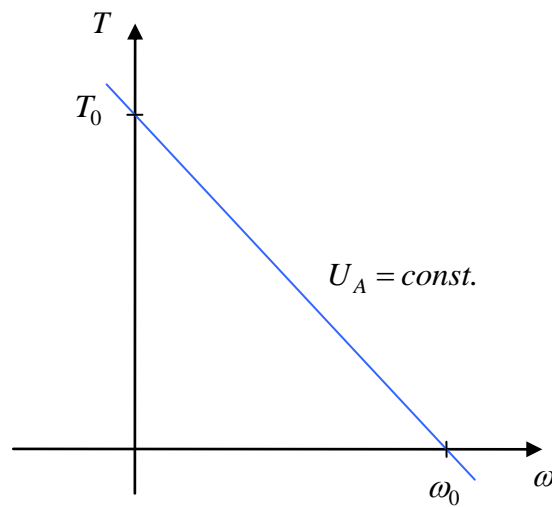


**Fig. 6-14:** Losbrech-Drehmoment und Leerlaufdrehzahl bei konstanter Ankerspannung

Losbrech-Drehmoment und –Ankerstrom ( $\omega = 0$ ):

$$I_{A0} = \frac{U_A}{R_A}, \quad T_0 = \frac{U_A \psi_E'}{R_A}$$

Leerlaufdrehzahl ( $T = 0$  bzw.  $I_A = 0$ )

$$\omega_0 = \frac{U_A}{\psi'_E} \tag{6.32}$$

Wird der Gleichstrommotor mit konstanter Ankerspannung betrieben, entsteht beim Einschalten aus dem Stillstand heraus ein sehr großer Anlaufstrom, der ggf. den zulässigen Maximalwert überschreitet. Bei kleinen Motoren mit geringer Trägheit, die schnell beschleunigen, kann ein derartiger kurzzeitiger Überstrom ggf. hingenommen werden. Andernfalls muss der Anlaufstrom begrenzt werden. Die klassische Vorgehensweise arbeitet mit Anlaufwiderständen vorgenommen, die mit steigender Drehzahl dann überbrückt werden.

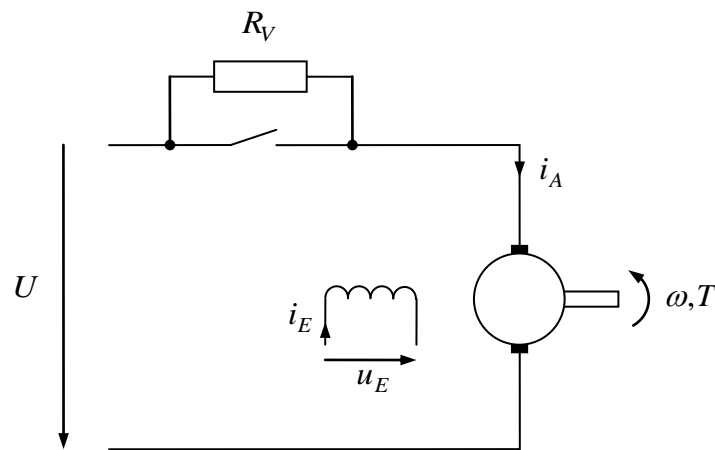


**Fig. 6-15:** Betrieb mit Vorwiderstand

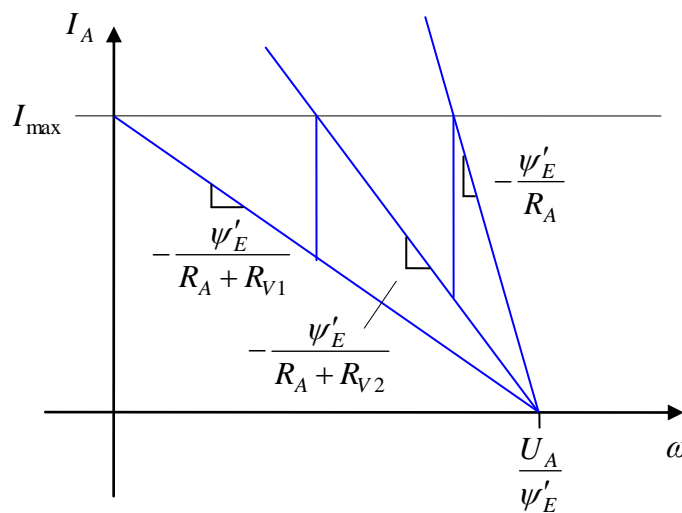


**Fig. 6-16:** Anfahren mit Vorwiderständen

## 6.10 Nebenschlussmotor

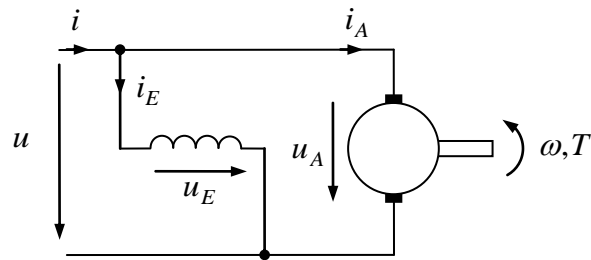


**Fig. 6-17:** Nebenschlusschaltung

$$u_A = R_A i_A + \psi'_E \omega + L_A \dot{i}_A = R_A i_A + L'_E i_E \omega + L_A \dot{i}_A \quad (6.33)$$

$$u_E = R_E i_E + L_E \dot{i}_E \quad (6.34)$$

$$T = \psi'_E i_A = L'_E i_E i_A \quad (6.35)$$

Nebenschluss:

$$u = u_A = u_E, \quad i = i_A + i_E$$

Stationäres Verhalten:

$$I_E = \frac{U}{R_E} \quad (6.36)$$

$$I_A = \frac{U - L'_E I_E \omega}{R_A} = \frac{U - L'_E U / R_E \omega}{R_A} = \frac{1 - L'_E / R_E \omega}{R_A} U \quad (6.37)$$

$$I = I_E + I_A = \left[ \frac{1}{R_A} + \frac{1}{R_E} - \frac{L'_E \omega}{R_A R_E} \right] U \quad (6.38)$$

$$T = L'_E I_E I_A = L'_E \frac{1 - L'_E / R_E \omega}{R_A R_E} U^2 \quad (6.39)$$

## 6.11 Reihenschlussmotor

$$u_A = R_A i_A + \psi'_E \omega + L_A \dot{i}_A = R_A i_A + L'_E i_E \omega + L_A \dot{i}_A \quad (6.40)$$

$$u_E = R_E i_E + L_E \dot{i}_E \quad (6.41)$$

$$T = \psi'_E i_A = L'_E i_E i_A \quad (6.42)$$

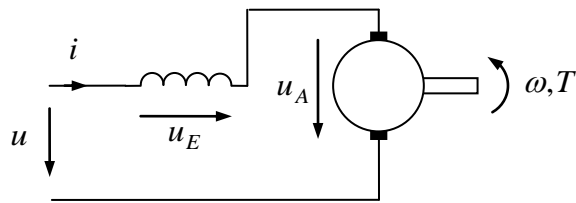


**Fig. 6-18:** Reihenschlusschaltung

Reihenschluss:

$$u = u_A + u_E \quad , \quad i = i_A = i_E$$

$$R = R_A + R_E \quad , \quad L = L_A + L_E$$

$$u = R i + L'_E i \omega + L \dot{i}$$

$$u = (R + L'_E \omega) i + L \dot{i} \quad (6.43)$$

$$u = R'(\omega) i + L \dot{i}$$

Drehzahlabhängiger effektiver Widerstand:

$$R'(\omega) = R + L'_E \omega \quad (6.44)$$

$$T = \psi'_E i = L'_E i^2 \quad (6.45)$$

Quadratische Abhängigkeit des Drehmoments vom Strom, Änderung des Vorzeichens ist nur durch Wechsel der Verschaltung von Erreger- und Ankerwicklung möglich,  $i = i_A = -i_E$ .

Daher kann ein Reihenschlussmotor auch mit Wechselspannung gespeist werden. Sinusförmige Speisung mit der Frequenz  $\omega_{el}$ , Schreibweise mit komplexen Effektivwertzeigern:

$$\underline{U} = R'(\omega) \underline{I} + j\omega_{el} L \underline{I} \quad (6.46)$$

$$\underline{I} = \frac{\underline{U}}{R'(\omega) + j\omega_{el} L} \quad (6.47)$$

Das Drehmoment pulsiert mit  $2\omega_{el}$ . Drehmomentmittelwert:

$$\bar{T} = L'_E \bar{i}^2 = L'_E I^2 = \frac{L'_E U^2}{R'^2(\omega) + \omega_{el}^2 L^2} \quad (6.48)$$

Drehmoment-Drehzahl-Charakteristik:

$$\left( R'^2(\omega) + \omega_{el}^2 L^2 \right) \bar{T} = L'_E U^2 \quad (6.49)$$

$$\left( (R + L'_E \omega)^2 + \omega_{el}^2 L^2 \right) \bar{T} = L'_E U^2 \quad (6.50)$$

Wird der Reihenschlussmotor mit konstanter Spannung betrieben und dabei mechanisch entlastet,  $T \rightarrow 0$ , wächst die Drehzahl über alle Grenzen,  $\omega \rightarrow \infty$  (s. Bild).

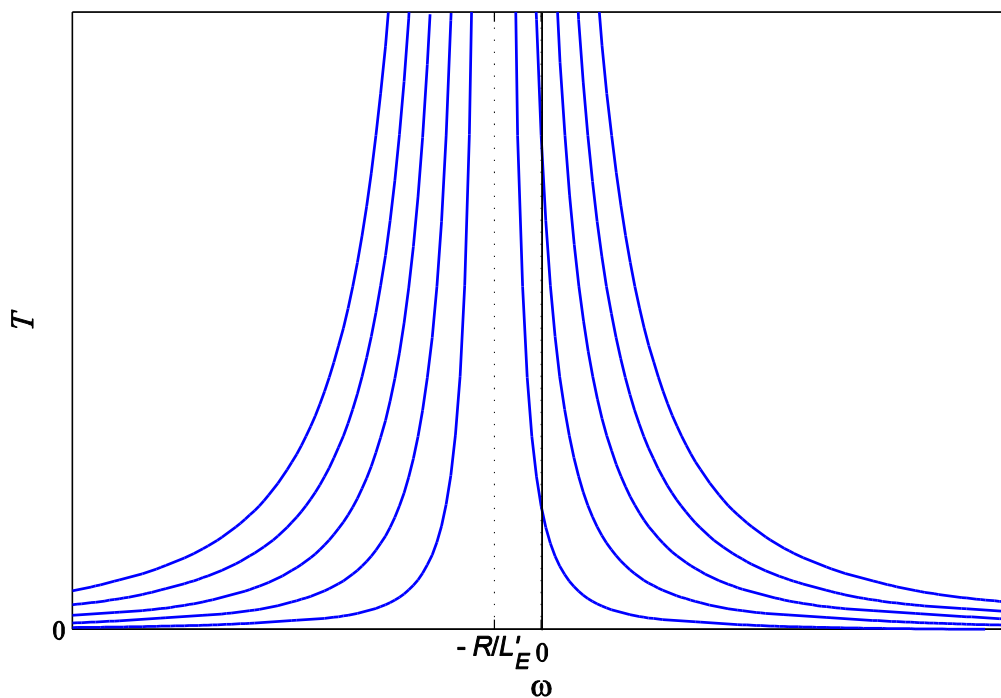


**Fig. 6-19:** Drehmoment-Drehzahl-Kennlinien des Reihenschlussmotors für verschiedene Spannungen  $U$  bei Gleichspannungsspeisung

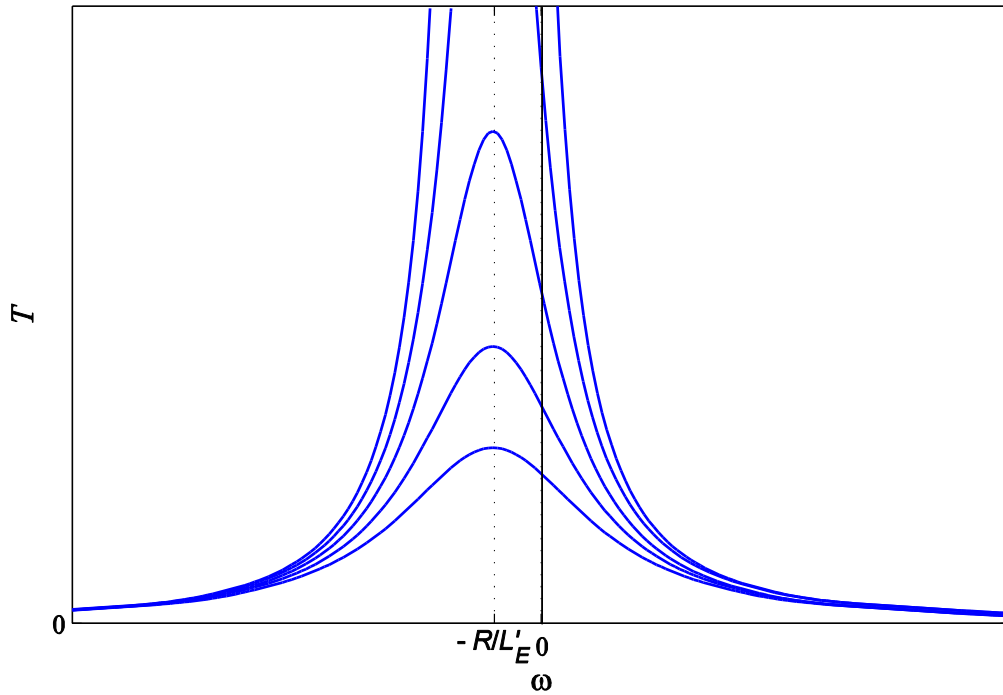


**Fig. 6-20:** Drehmoment-Drehzahl-Kennlinien des Reihenschlussmotors für GS-Speisung und verschiedene Frequenzen bei WS-Speisung, die Höhe der Spannungen  $U$  ist für alle Kurven konstant

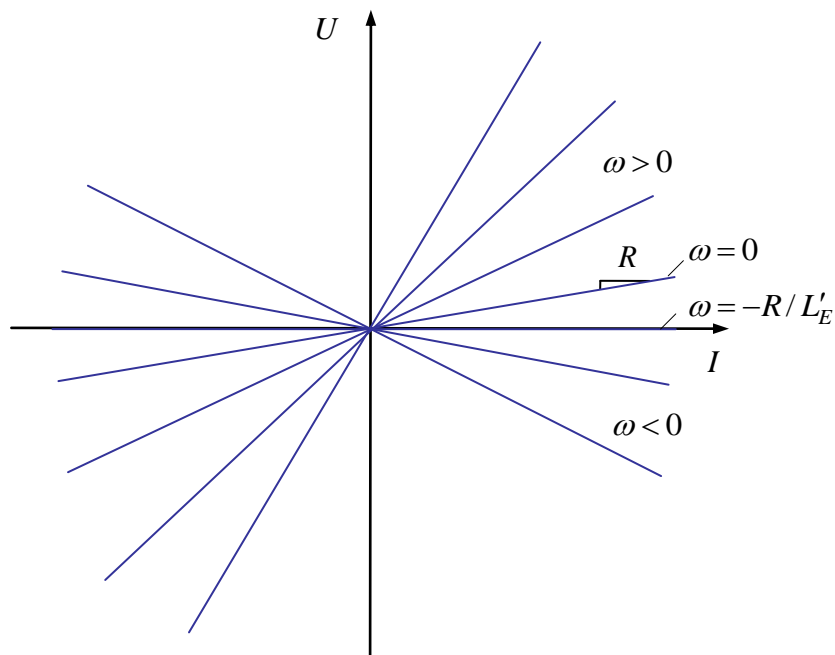


**Fig. 6-21:** Strom-Spannungs-Kennlinien des Reihenschlussmotors für verschiedene Drehzahlen

### 6.12 Controlled Operation

In order to operate the motor at a particular operation point in terms of torque and speed, a variable voltage supply is necessary. In case of one- or three-phase grids that can be realized by a controllable thyristor bridge. DC-DC converters are applied if a DC source is available. The type of the required DC-DC converter depends on the operation modes of the motor. If it is sufficient to operate the machine only in one direction of rotation in motoric operation mode, a simple buck (step-down) converter is sufficient. If both directions of rotation as well as motoric and regenerative (i.e. braking) modes must be covered, a 4-quadrant converter is required to feed the armature circuit. For the supply of the excitation circuit, however, a simple buck converter is still sufficient. The usage of a linear power amplifier is usually not appropriate due to the high losses.

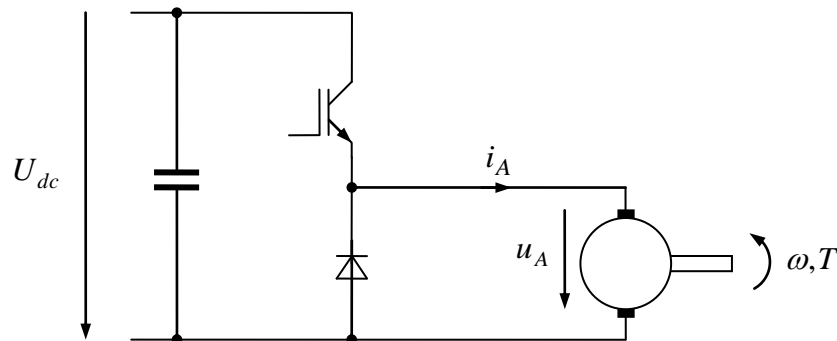


**Fig. 6-22:** Feeding the armature circuit by a buck converter

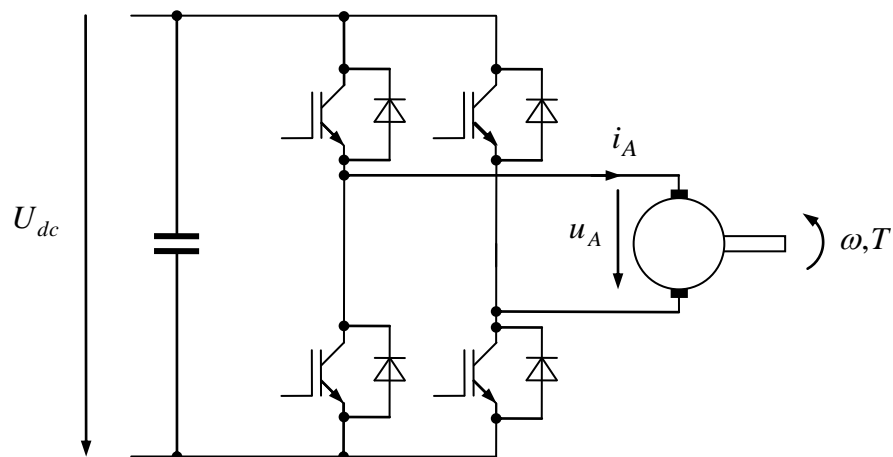


**Fig. 6-23:** Feeding the armature circuit by a 4-quadrant converter

In case of a simple speed control, the speed controller acts directly on the armature voltage. However, a feedforward compensation of EMF turns out as an advantageous detail. In doing so, the EMF action paths in the motor model and in the controller are mutually cancelled out, see Fig. 6-25. As a result, we will get an equivalent control system as shown in Fig. 6-26,

consisting only of a  $PT_1$  delay element and an integrator. For this simplified structure, the controller can be designed according to the Symmetrical Optimum method (Chapter 8.2). As it can be learnt from that chapter, though the achievable bandwidth of the closed-loop control system can be varied in some range, however, in any case the bandwidth is below the corner frequency of the plant transfer function. The important plant time constant is given here by the armature time constant  $\tau_A = L_A / R_A$ . With small time constants or low requirements with respect to dynamical performance, such a design may suffice. With higher dynamic demands which come up typically with motors of higher power rating where the armature time constants are even large, this kind of control is usually no longer applied.

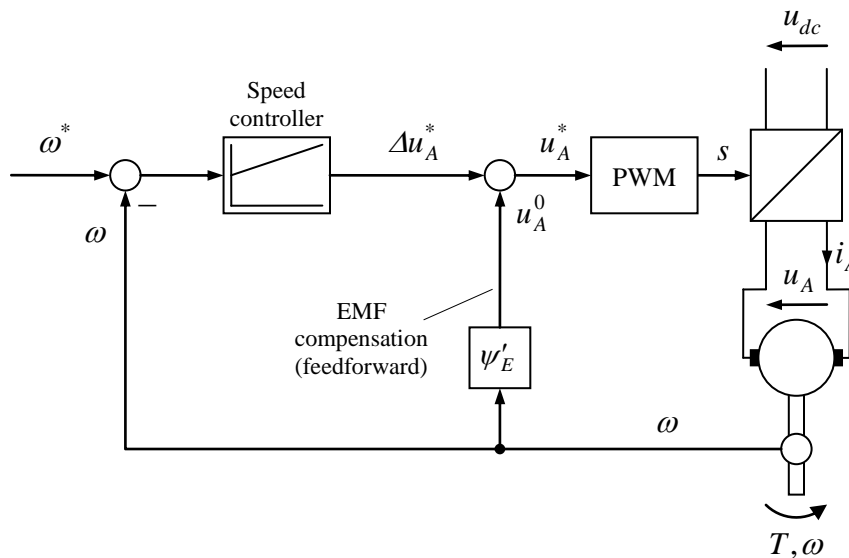


**Fig. 6-24:** Single-loop speed control

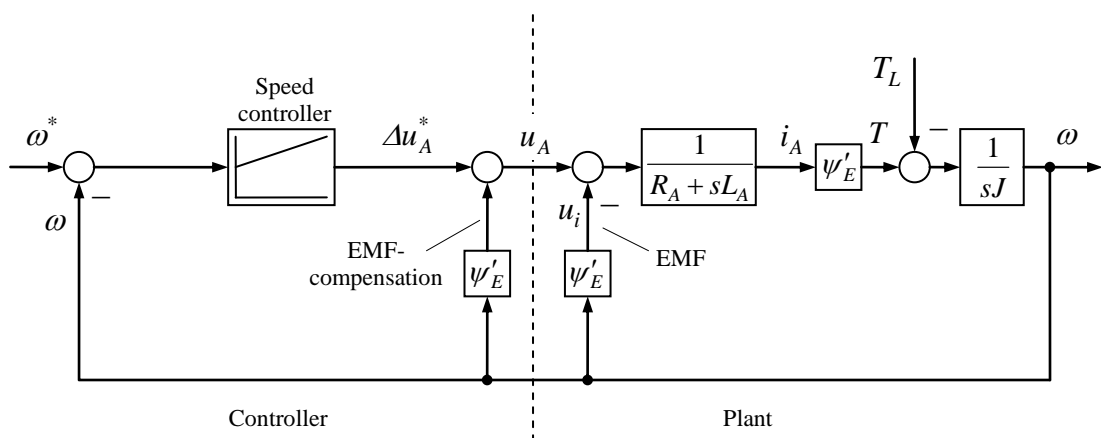


**Fig. 6-25:** Single-loop speed control:  
resulting control structure

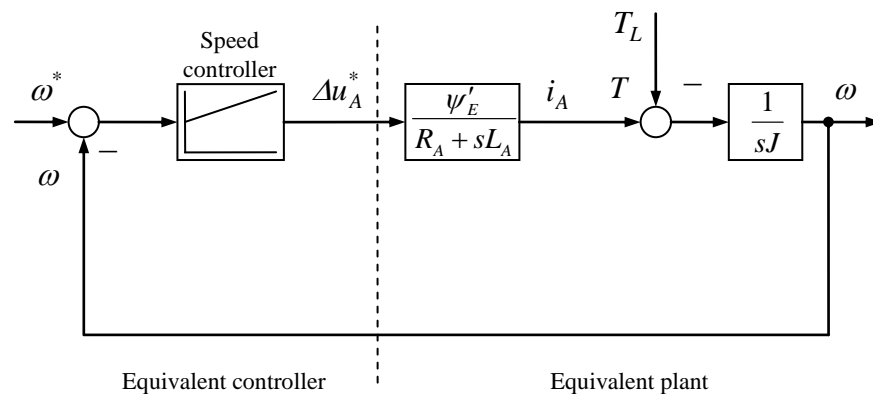


**Fig. 6-26:** Single-loop speed control: simplified equivalent control structure

Another drawback of the single-loop speed control is the fact that there is no direct supervision of the armature current. The armature current is a critical quantity as exceeding of the rated value may damage the devices due to heating-up. As the thermal time constants of the motor are usually large, an excess of the current rating can be tolerated for a short amount of time (usually some seconds). Even more critical are the feeding power electronic devices as their thermal time constants are very small, e.g. some fractions of a second. So, overcurrents are often not allowed at all. A control, which cannot guarantee that the current will retain within the allowed limits, is thus very critical.

However, it is possible to supervise the armature current using a cascade control structure with inner current control. Also the dynamic behavior will be improved.

The control is constructed in so-called cascaded manner. The task of the inner current control loops is to track the demanded current value, which is provided by the outer speed controller. Since armature current and torque are proportional, the inner current control can be seen as torque control. Similar to the single-loop speed control, an EMF feedforward compensation is recommended also here, see Fig. 6-27, Fig. 6-28, Fig. 6-29.

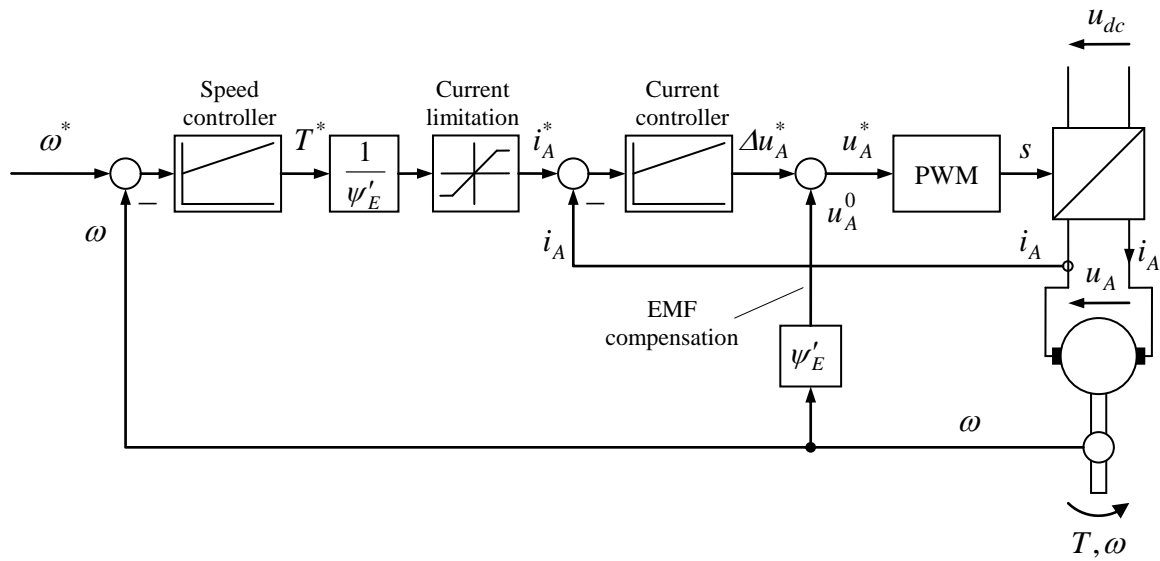


**Fig. 6-27:** Speed control with inner armature current control

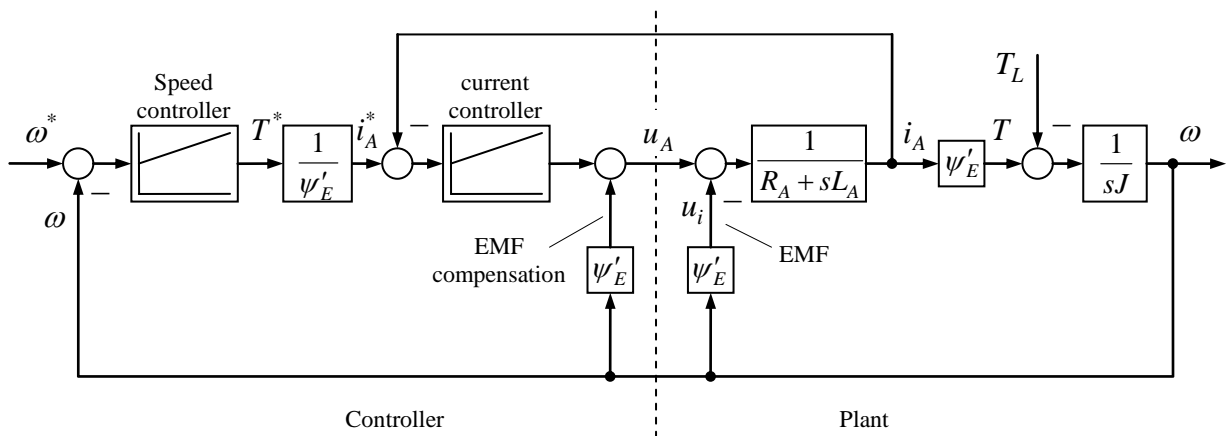


**Fig. 6-28:** Speed control with inner armature current control: control structure

(the limitation of the demanded current value as well as the saturation of the armature voltage are not depicted in this figure for reasons of simplification)

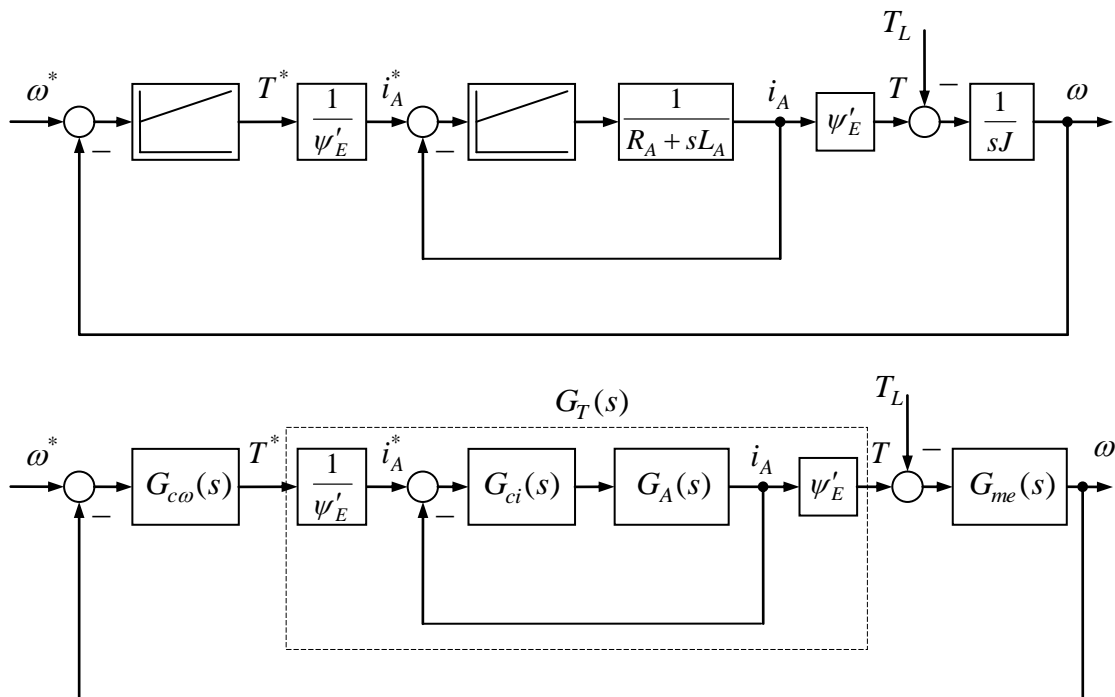


**Fig. 6-29:** Simplified control structure

The control design starts with design of the armature current control first. The plant time constant is also given by the armature time constant. However, unlike as with the single-loop control above, this part of the plant transfer function does not include an integrator. If applicable, another small time constant could be included into the transfer function in order to consider the influences of data sampling or sensor time constants. According to the symbols used with the Magnitude Optimum design (Chapter 8.1) this small time constant would be  $\tau_\sigma$ . The armature time constant  $\tau_A$  now plays the role of the large plant time constant  $\tau_s$ . The achievable control bandwidth is now in the range of the small time constant  $\tau_\sigma$ , while the large armature time constant is not important for the tracking behavior. So, the achievable dynamic performance of the current control turns out to be dimension better than the performance of the single-loop control.

Now, also the speed controller benefits from the good dynamic performance of the current control. The speed controller can be designed much faster as with the single-loop approach. In order to do so, the closed-loop inner current control  $G_T(s)$  (see Fig. 6-29) is being approximated by a delay component which time constant is usually much smaller than the armature time constant. The design of the speed controller can be again done with the Symmetrical Optimum approach, however, now resulting in a much better performance.

The supervision of the current allowed current rating, as discussed above, can now be realized easily by a simple limitation of the current reference value as shown in Fig. 6-27. In fact, there may occur deviations between demanded and actual current values. If the current controller is well tuned, these deviations will usually be only small so that the the actual current will really retain within the allowed limitation, where a small safety margin should be taken into account.

The main relations for the control loop are summarized as follows:

Differential equation for armature current and speed:

$$L_A \dot{i}_A = u_A - R_A i_A - u_i = u_A - R_A i_A - \omega \psi'_E \quad (6.51)$$

$$J \dot{\omega} = T - T_L \quad (6.52)$$

Laplace-Transformierte:

$$sL_A i_A(s) = u_A(s) - R_A i_A(s) - u_i(s) \quad (6.53)$$

$$sJ \omega(s) = T(s) - T_L(s) \quad (6.54)$$

Transfer functions:

Transfer function of the electrical sub-system (armature admittance)

$$G_A(s) = Y_A(s) = \frac{i_A(s)}{u_A(s) - u_i(s)} = \frac{1}{R_A + sL_A} \quad (6.55)$$

Torque transfer function

$$G_T(s) = \frac{T(s)}{T^*(s)} = \frac{G_{ci}(s)G_A(s)}{1 + G_{ci}(s)G_A(s)} \quad (6.56)$$

Transfer function of the mechanical sub-system

$$G_{me}(s) = \frac{\omega_A(s)}{T(s) - T_L(s)} = \frac{1}{sJ} \quad (6.57)$$

Speed tracking transfer function

$$G_\omega(s) = \frac{G_{c\omega}(s)G_T(s)G_{me}(s)}{1 + G_{c\omega}(s)G_T(s)G_{me}(s)} \quad (6.58)$$

Disturbance transfer function

$$G_{T_L}(s) = \frac{G_{me}(s)}{1 + G_{c\omega}(s)G_T(s)G_{me}(s)} \quad (6.59)$$

### 6.13 Operation at the Limits of Current and Voltages

The steady-state equations of the separately excited DC motor are

$$u_A = R_A i_A(s) + \omega \psi'_E \quad (6.60)$$

$$T = \psi'_E i_A \quad (6.61)$$

The maximum available torque results (at constant excitation flux) from the current limit of the motor or the feeding electric converter, respectively:

$$|i_A| \leq I_{\max},$$

$$T_{\max} = \psi'_E I_{\max}, \quad T_{\min} = \psi'_E I_{\max}.$$

Additionally, the voltage of the feeding converter is limited as well:

$$|u_A| \leq U_{\max}. \quad (6.62)$$

If the exciting magnetic flux is considered constant (with permanent excitation this is the case anyhow), the voltage will reach its limit at the speed of

$$\omega_1 = \frac{U_{\max} - R_A i_A}{\psi'_E} = \frac{U_{\max}}{\psi'_E} - \frac{R_A}{\psi'^2_E} T = \omega_0 - \frac{R_A}{\psi'^2_E} T \quad (6.63)$$

The speed cannot be increased beyond that point with constant excitation flux. The speed  $\omega_0$  is the idling speed. This value can be taken as roughly approximated speed limit. The exact speed limit  $\omega_1$ , however, depends not only on the excitation flux, but also on the armature current or the torque, respectively. With operation at maximum current  $i_A = \pm I_{\max}$ , the exact motoric and regenerative speed limits result to

$$\omega_{1mot} = \frac{U_{\max} - R_A I_{\max}}{\psi'_E}, \quad \omega_{1gen} = \frac{U_{\max} + R_A I_{\max}}{\psi'_E}.$$

Higher speeds are possible, however, if the flux is reduced accordingly. The flux must be reduced inversely proportional to the speed,

$$\psi'_E = \frac{U_{\max} - R_A I_A}{\omega} \approx \frac{U_{\max}}{\omega}, \quad (6.64)$$

in order not to violate the voltage limit. To do so, a variable supply of the excitation circuit is required (which is not possible with permanently excited motors). Then, the provided torque will also be reduced inversely proportional to the speed,

$$T_{\max} = \frac{U_{\max} - R_A I_{\max}}{\omega} I_{\max} \approx \frac{U_{\max} I_{\max}}{\omega} \quad (6.65)$$

in the motoric case, and for the regenerative case

$$T_{\min} = \frac{U_{\max} + R_A I_{\max}}{\omega} I_{\max} \approx \frac{U_{\max} I_{\max}}{\omega} \quad (6.66)$$

The maximum available mechanical power yields as

$$P_{\max} = \omega T_{\max} = (U_{\max} - R_A I_{\max}) I_{\max} \approx U_{\max} I_{\max} \quad (6.67)$$

and results to be constant. This operation area is called *flux weakening range* or *constant-power-range*. In the lower speed area with  $|\omega| < \omega_1$ , where the armature voltage is not saturated, the maximum power results to be proportional to the speed

$$P_{\max} = \omega T_{\max} = \omega \psi'_E I_{\max} \quad (6.68)$$

or

$$P_{\min} = \omega T_{\min} = -\omega \psi'_E I_{\max} \quad (6.69)$$

This area is called *armature* or *voltage control range* or *constant-torque-range*. The flux weakening range is often specified by the dimensionless ratio of the  $\omega_1$  and the maximum speed  $\omega_{\max}$ , which usually results from mechanical restrictions.

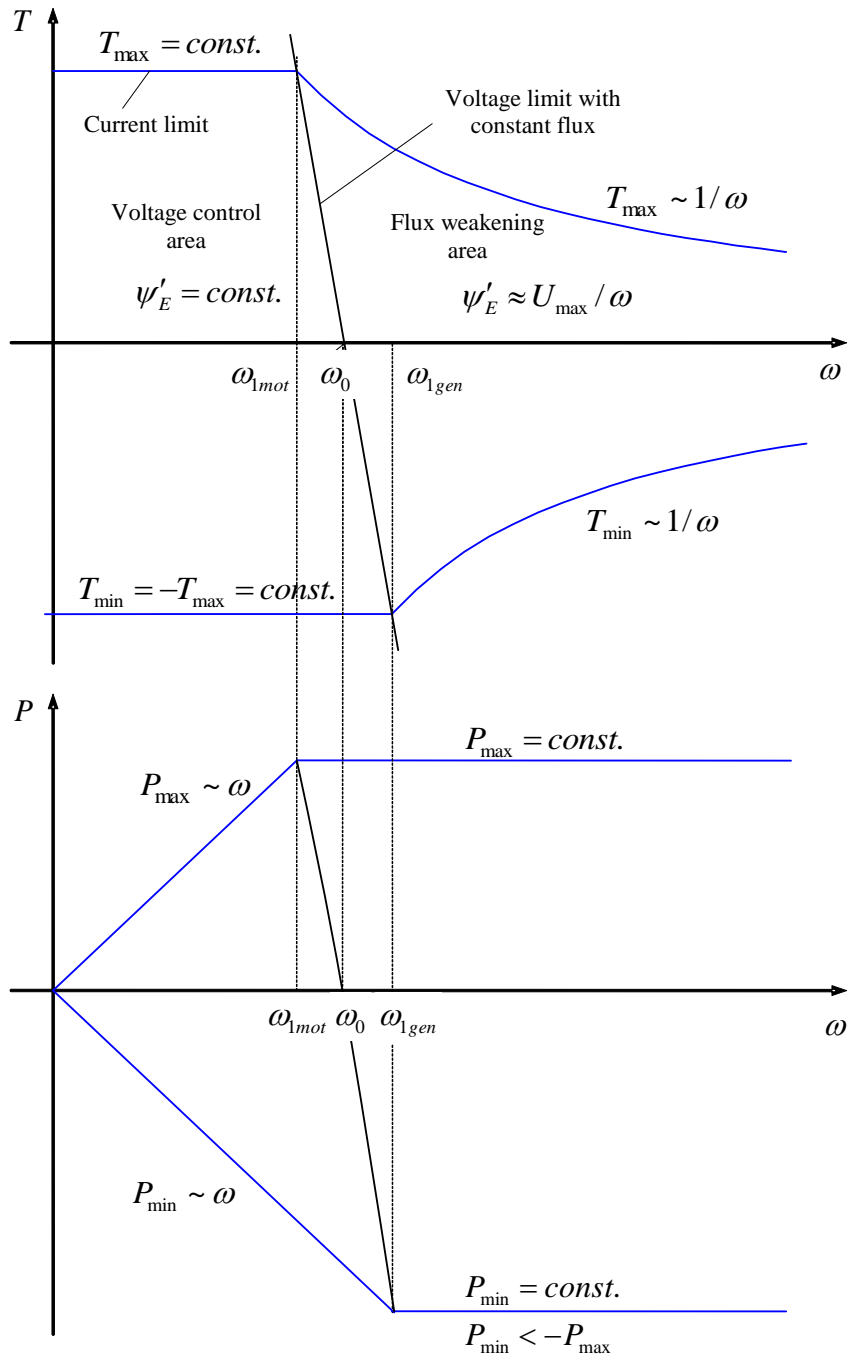


**Fig. 6-30:** Maximum available torque and power vs. speed

## 7 Electronically Commutated Motors

### 7.1 Functional Principle

The functional principle of electronically commutated motors is quite the same as of conventional permanent magnet DC motors. Both types of motors comprise an armature and a magnetic excitation from a permanent magnet. Unlike the mechanical commutation of a classical DC motor, the switching of the armature windings is performed electronically. In order to enable simple wiring between windings and the electronic switch, the armature of the electronically commutated motor is located in the stator. In return, the excitation, i.e. the permanent magnet is now located as moving part in the rotor. The most common construction principle provides for a rotor being located on the inside. However, a construction with external rotor is also possible.

Depending on the manufacturer's wording, electronically commutated motors (*EC motors*) can also be called *brushless DC motors (BLDC motors)*.

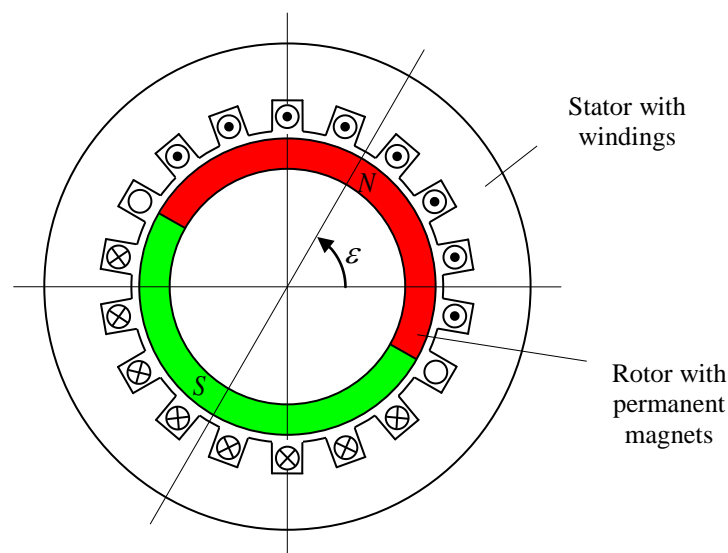


**Fig. 7-1:** DC motor with rotating excitation and armature winding in the stator

The advantages of electronically commutated motors as compared to mechanically commutated motors are as follows:

- The armature winding is located in the outer stator which can be cooled more easily as the internal rotor of a conventional DC motor. Due to better cooling, a more compact construction is possible.
- The mechanical commutator contributes to about one third of the overall length. An electronically commutated motor is much shorter.
- No wear of the brushes. An electronically commutated motor is almost free of maintenance.

Today, these advantages are compensated to a large extent by the higher cost of the electronic commutation. However, the electronic commutation exhibits some additional benefits.

While a mechanically commutated motor usually includes some tens armature segments, within an electronically commutated motors there are most commonly only three such segments that should be called phases. However, the function principle is not restricted to only three phases. Unlike classical DC motors, these winding segments are not connected in a ring, but as a star.

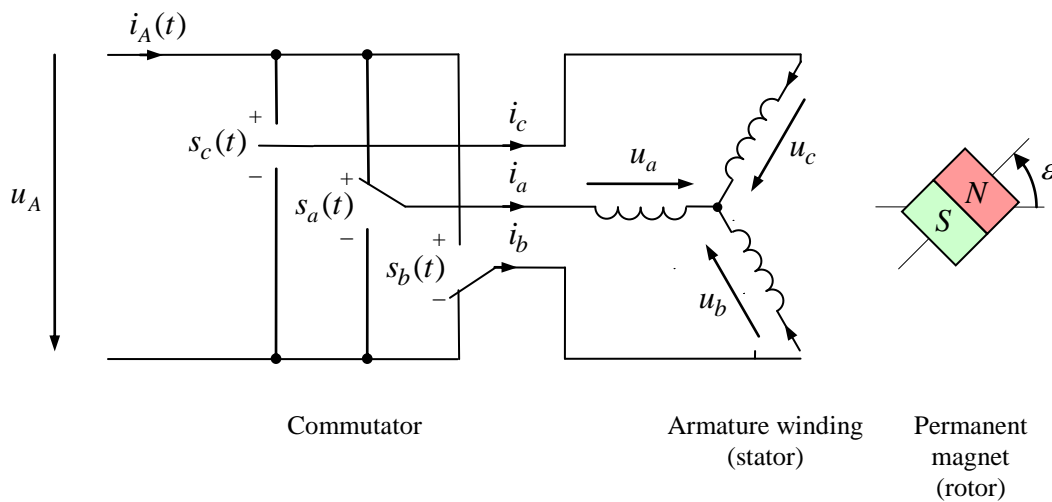


**Fig. 7-2:** Principle diagram of an electronically commutated motor

With a commutator as shown in the diagram, each of the terminals of the phase windings  $a$ ,  $b$ ,  $c$  can be connected to the positive or the negative potential of the supply voltage, or remains unconnected. So, the armature current  $i_A$  always flows through two out of the three phase windings, the third winding remains unconnected. Introducing the switching function

$$s_a, s_b, s_c \in \{-1;0;+1\},$$

where the value „0“ should denote the opened switch, the relations between armature current and voltage and the phase quantities can be written as follows:

$$i_A = \frac{1}{2} \sum_{k=a,b,c} s_k i_k \tag{7.1}$$

$$u_A = \sum_{k=a,b,c} s_k u_k \tag{7.2}$$

### 7.2 Induced Voltages

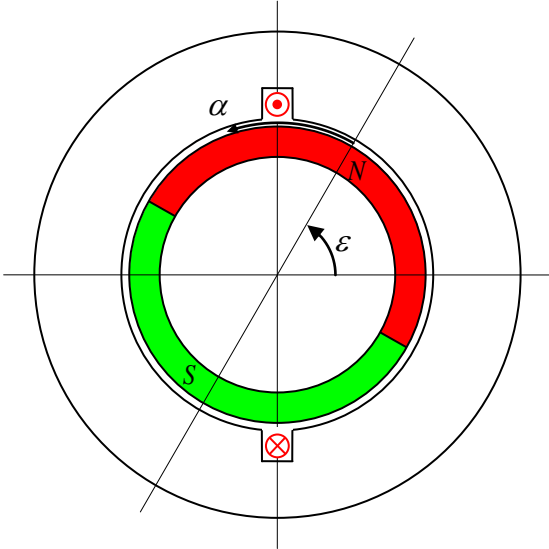


**Fig. 7-3:** On the induced voltage in a single armature winding turn  
 $\epsilon$  : position angle of the rotor with respect to the stator  
 $\alpha$  : rotor-fixed coordinate to be used for the description of the rotor field

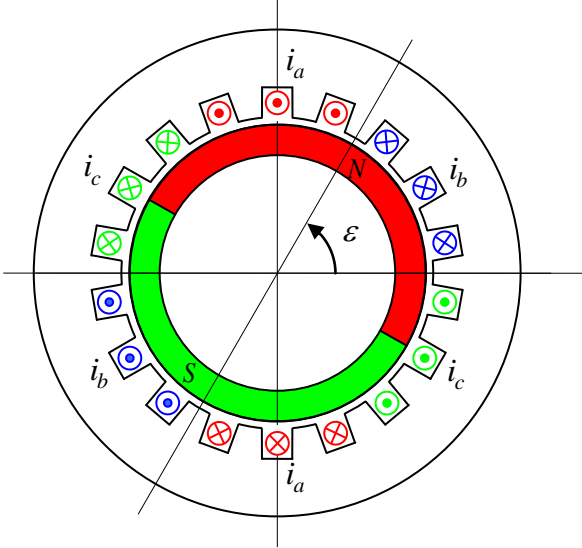


**Fig. 7-4:** Allocation of the turns to the three-phase winding system  
(dots and crosses do not indicate the actual directions of the current flows but only the direction of counting )

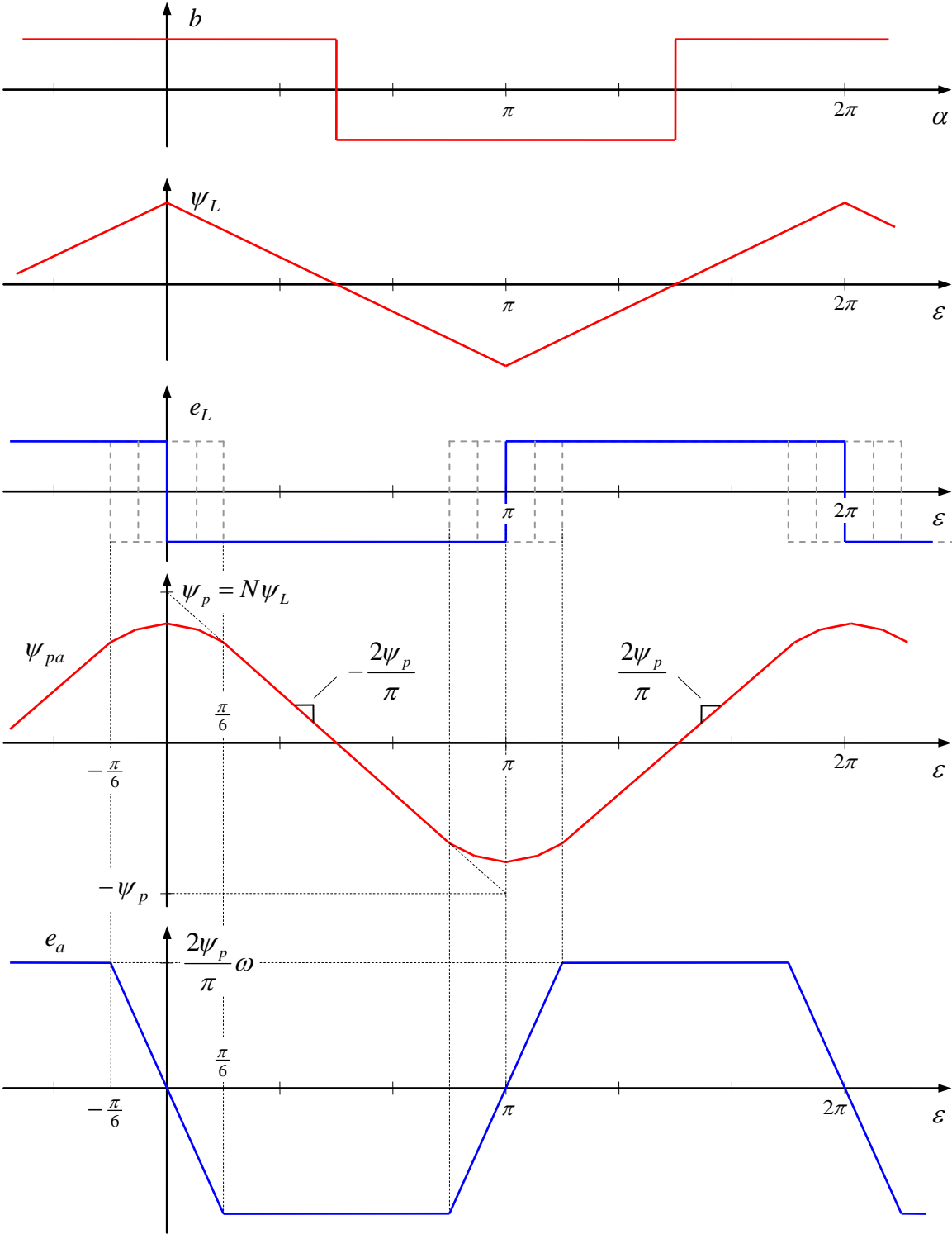
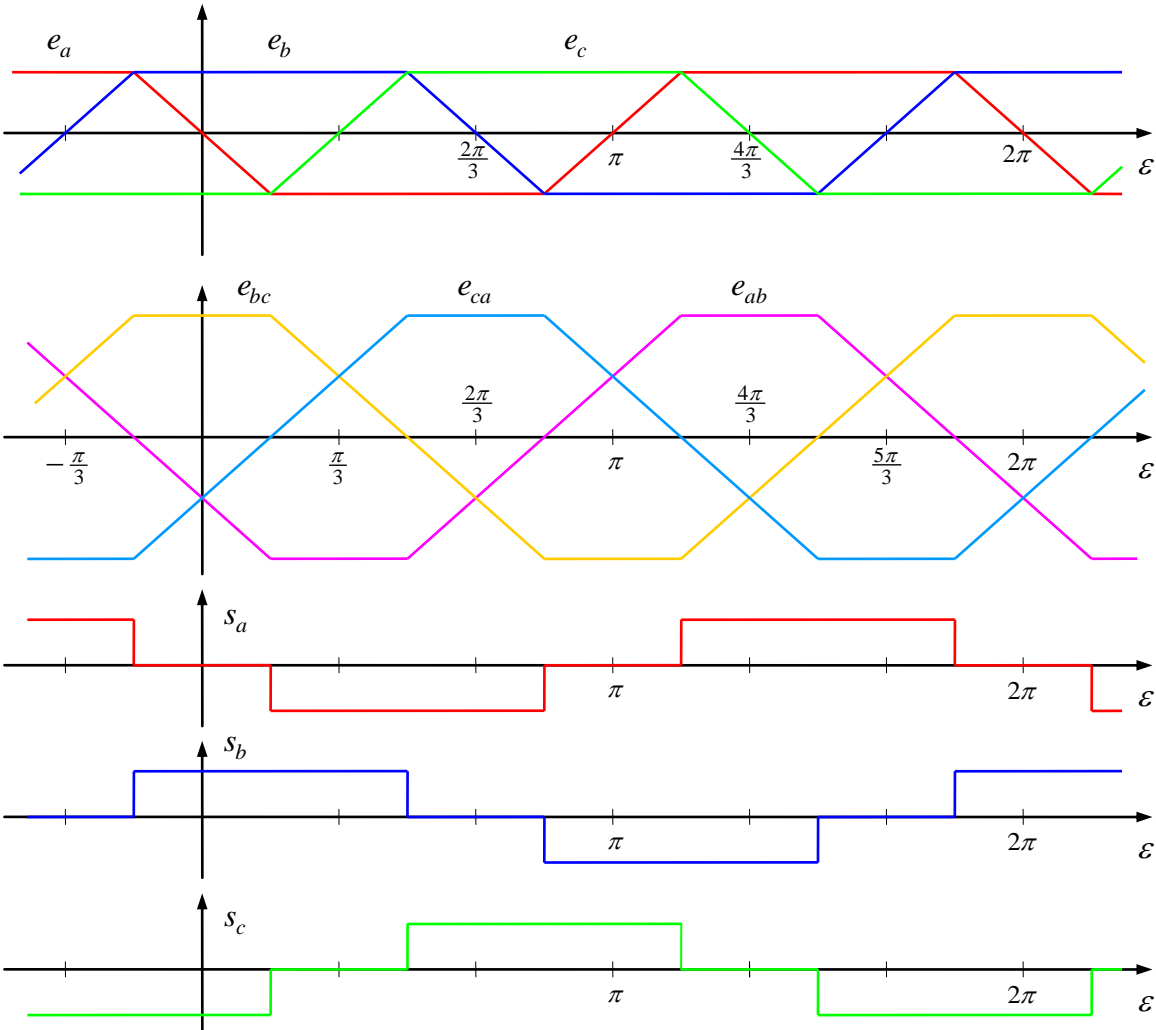
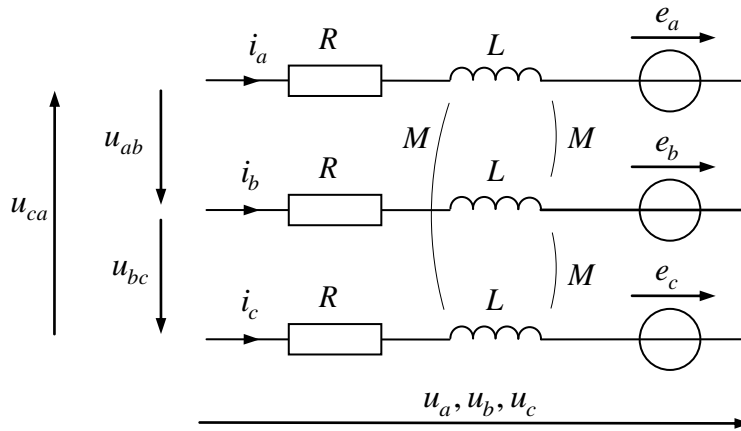


Fig. 7-5: Construction of the induced voltage of a turn and a complete winding



**Fig. 7-6:** Phase and phase-to-phase voltages and the required switching states of the commutator in order to rectify the armature voltages

### 7.3 Equivalent Circuit Diagram and Torque



**Fig. 7-7:** Equivalent circuit diagram with armature inductance and voltage sources representing the EMF

$$\begin{bmatrix} u_a \\ u_b \\ u_c \end{bmatrix} = R \begin{bmatrix} i_a \\ i_b \\ i_c \end{bmatrix} + L \frac{d}{dt} \begin{bmatrix} i_a \\ i_b \\ i_c \end{bmatrix} + \frac{d}{dt} \begin{bmatrix} \psi_{pa} \\ \psi_{pb} \\ \psi_{pc} \end{bmatrix} \quad (7.3)$$

where

$$\frac{d}{dt} \begin{bmatrix} \psi_{pa} \\ \psi_{pb} \\ \psi_{pc} \end{bmatrix} = \begin{bmatrix} e_a \\ e_b \\ e_c \end{bmatrix} \quad (7.4)$$

and the inductance matrix

$$\mathbf{L} = \begin{bmatrix} L & M & M \\ M & L & M \\ M & M & L \end{bmatrix} \quad (7.5)$$

The main or mutual inductance  $M$  describes the the flux linkage between two windings. It is negative,  $M < 0$ . Due to the symmetry of the three phase windings, only up to one half of the magnetic flux of one winding can be linked with another winding. The negative sign has to be considered, however. So, the following limit results

$$-M \leq \frac{1}{2}L \quad (7.6)$$

Excluding the commutation process from our consideration, one of the three phase windings  $i_a, i_b, i_c$  is always zero. In the remaining path of the current, the dynamic behavior e.g. in the case

$$i_c = 0, \quad i_A = i_a = -i_b, \quad u_A = u_a - u_b \quad (7.7)$$

is determined by

$$u_a = Ri_a + Li_a + Mi_b + e_a \quad (7.8)$$

$$u_b = Ri_b + Li_b + Mi_a + e_b \quad (7.9)$$

$$\begin{aligned} u_A = u_{ab} &= u_a - u_b \\ &= 2Ri_A + 2Li_A - 2Mi_A + e_{ab} \\ &= R_A i_A + L_A \dot{i}_A + e_A \end{aligned} \quad (7.10)$$

The effective armature resistance and the effective armature inductance result to

$$R_A = 2R, \quad L_A = 2L - 2M$$

The induced voltage, the EMF (the definition of  $\psi_p$  can be seen from the above timing diagram) results to

$$e_A = 2 \frac{2}{\pi} \psi_p \omega = \frac{4}{\pi} \psi_p \omega = \psi'_p \omega \quad (7.11)$$

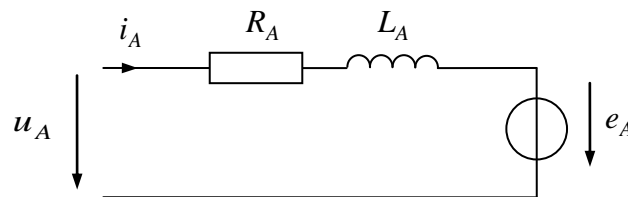


**Fig. 7-8:** Resulting equivalent circuit diagram of the armature circuit

The torque can be determined via the power balance as the mechanical power is equal to the electrical power of the voltage sources  $e_a, e_b, e_c$  :

$$P_{me} = \omega_{me} T = \sum_{k=a,b,c} i_k e_k \quad (7.12)$$

Assuming that one of the three currents is always zero while the other two are equal with inverted sign (and are equal to the armature current  $i_A$ ), it follows ( $p$  is the number of pole pairs)

$$\omega_{me} T = \frac{\omega}{p} T = 2i_A \frac{2\psi_p}{\pi} \omega \tag{7.13}$$

$$T = \frac{4}{\pi} p \psi_p i_A = p \psi'_p i_A \tag{7.14}$$

### 7.4 Converter

In order to supply the electronically commutated motor with variable voltage, a step-down converter (buck converter) can be applied similar to the mechanical commutated motor. Also in this case, a converter inductance is not required as the inductances of the motor take over this task. A circuitry with the combination of a buck converter with the electronically commutated motor is shown in the following figure. However, that structure should not be understood as realistic circuitry, but as an intermediate step only. In this configuration, the electrical commutator is only in charge of changing the polarity once in a fundamental period as it is also characteristic of the mechanical archetype. The buck converter, however, is operated with a higher switching frequency in a pulsing mode.

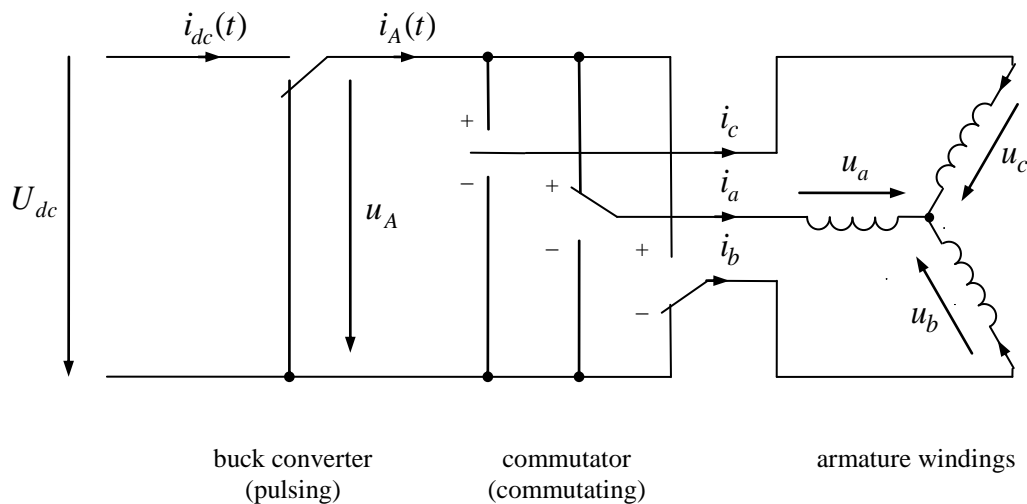


**Fig. 7-9:** Supply with a step-down (buck) converter

However, there is no need to employ different kinds of switches for the two functions pulsing buck converter and commutator. The electronic “commutator” whose major task has been considered up to now to ensure the correct polarity can take over the task of pulsing as well. That is shown in the following figure. In this structure, however, it is no longer possible to identify the armature current  $i_A$  and the armature voltage  $u_A$  at a certain point in the circuit diagram.

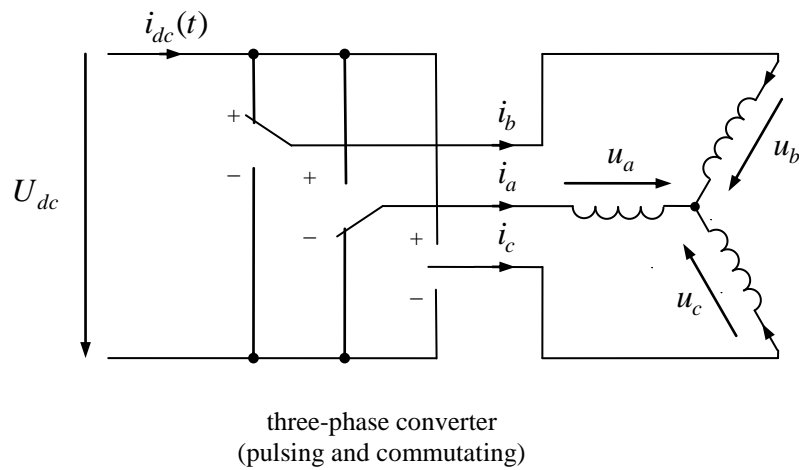


**Fig. 7-10:** Unification of the functions „pulsing“ and „commutating“ within one three-phase converter

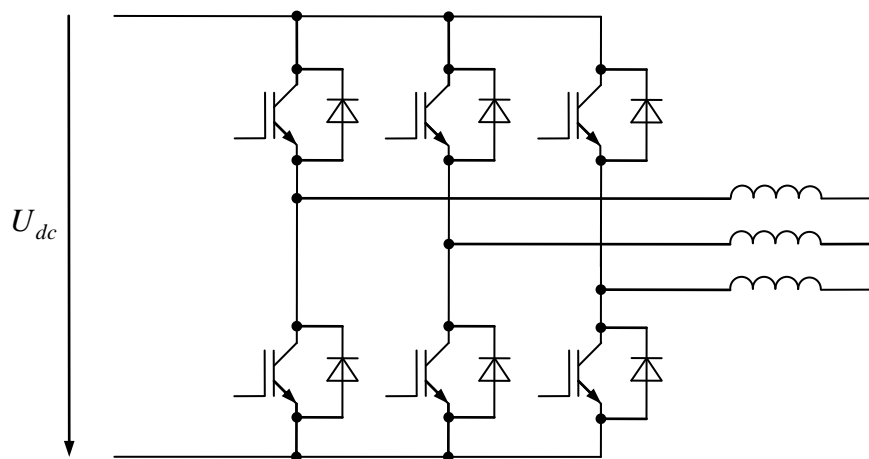


**Fig. 7-11:** Realization of a three-phase converter

### 7.5 Commutation

In order to investigate the process of commutation e.g. between phases *a* and *b*, the current of the third phase *c* which does not take part in the commutation is assumed to remain approximately constant.

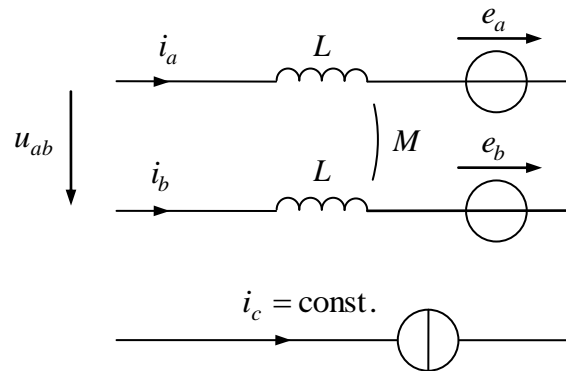


**Fig. 7-12:** Equivalent circuit diagram for the commutation

The inductance in the commutation mesh is

$$L_K = 2L - 2M ,$$

which is identical to the effective armature inductance. The ohmic resistances shall be neglected during the commutation. The commutation starts when the conducting transistor is switched off. The current changes its path to the free-wheeling diode. As a result, the driving commutation voltage is then the negative DC supply voltage. This leads to the simplified equivalent circuit diagram for the commutation mesh:

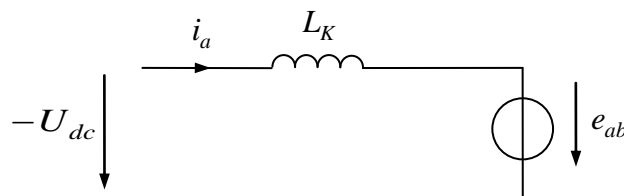


**Fig. 7-13:** Simplified equivalent circuit diagram of the commutation mesh

The starting values of the commutation are

$$i_a(t_{K1}) = i_A , \quad i_b(t_{K1}) = 0 .$$

The commutation is completed when the following end values are reached:

$$i_a(t_{K2}) = 0 , \quad i_b(t_{K2}) = i_A .$$

The differential equation for the commutation is as follows

$$L_K \dot{i}_a = -U_{dc} - e_{ab} \tag{7.15}$$

For the considered example, the commutation should take place symmetrically with respect to the angle  $\varepsilon_K = -\pi/6$  (see timing diagrams above). Around this instant, the induced voltage crosses zero,  $e_{ab} = 0$ . As a result, only the external voltage  $U_{dc}$  is the driving voltage in the commutation mesh. So, the commutation time can be simply calculated as

$$T_K = t_{K2} - t_{K1} = \frac{i_a(t_{K1})L_K}{U_{dc}} = \frac{i_A L_K}{U_{dc}} \quad (7.16)$$

For a more detailed investigation, the accurate behavior of  $e_{ab}$  during the commutation shall be taken into account:

$$i_A = i_a(t_{K2}) - i_a(t_{K1}) = \int_{t_{K1}}^{t_{K2}} \dot{i}_a(t) dt = -\frac{U_{dc} T_K}{L_K} - \frac{1}{L_K} \int_{t_{K1}}^{t_{K2}} e_{ab}(t) dt \quad (7.17)$$

In spite of not assuming  $e_{ab}(t)$  as zero, the corresponding integral of  $e_{ab}(t)$  is zero anyhow, provided that the commutation is symmetrical with respect to the angle  $\varepsilon_K$ . Although the particular trajectories of  $i_a(t)$  will change depending on  $e_{ab}(t)$ , the total commutation time remains constant. However, that requires the commutation to be triggered in advance with an angle of

$$\varepsilon_{K1} = \varepsilon_K - \Delta\varepsilon_K \quad (7.18)$$

That way, the commutation interval is symmetrical with respect to the center angle  $\varepsilon_K$  and will be finished at the angle

$$\varepsilon_{K2} = \varepsilon_K + \Delta\varepsilon_K \quad (7.19)$$

The angle advance is calculated from

$$\Delta\varepsilon_K = \frac{T_K}{2} \omega = \frac{i_A L_K \omega}{2U_{dc}} \quad (7.20)$$

A larger advance can be applied in order to utilize the induced voltage additionally driving the commutation and thus to shorten the commutation time. This can be advantageous particularly in high speed operation when the available time for commutation is short. A delayed commutation trigger would lengthen the commutation time having a negative impact particularly at higher speeds.

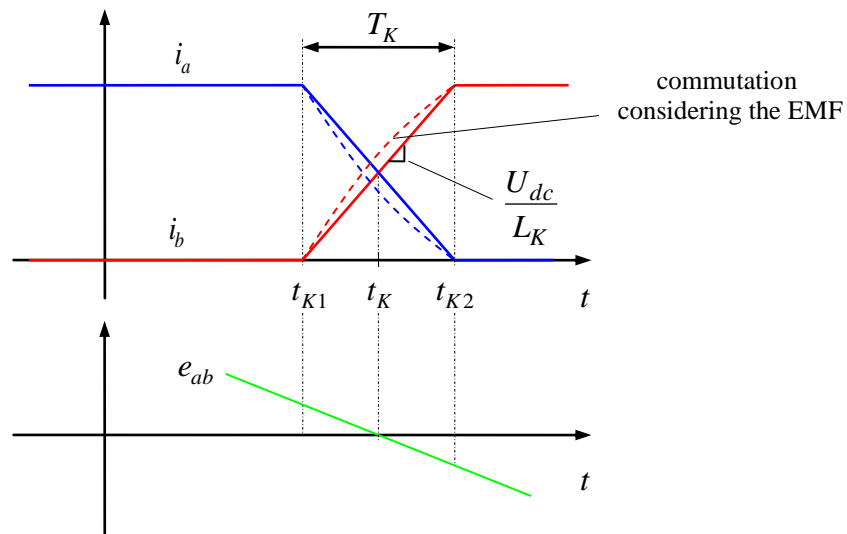


**Fig. 7-14:** Trajectories during the commutation

Unlike the mechanically commutated DC motor, where the commutation of the armature current takes place locally only within the commutator contacts and the carbon brushes, the the electrical commutation also includes the DC bus.

### 7.6 Control

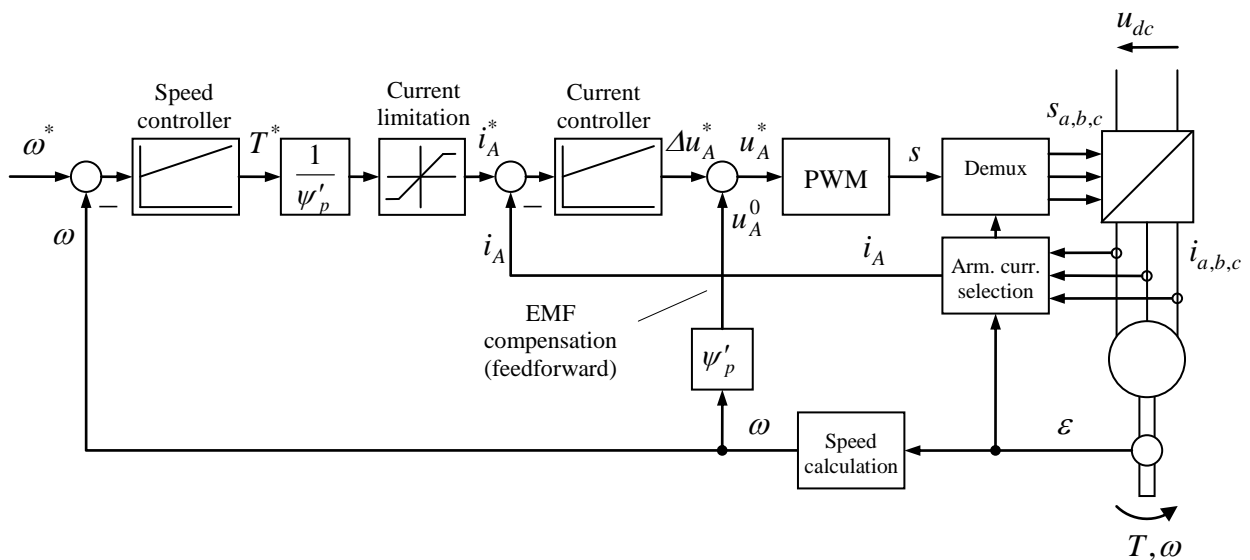


**Fig. 7-15:** Speed control with inner current control and PWM

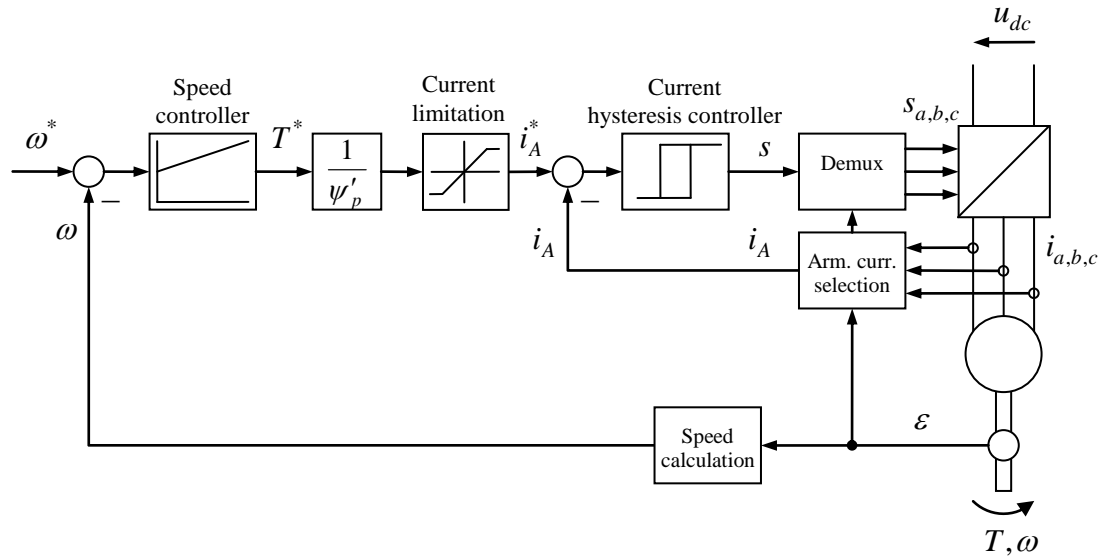


**Fig. 7-16:** Speed control with inner hysteresis current control

The calculation of the armature current  $i_A$  can be performed depending on the position angle  $\varepsilon$  by selection of one of the phase currents  $i_a, i_b, i_c$  with appropriate sign according to the following table:

Table of the commutator switching positions and the relevant armature current

$\varepsilon$	$s_a$	$s_b$	$s_c$	$i_A =$
$-30^\circ < \varepsilon < 30^\circ$	0	+1	-1	$i_b = -i_c$
$30^\circ < \varepsilon < 90^\circ$	-1	+1	0	$i_b = -i_a$
$90^\circ < \varepsilon < 150^\circ$	-1	0	+1	$i_c = -i_a$
$150^\circ < \varepsilon < 210^\circ$	0	-1	+1	$i_c = -i_b$
$210^\circ < \varepsilon < 270^\circ$	+1	-1	0	$i_a = -i_b$
$270^\circ < \varepsilon < 330^\circ$	+1	0	-1	$i_a = -i_c$

If regenerative operation is excluded, the armature current will always be positive or zero so that it can be calculated independent of the position from

$$i_A = \frac{1}{2} \sum_{k=a,b,c} |i_k| ,$$

which can be realized quite easily.

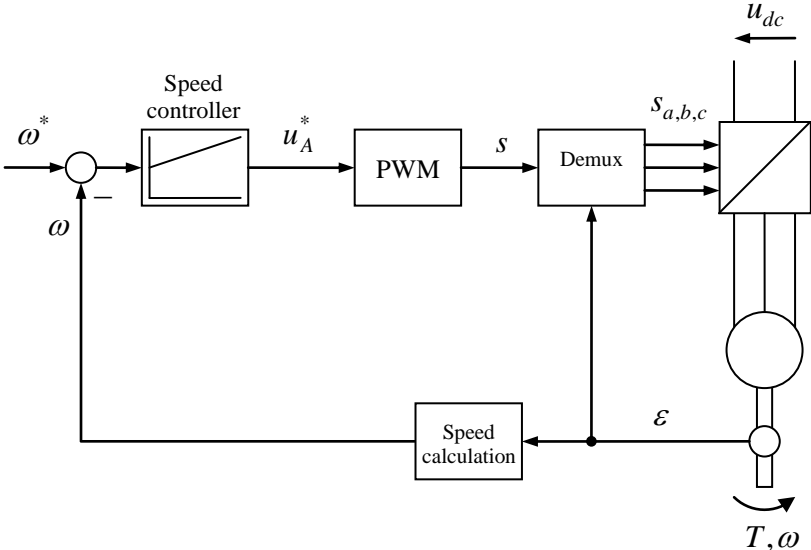


**Fig. 7-17:** Simplified speed control without inner current control and EMF compensation

## 8 Design of Current and Speed Control

In different contexts such as for the magnetic bearing, switched reluctance motor, DC motor – both variants with mechanical and electronic commutation – subordinate current controllers are to be employed. All of them have quite a similar structure and can be designed similarly using standard controller design methods. The same applies for the speed control.

For the current control, we should start with a plant transfer function (i.e. the admittance) of a  $RL$ -element:

$$Y(s) = \frac{I(s)}{U(s)} = G_s(s) = \frac{1}{R + sL} = \frac{1}{R} \frac{1}{1 + s\tau_s} \quad (8.1)$$

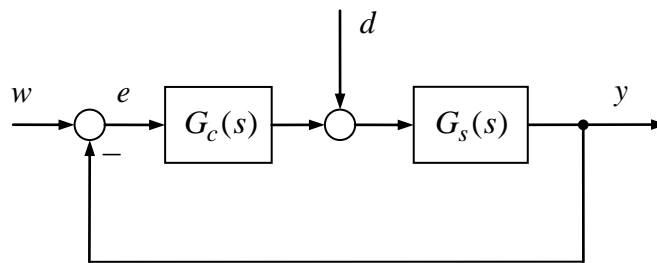


**Fig. 8-1:** Considered standard control loop with control variable  $y$ , set value  $w$ , and disturbance variable  $d$

Other influences like the EMF shall not be considered here. It is assumed that the EMF has already been compensated by a feedforward action of the controller (in term of control engineering, we refer to disturbance compensation).

Additionally to the behavior of the  $RL$ -element, another time constant  $\tau_\sigma$  shall be taken into account, which may be due to, e.g., the delays of sensors or the voltage actuator. Thus, we should start from the transfer function

$$G_s(s) = V_s \frac{1}{1 + s\tau_s} \frac{1}{1 + s\tau_\sigma} \quad (8.2)$$

It is assumed that

$$\tau_s > \tau_\sigma \quad (8.3)$$

The controller is now assumed to be a  $PI$ -type with reset time  $T_n$  and controller gain  $V_c$  :

$$G_c(s) = V_c \frac{1 + sT_n}{sT_n} \quad (8.4)$$

Then, the loop transfer function results to<sup>7</sup>

$$L(s) = G_s(s)G_c(s) = V_s V_c \frac{1}{1 + s\tau_s} \frac{1}{1 + s\tau_\sigma} \frac{1 + sT_n}{sT_n} \quad (8.5)$$

### 8.1 Controller Design with Pole-Zero-Cancellation (Magnitude Optimum)

If the controller reset time is chosen equal to time constant of the plant,

$$T_n = \tau_s \quad (8.6)$$

the corresponding plant pole will be cancelled by the controller zero and the loop transfer function results to

$$L(s) = V_s V_c \frac{1}{sT_n} \frac{1}{1 + s\tau_\sigma} \quad (8.7)$$

With the normalized gain

$$\gamma = \frac{\tau_\sigma}{\tau_s} V_s V_c = \tilde{V}_s V_c \quad (8.8)$$

the loop transfer function is represented as

$$L(s) = \gamma \frac{1}{s\tau_\sigma} \frac{1}{1 + s\tau_\sigma} \quad (8.9)$$

---

<sup>7</sup> Though the same letter is used for the loop transfer function as well as for the inductance, there is no danger of confusion, since inductances will not occur in the following.

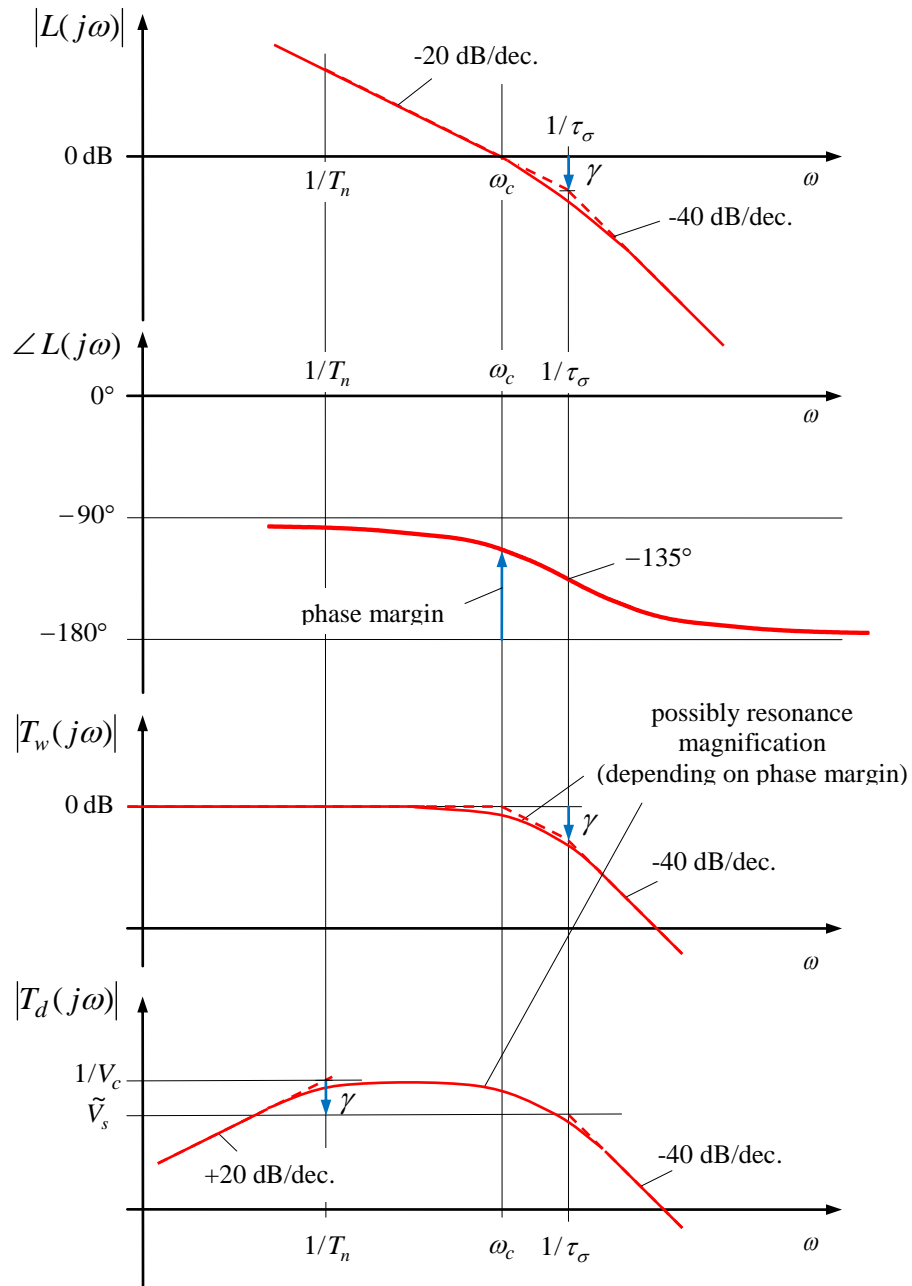


**Fig. 8-2:** Bode plots for control design according the magnitude optimum in double-logarithmic scaling

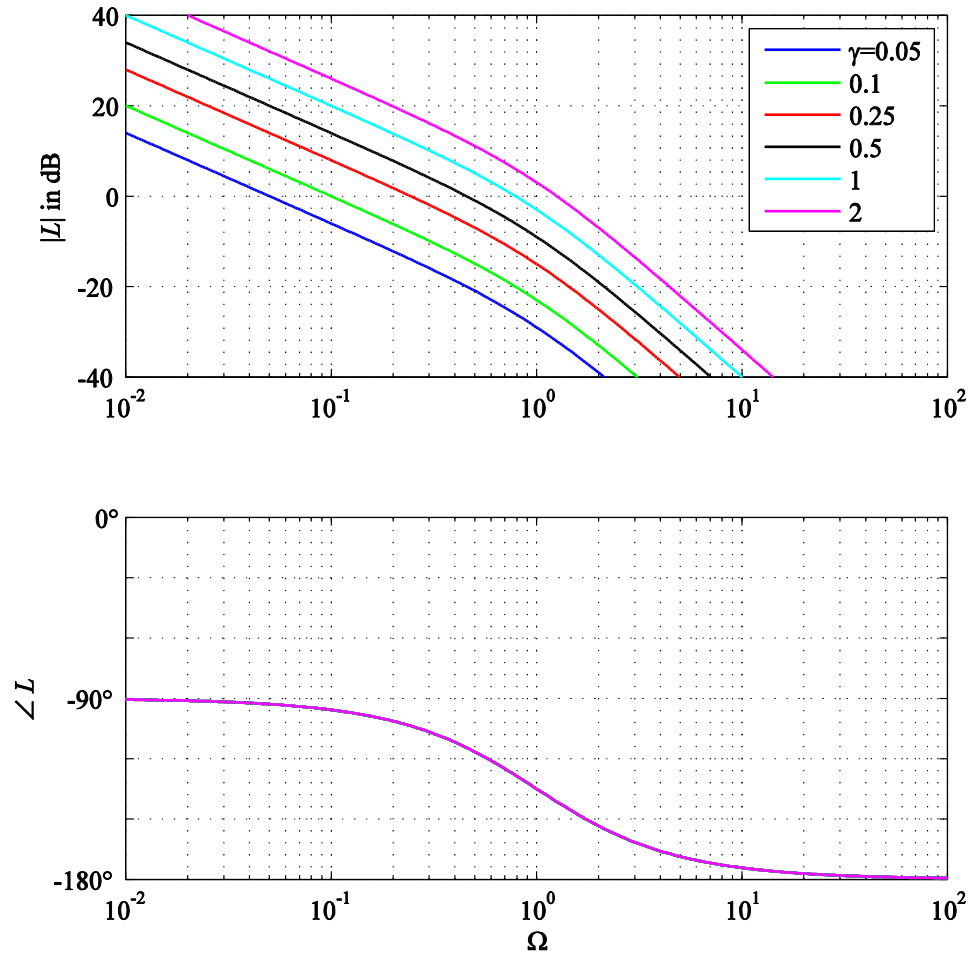


**Fig. 8-3:** Bode plot of the loop gain  $L$  vs. normalized frequency  $\Omega = \omega\tau_\sigma$  for different values of  $\gamma$ , only the magnitude is affected by this parameter

The control transfer function (tracking of reference input) results as

$$T_w(s) = \frac{L(s)}{1+L(s)} = \frac{\gamma}{s\tau_\sigma(1+s\tau_\sigma) + \gamma} = \frac{1}{1 + s\frac{\tau_\sigma}{\gamma} + s^2\frac{\tau_\sigma^2}{\gamma}} \quad (8.10)$$

Comparing this with the standard form of a  $PT_2$ -element,

$$T_w(s) = \frac{L(s)}{1+L(s)} = \frac{1}{1 + s\frac{\tau_\sigma}{\gamma} + s^2\frac{\tau_\sigma^2}{\gamma}} = \frac{1}{1 + 2d\frac{s}{\omega_0} + \frac{s^2}{\omega_0^2}} \quad (8.11)$$

yields

$$\omega_0 = \frac{\sqrt{\gamma}}{\tau_\sigma} \quad (8.12)$$

$$d = \frac{1}{2\tau_\sigma\omega_0} = \frac{1}{2\sqrt{\gamma}} \quad (8.13)$$

It is reasonable to normalize the frequency with respect to the time constant  $\tau_\sigma$ , i.e.

$$\Omega_0 = \omega_0\tau_\sigma = \sqrt{\gamma} \quad (8.14)$$

The free gain parameter  $\gamma$  influences the damping factor  $d$  as well as the characteristic frequency  $\omega_0$  or  $\Omega_0$ , respectively, of the control transfer function. In any case of the control design, however, the characteristic frequency will not be far from  $1/\tau_\sigma$ . That means that the dynamic capability of the system, which is in the end limited by the time constant  $\tau_\sigma$  is exploited to a rather high extent.

The resulting Bode plots of the control transfer functions are shown in the following figures. As it can be clearly seen, a higher Bandwidth can be achieved at the cost of poorer damping, higher resonance peak or higher overshoot in the time domain. Typical damping values lie in the range between  $1/\sqrt{2}$  and 1, depending on the acceptable overshoot. The design with the value

$$\gamma = \frac{1}{2} \quad \text{or} \quad d = \frac{1}{\sqrt{2}}$$

is called *Magnitude Optimum*<sup>8</sup>.

The *bandwidth* of the control transfer behavior (-3 dB frequency) can be determined straight forward in an analytical manner. Advantageously, the frequency should again be referred to the time constant  $\tau_\sigma$ :

$$T_w(j\Omega) = \frac{\gamma}{\gamma + j\Omega - \Omega^2} \quad (8.15)$$

$$|T_w(j\Omega_b)|^2 = \frac{1}{2} \quad (8.16)$$

$$2\gamma^2 = |\gamma + j\Omega_b - \Omega_b^2|^2 = (\gamma - \Omega_b^2)^2 + \Omega_b^2 = \gamma^2 - 2\gamma\Omega_b^2 + \Omega_b^4 + \Omega_b^2 \quad (8.17)$$

$$(1 - 2\gamma)\Omega_b^2 + \Omega_b^4 - \gamma^2 = 0 \quad (8.18)$$

$$\Omega_b^2 = \gamma - \frac{1}{2} + \sqrt{\left[\gamma - \frac{1}{2}\right]^2 + \gamma^2} \quad (8.19)$$

---

<sup>8</sup> Please see the comprehensive literature in order to learn more about background, motivation, and title of the method, e.g. Lutz, Wendt: Taschenbuch der Regelungstechnik.

$$\Omega_b = \sqrt{\gamma - \frac{1}{2} + \sqrt{\left[\gamma - \frac{1}{2}\right]^2 + \gamma^2}} \quad (8.20)$$

For the standard design  $\gamma = 1/2$  a bandwidth of  $\Omega_b = 1/\sqrt{2}$  results.

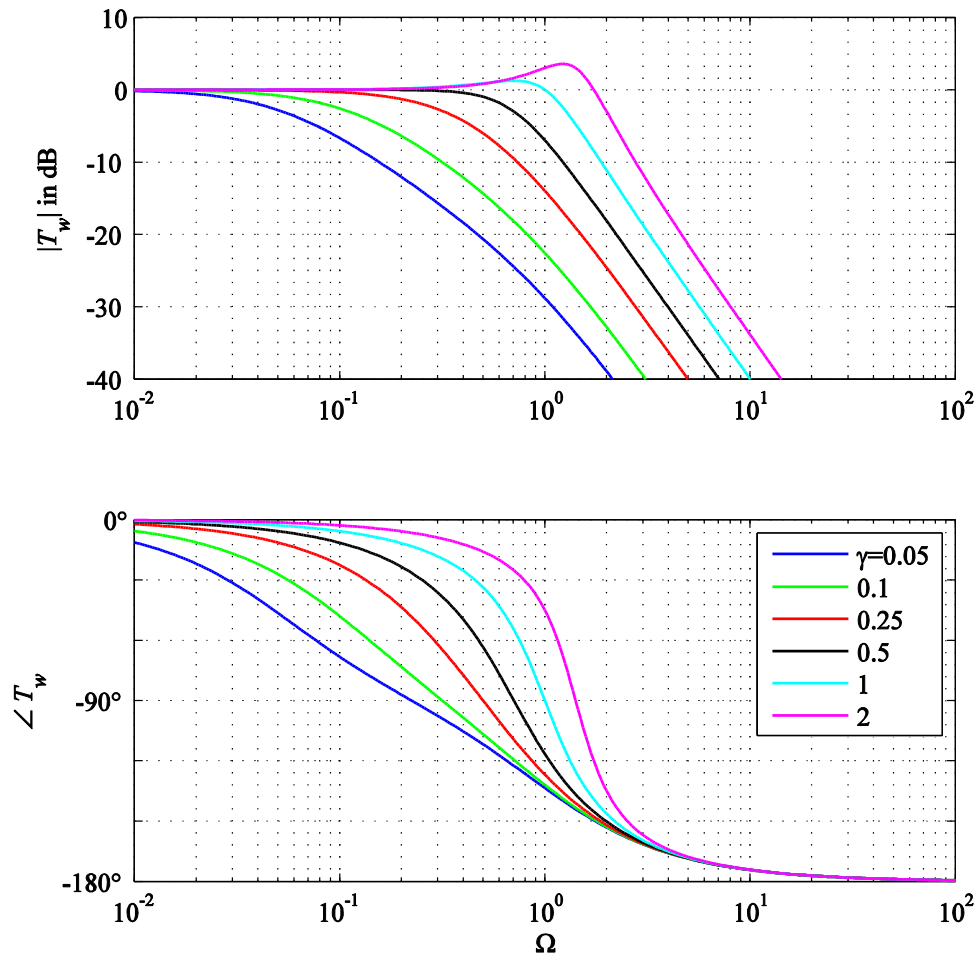


**Fig. 8-4:** Bode plot of the control tracking transfer function  $T_w$  vs. normalized frequency  $\Omega = \omega\tau_\sigma$  for different values of  $\gamma$ ,

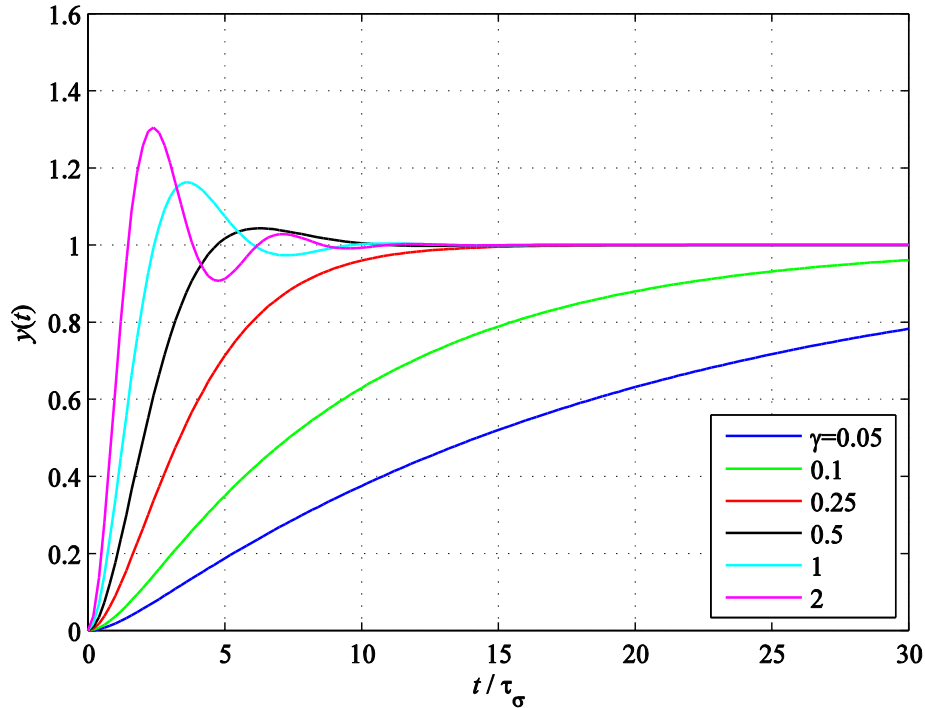


**Fig. 8-5:** Response of the control variable  $y(t)$  to a step-like change of the set point  $w(t) = \sigma(t)$  (tracking behavior)

The Magnitude Optimum is a relatively simple design method that yields rather good reference tracking dynamics. However, attention should also be paid to the disturbance behavior. The disturbance transfer function from the disturbance input  $d$  to control variable  $y$  is

$$T_d(s) = \frac{G_s(s)}{1+L(s)} = V_s \frac{s\tau_\sigma}{(s\tau_\sigma(1+s\tau_\sigma) + \gamma)(1+s\tau_s)} = \tilde{V}_s \frac{s\tau_s}{(s\tau_\sigma(1+s\tau_\sigma) + \gamma)(1+s\tau_s)} \quad (8.21)$$

or, in the representation with the normalized frequency:

$$T_d(j\Omega) = V_s \frac{j\Omega}{(-\Omega^2 + j\Omega + \gamma)(1 + j\Omega\tau_s/\tau_\sigma)} \quad (8.22)$$

It can be seen that the pole  $s = -1/\tau_s$  that has been cancelled in the control transfer function is still present in the disturbance transfer function. Particularly, if  $\tau_s$  is large compared to  $\tau_\sigma$  disturbances will take a relatively long time to be rejected. As the disturbance step response figure shows, even with high controller gain, the control error decreases only slowly with a creeping behavior. Such a disturbance can occur in the current control loop of a DC motor in the case the EMF is not or not precisely compensated for by the feedforward controller action (cp. Section 6.12). In case of operation with constant or slowly varying speed such a slow disturbance rejection would not cause any problems. However, if the speed and thus the EMF changes rapidly, a quick disturbance rejection is desired. In that case the design method described in the following section, the Symmetrical Optimum, may be more suitable.

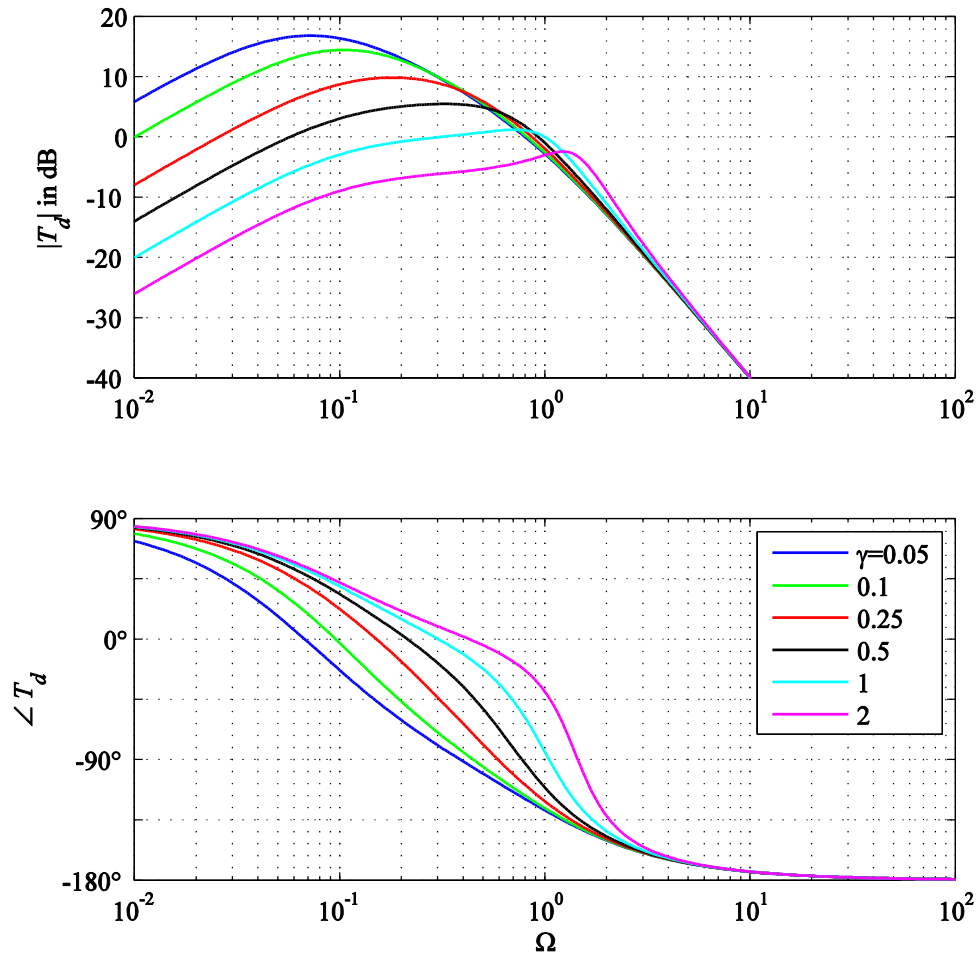


**Fig. 8-6:** Bode plot of the disturbance transfer function  $T_d$  vs. normalized frequency  $\Omega = \omega\tau_\sigma$  with  $\tilde{V}_s = 1$ ,  $\tau_s/\tau_\sigma = 10$

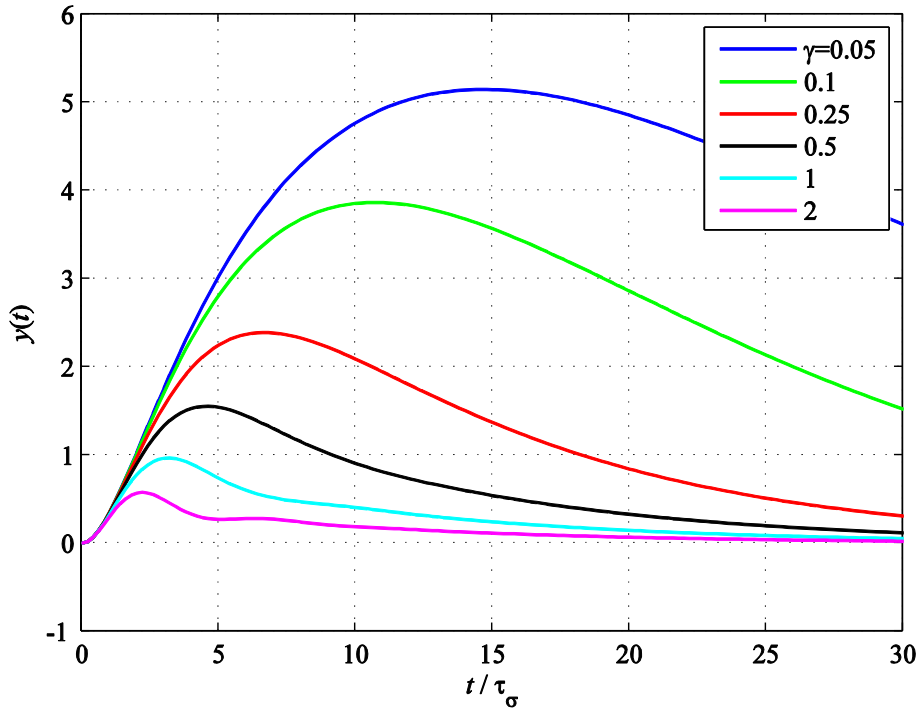


**Fig. 8-7:** Response of the control variable  $y(t)$  to step-like change of the disturbance  $d(t) = \sigma(t)$ , with  $\tilde{V}_s = 1$ ,  $\tau_s / \tau_\sigma = 10$

The magnitude crossover frequency  $\Omega_c$  of the loop gain can also be determined analytically:

$$1 = |L(j\Omega_c)|^2 = \gamma^2 \frac{1}{\Omega_c^2} \frac{1}{1 + \Omega_c^2} \quad (8.23)$$

$$\begin{aligned} \Omega_c^2(1 + \Omega_c^2) &= \gamma^2 \\ \Omega_c^4 + \Omega_c^2 - \gamma^2 &= 0 \end{aligned} \quad (8.24)$$

$$\Omega_c^2 = -\frac{1}{2} + \sqrt{\frac{1}{4} + \gamma^2}$$

$$\Omega_c = \sqrt{-\frac{1}{2} + \sqrt{\frac{1}{4} + \gamma^2}} \quad (8.25)$$

## 8.2 Symmetrical Optimum

The control design method introduced in the preceding section uses the controller reset time for a pole-zero-cancellation. With that design method, good reference tracking dynamics result while the disturbance behavior is not considered. Aiming for a better disturbance rejection while keeping the *PI* controller type, the controller reset time should be determined in a different way. As a tendency, the reset time should be reduced to enable a quicker reaction of the integral part of the controller. The situation becomes very simple if the plant time constant  $\tau_s$  is assumed to be much larger than the small time constant  $\tau_\sigma$  and also larger than the controller reset time  $T_n$ :  $\tau_s \gg \tau_\sigma, T_n$ . In this case, the small time constant can be approximated only by an integrative behavior:

$$G_s(s) = V_s \frac{1}{1+s\tau_s} \frac{1}{1+s\tau_\sigma} \approx V_s \frac{1}{s\tau_s} \frac{1}{1+s\tau_\sigma} = V_s \frac{\tau_\sigma}{\tau_s} \frac{1}{s\tau_\sigma} \frac{1}{1+s\tau_\sigma} = \tilde{V}_s \frac{1}{s\tau_\sigma(1+s\tau_\sigma)}. \quad (8.26)$$

In case of a speed control, the plant really includes such an integrator. The loop transfer function results to

$$L(s) = G_c(s)G_s(s) = \tilde{V}_s V_c \frac{1+sT_n}{sT_n} \frac{1}{s\tau_\sigma} \frac{1}{1+s\tau_\sigma} = \tilde{V}_s V_c \frac{1}{s^2 T_n \tau_\sigma} \frac{1+sT_n}{1+s\tau_\sigma}. \quad (8.27)$$

The idea of the control design can be outlined very well using approximated magnitude Bode plots. For small frequencies, the magnitude plot decreases first with -40 dB per decade. The phase delay is -180° accordingly. At the corner frequency  $1/T_n$  the phase is increased by the controller zero, but decreased again at the corner frequency  $1/\tau_\sigma$  (plant pole). The maximum phase angle is achieved exactly between the two corner frequencies (in terms of the logarithmic scaling). The largest phase margin is obtained if the gain is chosen in that way so that the magnitude crossover frequency  $\omega_c$  is exactly at this point. Let

$$\frac{T_n}{\tau_\sigma} = a^2 \quad (8.28)$$

be the ratio between reset time and the small time constant. Then, the crossover frequency should be located at

$$\omega_c = \frac{1}{a\tau_\sigma} = \frac{a}{T_n} \quad (8.29)$$

In doing so, the ratio  $a$  can be interpreted as two different frequency ratios as also shown in the figure:

$$a = \frac{\omega_c}{1/T_n} = \frac{1/\tau_\sigma}{\omega_c}. \quad (8.30)$$

With respect to terms of geometry,  $a$  is called *double ratio*. On a logarithmic frequency axis the geometric distances from the crossover frequency  $\omega_c$  is exactly the same to both corner frequencies  $1/\tau_\sigma$  and  $1/T_n$ .

At the crossover frequency, the loop gain must be 1,

$$|L(j\omega_c)| = 1, \quad (8.31)$$

that leads to the design of the controller gain:

$$1 = \left| \tilde{V}_s V_c \frac{1}{-\omega_c^2 T_n \tau_\sigma} \frac{1 + j\omega_c T_n}{1 + j\omega_c \tau_\sigma} \right| = \tilde{V}_s V_c \left| \frac{1 + ja}{1 + j/a} \right| = \tilde{V}_s V_c a \left| \frac{1 + ja}{a + j} \right| = \tilde{V}_s V_c a \quad (8.32)$$

$$\tilde{V}_s V_c = \frac{1}{a} \quad \text{or} \quad V_c = \frac{1}{a \tilde{V}_s}$$

With that, loop and reference transfer functions result to

$$L(s) = \frac{1}{a^3 s^2 \tau_\sigma^2} \frac{1 + a^2 s \tau_\sigma}{1 + s \tau_\sigma} \quad (8.33)$$

$$T_w(s) = \frac{L(s)}{1 + L(s)} = \frac{1 + a^2 s \tau_\sigma}{1 + a^2 s \tau_\sigma + a^3 s^2 \tau_\sigma^2 (1 + s \tau_\sigma)} = \frac{1 + a^2 s \tau_\sigma}{1 + a^2 s \tau_\sigma + a^3 s^2 \tau_\sigma^2 + a^3 s^2 \tau_\sigma^2} \quad (8.34)$$

The controller transfer function can be expressed with the double ratio  $a$  as

$$G_c(s) = \frac{1}{a \tilde{V}_s} \frac{1 + s \tau_\sigma a^2}{s \tau_\sigma a^2} = \frac{1}{a^3 \tilde{V}_s} \frac{1 + s \tau_\sigma a^2}{s \tau_\sigma} \quad (8.35)$$

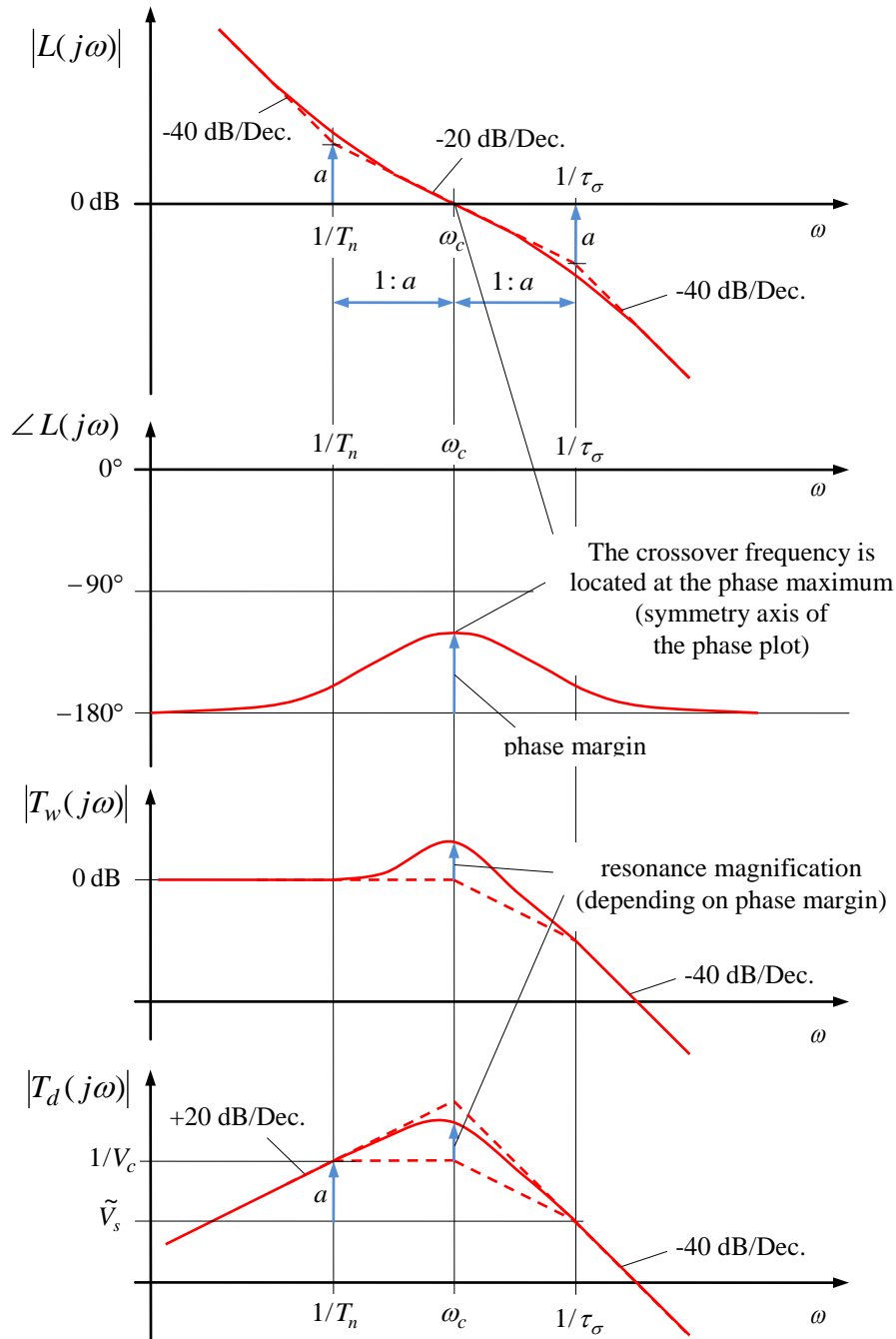


**Fig. 8-8:** Bode plots with the Symmetrical Optimum design method in double-logarithmic scaling

(The resonance peaks depending on the phase margins, in particular, distort the curve shapes. However, sometimes the piecewise straight lines (dashed) allow a better understanding of the design method than the exact plot.)

The bandwidth of the control transfer function is approximately determined by the magnitude crossover frequency  $\omega_c = 1/a\tau_\sigma$  when regarding the approximation

$$T_w(j\omega) = \frac{L(j\omega)}{1 + L(j\omega)} \approx \begin{cases} L(j\omega) & \text{für } |L(j\omega)| \ll 1 \\ 1 & \text{für } |L(j\omega)| \gg 1 \end{cases} \quad (8.36)$$

In order to achieve a high bandwidth, a small ratio  $a$  should be chosen. Of course that is done at the cost of a small phase margin and high resonance peaks. On the other hand, the disturbance behavior will benefit from aiming at a high crossover frequency  $\omega_c$ . The higher  $\omega_c$  and thus  $1/T_n$ , the smaller is the frequency band of poor disturbance rejection between  $1/T_n$  and  $\omega_c$ . The disturbance transfer function results as follows:

$$\begin{aligned}
 T_d(s) &= \frac{G_s(s)}{1+L(s)} = \frac{T_w(s)}{G_c(s)} \\
 &= a^3 \tilde{V}_s \frac{s \tau_\sigma}{1 + a^2 s \tau_\sigma + a^3 s^2 \tau_\sigma^2 + a^3 s^2 \tau_\sigma^2}
 \end{aligned}
 \tag{8.37}$$

The following figures show the Bode plots and step responses for different values of the double ratio  $a$  as design parameter.

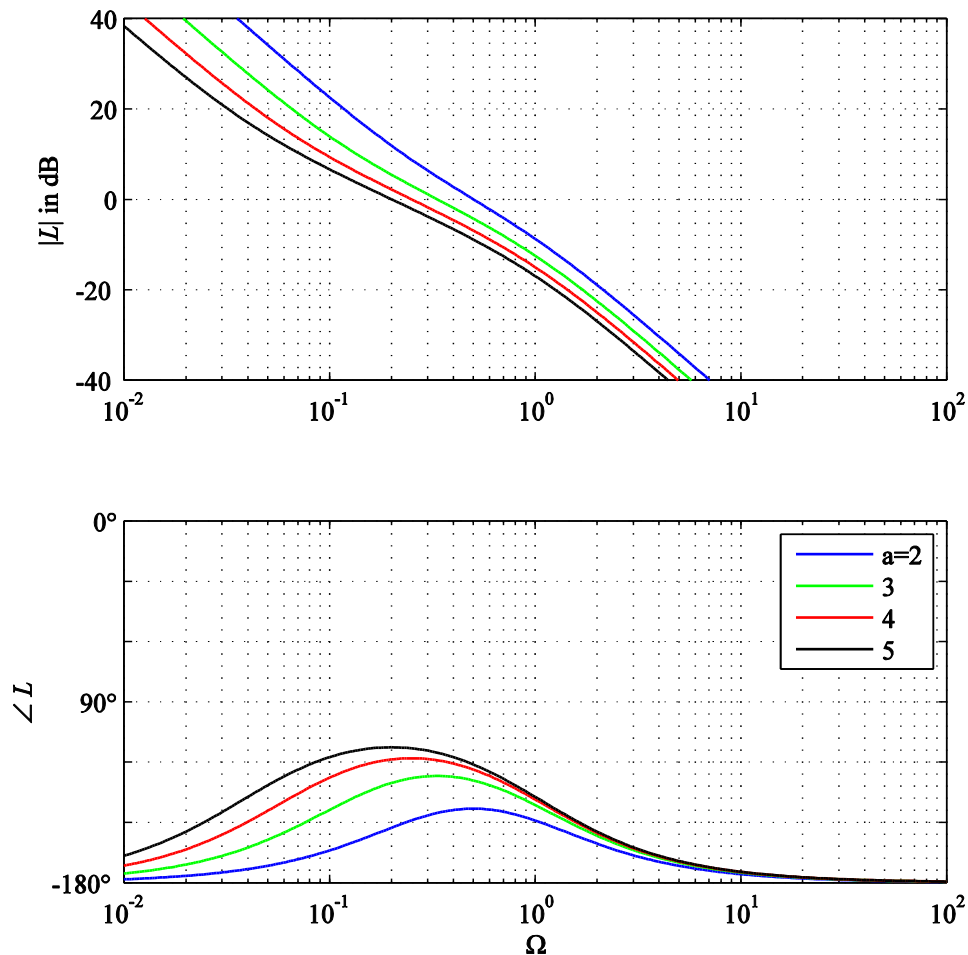


**Fig. 8-9:** Bode plot of loop transfer function  $L$  with Symmetrical Optimum design vs. normalized frequency  $\Omega = \omega \tau_\sigma$

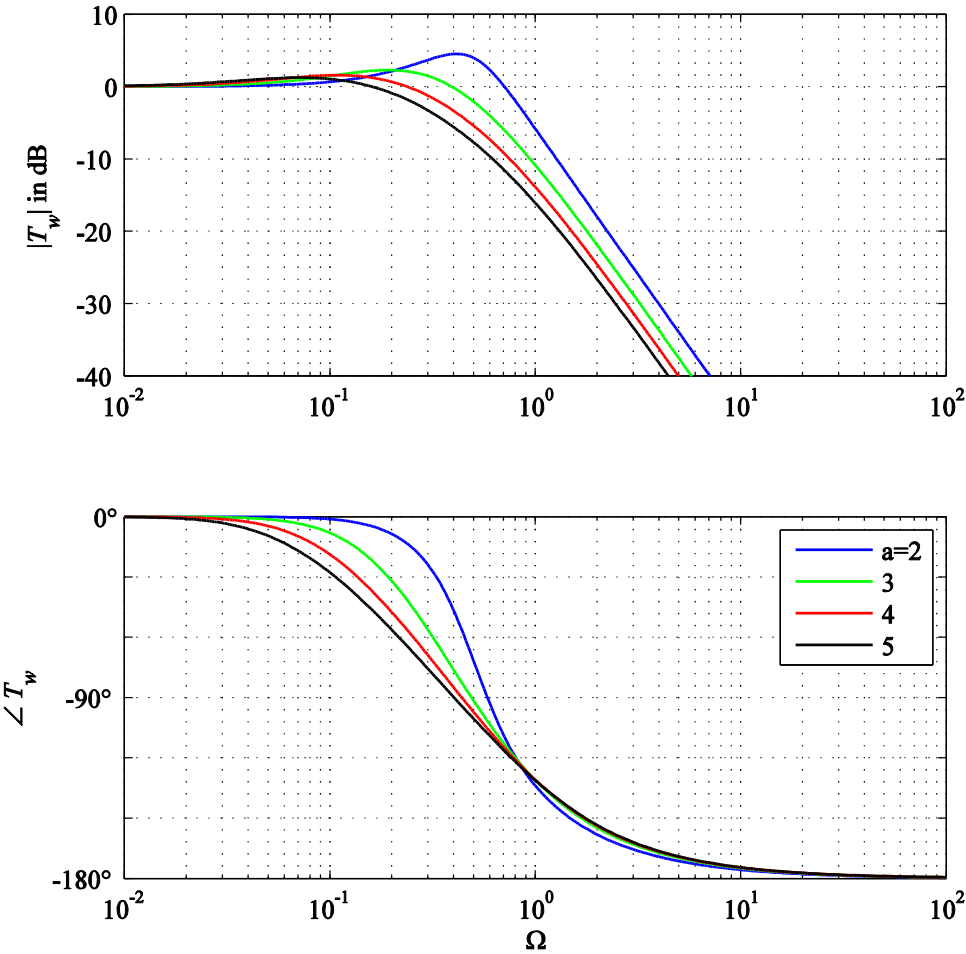


**Fig. 8-10:** Bode plot of the control tracking transfer function  $T_w$  vs. normalized frequency  $\Omega = \omega \tau_\sigma$

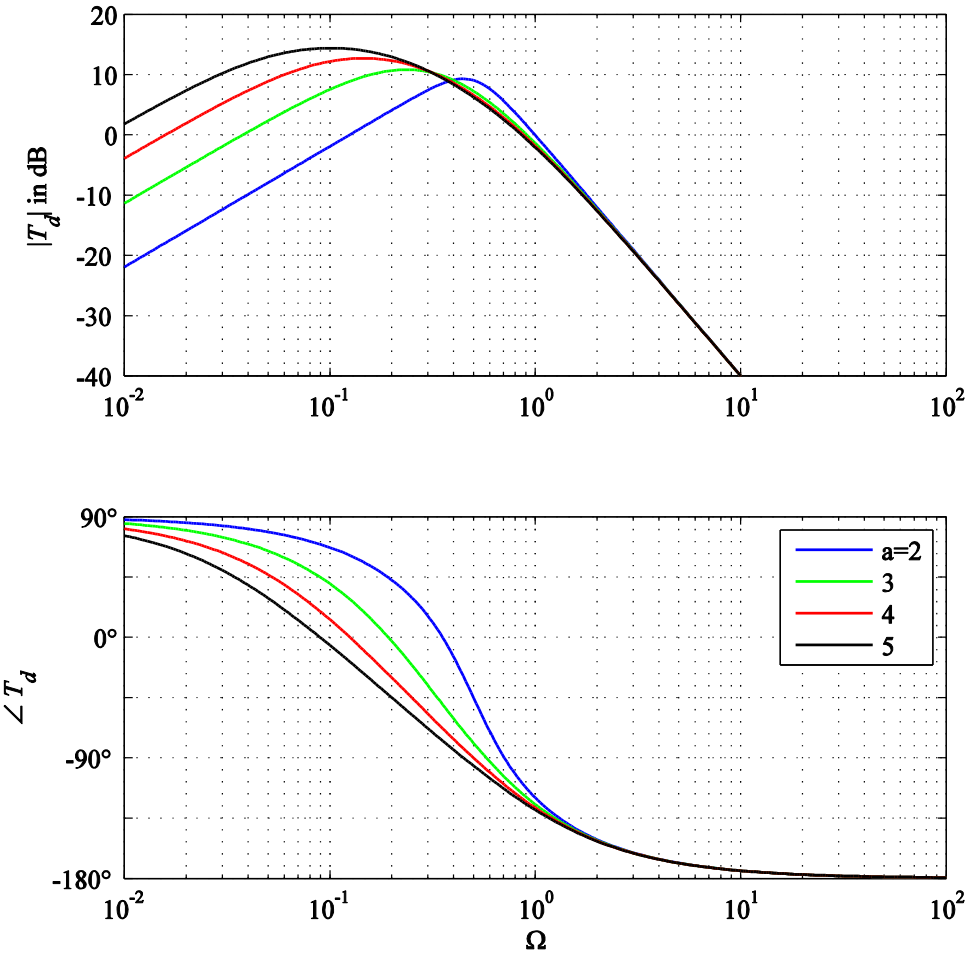


**Fig. 8-11:** Bode plot of the disturbance transfer function  $T_d$  vs. normalized frequency  $\Omega = \omega \tau_\sigma$  with  $\tilde{V}_s = 1$

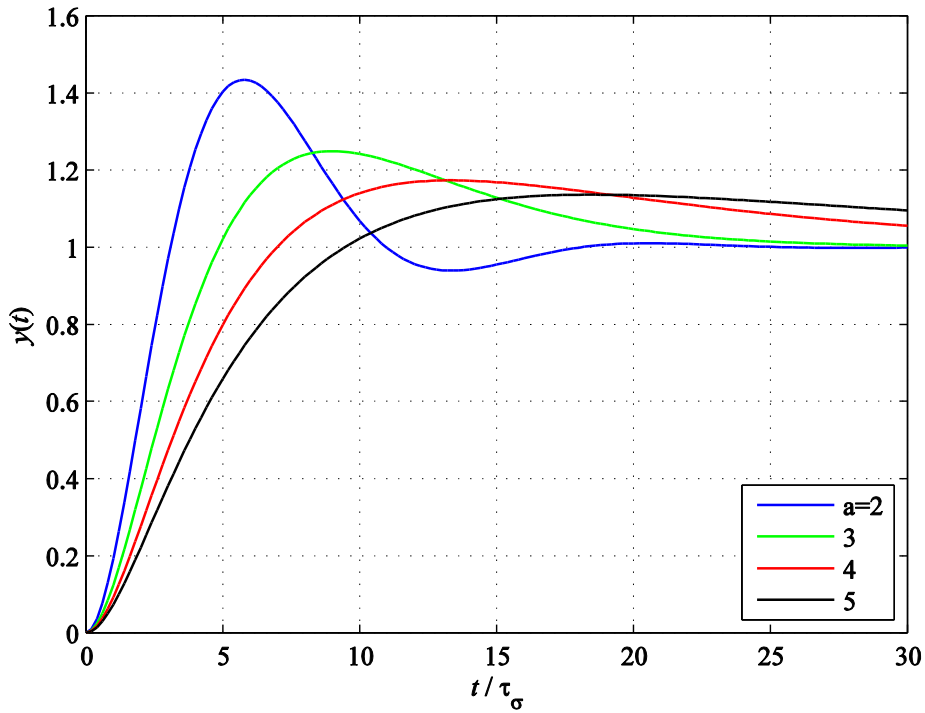


**Fig. 8-12:** Response of the control variable  $y(t)$  to a step-like change of the set point  $w(t) = \sigma(t)$  (tracking behavior)

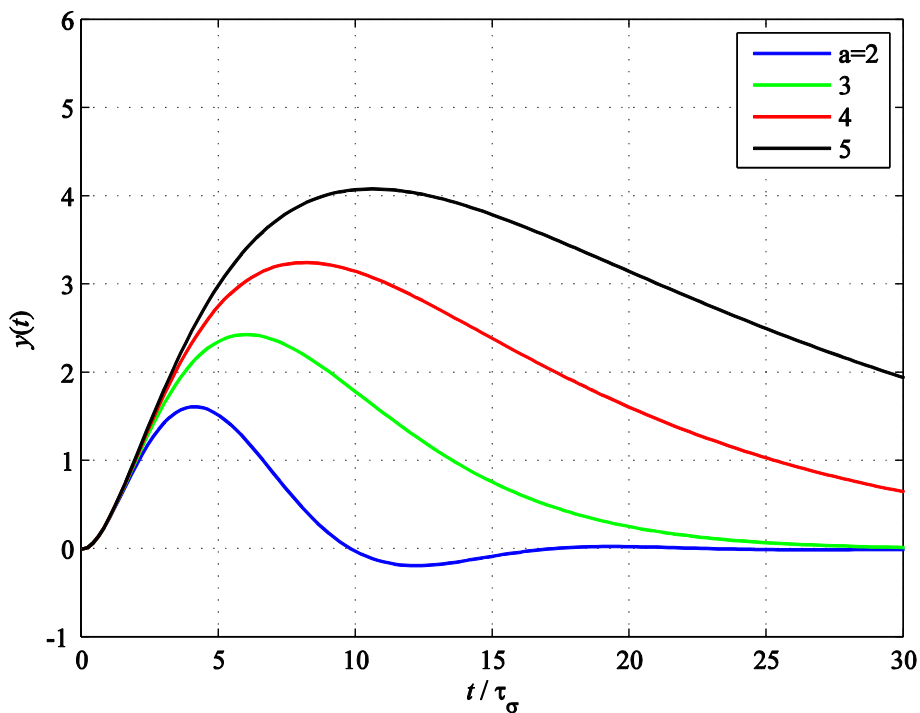


**Fig. 8-13:** Response of the control variable  $y(t)$  to a step-like change of the disturbance input  $d(t) = \sigma(t)$  with  $\tilde{V}_s = 1$

A popular standard design of the Symmetrical Optimum is  $a = 2$ . With that value, the phase margin results to  $37^\circ$ . In time domain, the resulting 43% overshoot of the reference step

response is not satisfactory, however. The reason for this large overshoot is mainly due to the zero of the reference transfer function at  $s = 1/(a^2\tau_\sigma)$ . With help of an additional  $T_1$  prefilter,

$$G_f(s) = \frac{1}{1 + a^2\tau_\sigma s} = \frac{1}{1 + T_n s} \tag{8.38}$$

the transfer function zero is cancelled, reducing the step response overshoot to only 8%, but doubling the rise time in return (see following figure).

The value  $a = 3$  represents the special case of a triple pole of the reference and disturbance transfer functions at  $s = 1/(3\tau_\sigma)$ . With the prefilter applied, the step response does not show any overshoot in that case.

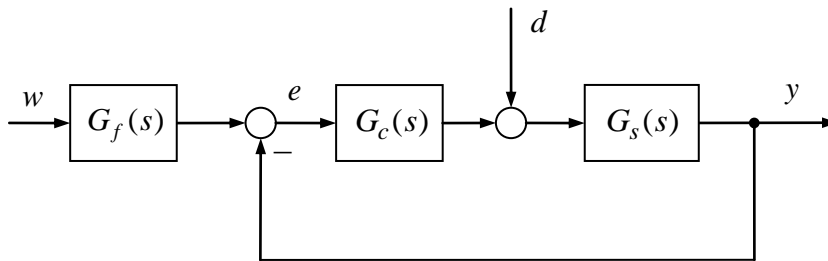


**Fig. 8-14:** Control loop with prefilter

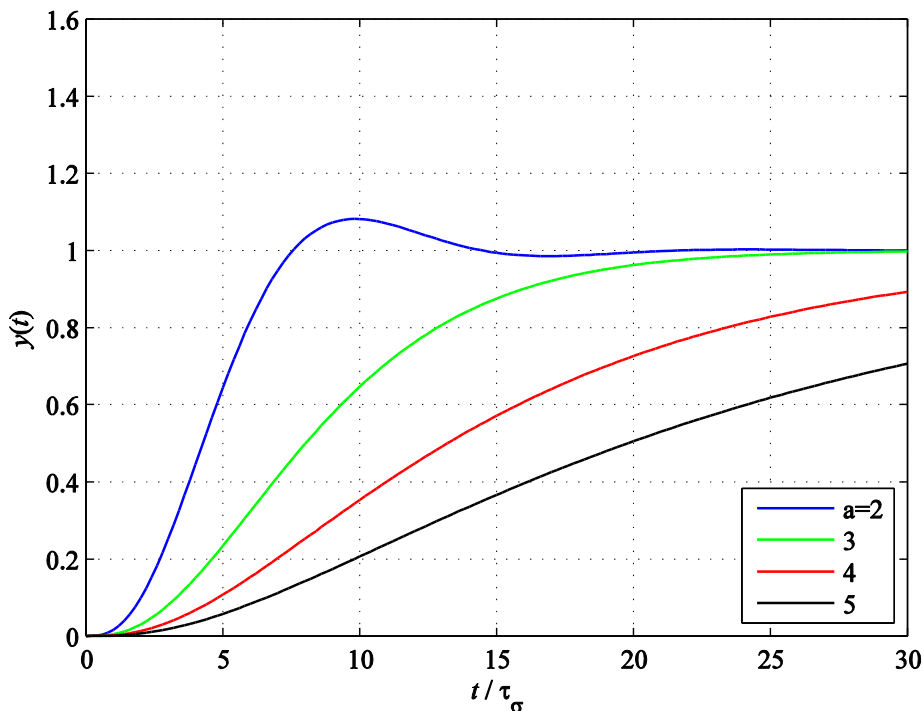


**Fig. 8-15:** Response of the control variable  $y(t)$  to a step-like change of the reference input  $w(t) = \sigma(t)$  with additional  $T_1$ -prefilter (tracking behavior)

The Symmetrical Optimum was only introduced for the case of a plant with integrating behavior and one time constant. Nevertheless, this assumption can also be seen as a suitable approximation for a plant with two distant time constants  $\tau_\sigma \ll \tau_s$  (as assumed with the Magnitude Optimum). In literature, however, also the exact case without such an approximation is covered.

The disturbance suppression characteristics of the Symmetrical Optimum are superior compared with Magnitude Optimum in case of large ratios of the time constants  $\tau_s / \tau_\sigma$ . This is due to the fact that the large time constant is not being cancelled by the controller reset time, but a much shorter controller reset time is chosen, instead. As far as only tracking control performance is concerned, the Magnitude Optimum outperforms the Symmetrical Optimum.